

**HUNTING FOR EMERGING POLYFLUORINATED POLLUTANTS:
FROM THEORETICAL PREDICTION TO EXPERIMENTAL DETECTION**

by © Xiaolei Li

A thesis submitted to the School of Graduate Studies
in partial fulfillment of the requirements for the degree of

Doctor of Philosophy

Chemistry Department

Memorial University of Newfoundland

August 2023

St. John's Newfoundland and Labrador

Abstract

A large number of chemicals are manufactured, used, and ultimately released to the environment every year, but only a few are regulated. Some chemicals are recognized as persistent organic pollutants (POPs) that are persistent, bioaccumulative, and can undergo long-range transport. Per- and poly-fluoroalkyl Substances (PFASs) have continued to attract attention since perfluorooctanoic acid and perfluorooctane sulfonate were first identified as POPs. However, the environmental behaviors of other polyfluorinated chemicals, such as longer chain (mixed) halogenated n-alkanes (PXAs), have never been investigated, although these chemicals are widely used. The lack of experimental data has hindered the assessment of these chemicals.

We have developed two strategies to better estimate the environmental fate of an unknown compound without sufficient experimental data. The first strategy presented is an approach using quantitative structure-property relationships, density functional theory (DFT), chemical fate models, and partitioning space to prioritize all possible PXAs. The results suggest that PXAs with elemental compositions characterized by a more significant number of carbon and fluorine atoms but fewer chlorine and bromine atoms may pose a risk. These chemicals are likely constituents of substances used as lubricants, plasticizers, and flame retardants.

In the second strategy, we analyzed the potential of conceptual DFT descriptors (global electronegativity, electrophilicity index, hardness, and polarizability) to predict a chemical's environmental behavior. The model shows that chemicals with POPs potential tend to possess a discrete zone in spaces defined by these descriptors from

those with less or no POPs potential. Fluorinated chemicals tend to have a higher hardness than other compounds, which may explain their potential to bind with proteins.

The results of PXA research also underline the urgent need to identify and monitor these suspected pollutants, most appropriately using mass spectrometry. We demonstrated that the novel cyclic ion mobility-mass spectrometer (cIMS-MS), coupled with gas chromatography atmospheric pressure chemical ionization (GC-APCI), can reveal the presence of unknown PFASs based on the ratio of their mass and collision cross section. PFASs compounds are revealed without prior knowledge of their occurrence in dust samples using cIMS-MS data. The method also indicates the presence of chlorofluoro n-alkanes as an emerging class of "forever chemicals" that contaminate the indoor environment.

Acknowledgments

I would like to express my heartfelt gratitude to my supervisor, Dr. Karl Jobst, for his unwavering support and guidance throughout my Ph.D. studies. Working with Dr. Jobst has been an incredible pleasure, and I am truly grateful for his mentorship. I would not have achieved any of my accomplishments without his constant help and encouragement. Dr. Jobst has not only pushed me to excel in my research but has also inspired me to become a better version of myself. The knowledge and skills I have acquired under his guidance will benefit me for a lifetime, and I am grateful for this transformative journey.

I extend my sincere thanks to my supervisory committee, Dr. Christina Bottaro and Dr. Francesca Kerton, for their support and guidance. Their expertise and wisdom have been invaluable, not only in academics but also in various aspects of life. I consider myself fortunate to have had such remarkable individuals as role models during my studies.

I am grateful to the Department of Chemistry, the School of Graduate Studies, and the Teaching Assistant's Union at Memorial University for their support and resources that have contributed to my academic and personal growth. I would also like to acknowledge the financial assistance provided by the Natural Sciences and Engineering Research Council (NSERC) Postgraduate Scholarships Doctoral program, as well as Dr. Linqi Chen and J. Beryl Truscott for their support. I also thank NSERC and the Ontario Ministry of the Environment, Conservation and Parks (MECP) for their funding support and the Advanced research computing in Atlantic Canada (ACENET:

www.ace-net.ca) and Compute/Calcul Canada (www.computecanada.ca) for their computation resources.

My deepest appreciation goes to my dear husband, Dr. Yang Zhang, for his unwavering support, understanding, and encouragement throughout this journey. His presence has been a constant source of strength and inspiration. I am also grateful to my son, Alex, for always being there for me and being a constant reminder of what truly matters in life.

I would like to acknowledge all my collaborators for their contributions to my research. Their expertise and collaboration have enriched my work and made it possible to achieve significant outcomes. I am also grateful to my team colleagues, Roshanak Amiri, Meera Bissram, Amber MacNeil, Tania Chevez, and my Chinese friends in St. John's for their friendship and support. The memories we have created together will be cherished forever. In conclusion, I am indebted to the support, guidance, and contributions of all those mentioned above. They have played a significant role in shaping my Ph.D. journey and have my deepest appreciation.

Preface

The majority of the computational and experimental results presented in this thesis have been obtained by the author over a three-year period of research in the field of environmental analytical chemistry. The author's primary focus has been on the identification and assessment of fluorinated chemicals existing in the environment, as well as the development of approaches for the risk assessment of both known and new fluorinated chemicals. Such investigations have required close collaboration between experimental and theoretical chemists. The author took responsibility for collecting the references and writing the initial draft of Chapter 2 and made corrections to the chapter based on feedback and guidance provided. In Chapter 3 and 4, the author played a central role in developing the methodology, conducting calculations, reviewing and analyzing data, and validating results and also prepared figures and tables and addressed the necessary revisions under the direction of Dr. Karl Jobst. Finally, in Chapter 5, the author took the lead in developing the model simulation, devising the sample preparation methodology, reviewing and analyzing data, creating relevant figures and tables and writing part of the manuscript.

The author extends heartfelt gratitude to the collaborators who have made substantial contributions to this research. Special thanks are owed to Prof. Frank L. Dorman for providing the essential gas chromatography instrumental resources required for Chapters 2 and 5. Prof. Dorman's support has been instrumental in the successful execution of this research. Prof. Paul A. Helm (Chapter 2), Sonya Kleywegt (Chapters 2, 3), Dr. André Simpson, and Dr. Myrna J. Simpson (Chapters 2, 3, 5) provided mentorship, insightful discussion and project administration. Chapter 3 was inspired by the enlightening discussions on bromochloro pollutants with Dr. Amila O.

De Silva and Dr. Derek C.G. Muir, who have provided their expertise in environmental fate modeling, significantly shaping the content of the chapter. Tannia Chevez assisted with the calculations in Chapter 3. Dr. James S.M. Anderson contributed to the conceptual density functional theory part in Chapter 4. Amber MacNeil synthesized and confirmed chlorofluoro phthalimides, and Roshanak Amiri aided with the Mobcal calculation in Chapter 5. These collaborators have provided valuable insights, suggestions, and critical evaluations that have greatly influenced the presentation of the results. The author also acknowledges the permission granted by Elsevier Science, Springer, MDPI, and the American Chemical Society to reproduce previously published data and text, which has contributed to the completeness and accuracy of the thesis.

Overall, the collaborative efforts and contributions of all individuals mentioned above have been instrumental in shaping the research outcomes and enriching the quality of this thesis.

Table of Contents

Abstract	i
Acknowledgments.....	iii
Preface.....	v
Table of Contents	vii
List of Tables	xi
List of Figures	xiii
List of abbreviations and symbols	xvii
Chapter 1	1
1.1 Background	3
1.2 Computational and experimental techniques for environmental risk assessment....	5
1.2.1 Quantitative structure-property relationship	5
1.2.2 Density functional theory	7
1.2.3 Gas chromatography atmospheric pressure chemical ionization (GC-APCI)	9
1.2.4 Ion mobility spectrometry mass-spectrometry.....	11
1.2.5 Gas chromatography cyclic ion mobility mass spectrometer	18
1.3 Data analysis technique involved in IMS	21
1.3.1 Ion-neutral collision cross-section	21
1.3.2 Unwrapping "wrapping around" data in GC-cIMS-MS	22
1.3.3 The potential of CCS in target screening	24
1.4 Present progress in non-target analysis using IMS-MS.....	25
1.4.1 Automated annotation.....	25
1.4.2 CCS and m/z conformation space.....	27
1.5 Aims of this research	29
Chapter 2.....	31
2.1 Introduction.....	33
2.2 Gas chromatography-atmospheric pressure ionization techniques.....	43
2.2.1 Atmospheric pressure chemical ionization (APCI)	44
2.2.2 Atmospheric pressure photoionization.....	46
2.2.3 Atmospheric pressure Laser ionization (APLI)	49
2.2.4 Electrospray ionization (ESI).....	49

2.2.5 Penning ionization (PI)	50
2.2.6 Dielectric barrier discharge ionization (DBDI)	51
2.3 Strategies to identify unknowns by GC-API	52
2.3.1 Multidimensional chromatography	52
2.3.2 Data-independent identification	55
2.3.3 Evaluating confidence in structure assignments	60
2.3.4 Ion-molecule reactions for separation and structural elucidation	61
2.3.5 Retrospective analysis and compound discovery.....	64
2.3.6 Computational tools to predict mass spectra	66
2.4 Summary and outlook	68
Chapter 3	71
3.1 Introduction.....	73
3.2 Experimental methods	75
3.2.1 Generating representative SMILES structures of the PXAs.....	75
3.2.2 Persistence, bioaccumulation potential and chemical fate modeling.....	76
3.2.3 Prediction of PXA mass spectra.....	78
3.3 Results and Discussion	79
3.3.1 Development of a set of representative PXA structures	79
3.3.2 Screening PXAs that are potential POPs using chemical fate models and partitioning space	82
3.3.3 Prediction of partitioning coefficients using density functional theory	87
3.3.4 Potential sources of PXAs to the environment	94
3.3.5 Is it possible to identify the PXAs using high-resolution mass spectrometry?... 96	
Chapter 4	101
4.1 Introduction.....	103
4.2 Computational methods	106
4.2.1 Chemical lists.....	106
4.2.2 Chemical property calculations.....	107
4.2.3 Data analysis	108
4.3 Results and discussion	109
Chapter 5	119
5.1 Introduction.....	121

5.2 Experimental Methods	123
5.2.1 Chemical Standards	123
5.2.2 Instrumental analysis	124
5.2.3 Chemical Databases and CCS Prediction	125
5.2.4 Indoor Dust Samples	126
5.2.5 Data Processing	126
5.2.6 Quality Assurance and Quality Control	126
5.3 Results and Discussion	127
5.3.1 Differentiating polyfluorinated and non-fluorinated compounds based on m/z and CCS	127
5.3.2 Evaluation of the method using a standard reference material of indoor dust..	130
5.3.3 Identification of previously unknown chlorofluoro n-alkanes in indoor dust ..	138
5.4 Conclusions	141
Chapter 6	143
6.1 Conclusions	145
6.2 Future work	147
References	151

List of Tables

Table 1.1 Resolving power of different IMS platforms.....	18
Table 2.1 Recent studies that employ GC-API techniques for (non)targeted analysis of environmental pollutants.....	37
Table 3.1. Summary of the number of persistent and bioaccumulative PXAs identified in this study using the criteria developed by Muir and Howard, Howard and Muir, Brown and Wania, Rorije <i>et al.</i> and Scheringer <i>et al.</i>	77
Table 3.2 The physical-chemical properties and statics of all C ₁₀ H ₁₈ Cl ₄ isomers predicted by EPISuite.	82
Table 3.3 Partitioning coefficients computed using DFT (MO6-2X/6-311+G**) and experimentally determined values of available halogenated n-alkanes	89
Table 3.4 The breakdown of screened compositions using experimental and DFT correction.	93
Table 3.5 Different categories of screened PXAs number separated against the category of 184,600 PXA under different resolutions.....	98
Table 5.1 Summary of tentatively identified PFASs present in NIST SRM 2585. ...	132

List of Figures

Figure 1.1 Locations of all chemicals in the EPISuite database which match the structural profile of known Arctic contaminants	6
Figure 1.2 The GC atmospheric pressure chemical ion source; (b) general scheme for positive mode ionization in dry ion source	11
Figure 1.3 Stacked ring ion guide (top) and a real T-wave collision cell (bottom) of Waters T-wave; (b) Schematic diagram (top) and real picture (bottom) of the Agilent ion mobility instrument.....	13
Figure 1.4 Schemes of different ion confinement with selective release IMS	15
Figure 1.5 Multipass experiment increases the separation of TCDD isomers	16
Figure 1.6 Scheme of Waters cyclic ion mobility coupled with time-of-flight mass spectrometry (b) the GC-cIMS-MS platform used (c) cyclic ion mobility cell.....	19
Figure 1.7 Comparison of "wrapping" and "unwrapping" retention time vs. drift time contour plots obtained by GC-cIMS	23
Figure 1.8 CCS as an additional dimension for automated annotation. (a) The CCS value reduces false positives when combined with m/z data	26
Figure 1.9 Examples of CCS vs. m/z conformation zone.....	28
Figure 2.1 Partial mass spectra obtained using GC-APPI (top) and GC-APCI (bottom) for (a) decabromo-diphenyl ether (BDE-209) and its ¹³ C-labelled counterpart, and (b) 1,8-dibromo-2,6-dichloro-9H-carbazole.....	48
Figure 2.2 (a) Comprehensive two-dimensional gas chromatography (GC×GC) affords unparalleled separation of organic pollutants from in plasma; (b) Modulated gas chromatogram obtained from 2,3,7,8-tetrachlorodibenzo-p-dioxin.....	53
Figure 2.3 Kendrick mass defect (KMD) plots of (a) a coal tar seal coat product, and (b) an asphalt sealcoat product. (c) Two-dimensional hierarchical cluster analysis with heat map plot of various environmental PAH sources.	53
Figure 2.4 Comparison of (a) GC-DIA, (b) GC×GC-DIA, and (c) deconvolved GC-SQDIA spectra of a tetrabromodiphenyl ether.	57

Figure 2.5 (a) Scheme of reaction between 2,3,7,8-TCDD and O_2^- ; (b~e) APCI-spectra of 2,3,7,8-TCDD, 2,3,7,8-TBDD, and 2,3Br-7,8Cl-DD. Ether cleavage products (ECPs) are observed at m/z 176 and 266 for the 2,3,7,8-TCDD and 2,3,7,8-TBDD species.	62
Figure 2.6 Distribution of 610 prioritized persistent, bioaccumulative (P, B) compounds (in red) and commercial chemicals (in blue) from the North American chemical inventories in the compositional spaces defined by m/z of the molecular ion and the ratio of its isotopic peaks $(A + 2):A$	59
Figure 2.7 (a) EI mass spectrum calculated by QCEIMS and experimental EI mass spectrum of 3,6-dichloro-1,8-dibromo-carbazole. (b) calculated spectrum and 40 eV literature spectrum of the most populated caffeine protomer at 600 K, single collision at 100 eV	65
Figure 3.1 Distribution of elemental compositions corresponding to (mixed) halogenated n-alkanes (PXAs) of varying carbon length	79
Figure 3.2 Partitioning space for 184,600 PXAs	83
Figure 3.4 Partitioning space for 184,600 PXAs using DFT correction.....	84
Figure 3.4 Breakdown of the PXAs identified using partitioning space based on (a) the types of halogens present; and (b) the carbon chain length.....	85
Figure 3.5 Comparison of the experimental $\log K_{OW}$, $\log K_{OA}$ and $\log K_{AW}$ partitioning coefficients with those computed using the $MO6-2X/6-311+G^{**}$	88
Figure 3.6 The relationship between DFT and EpiSuite values obtained for (a) $\log K_{OW}$; and (b) $\log K_{OA}$	91
Figure 3.7 Distributions of (a) fluorine; (b) chlorine; (c) bromine; and (d) total halogen content by weight	92
Figure 4.1 Distribution of CDFT descriptors among suspected POPs (red) and all industrial chemicals (grey): (a) Hardness; (b) Global electronegativity; (c) Electrophilicity index; (d) Polarizability	110
Figure 4.2 Chemical space defined by CDFT properties: (a) Polarizability and Hardness; (b) Electrophilicity and Polarizability (c) Electrophilicity and Hardness.....	98
Figure 4.3 Hardness (Ht) vs. the logarithm of the Bioconcentration Factor (BCF) predicted by EpiSuite. Known or suspected POPs are coloured red. All remaining compounds on the DT list are in grey.	111

Figure 4.4 (a) Scores plot and; (b) loadings plot obtained by PCA. Note: POPs have been split into PFAS and all remaining POPs.	114
Figure 5.1 (a) Predicted CCS_{N_2} vs. m/z for c. 20,000 substances listed in the Canadian DSL and US TSCA chemical inventories; (b) Experimental $^{TW}CCS_{N_2}$ vs. m/z of ions detected in SRM 2585, a reference material of indoor dust, using GC-cIMS	128
Figure 5.2 Retention time vs. drift time contour plots obtained from NIST SRM 2585 displaying (a) all ions; and (b) only ions characterized by CCS values that are less than the sum of 100 \AA^2 and one-fifth of their mass	130
Figure 5.3 Negative ion mode mass spectra obtained from (a) the main product of the synthesis (Cl/F-1); and (b) the same compound found in SRM 2585; Retention time vs. drift time contour plot of the molecular ions M^{*+} of Cl/F-1 after (c) one pass and (d) ten passes through the cyclic ion mobility cell	135
Figure 5.4 Mass spectra obtained from (a) a dechlorinated impurity produced in the synthesis of Cl/F-1; and (b) the same compound found in SRM 2585.....	136
Figure 5.5 Optimized geometries of selected homologs and isomers of Cl/F-1.....	137
Figure 5.6 Total ion contour plots obtained from indoor dust sample CSF1.....	139

List of abbreviations and symbols

8:2 FTOH	8:2 fluorotelomer alcohol
AMAP	Arctic Monitoring and Assessment Programme
APCI	atmospheric pressure chemical ionization
API	atmospheric pressure ionization
APLI	atmospheric pressure laser ionization
APPI	atmospheric pressure photoionization
Atm-HL	half-life in the atmosphere
B	bioaccumulative
BAF	bioaccumulation factor
BCF	bioconcentration factor
BDE	decabromo-diphenyl ether
CCS	collision cross-section
CID	collision induced dissociation
CV	coefficient of variance
(C)DFT	(conceptual) density functional theory
DBDI	dielectric barrier discharge ionization
DDA	data-dependent acquisition
(SQ)DIA	(scanning quadrupole) data-independent acquisition
DSL	Canadian Domestic Substances List
DT	drift tube
EA	electron affinity
ESI	electrospray ionization
GC-cIM-MS	gas chromatography-cyclic ion mobility mass spectrometry
GC-HRMS	gas chromatography -high-resolution mass spectrometry
GCxGC	two-dimensional gas chromatography

HBCCD	hexabromocyclododecane
HF	Hartree-Fock
HOMO	highest occupied molecular orbital
HSAB	soft acids and bases
ID(Q)L	instrument detection(qualification) limit
IECSC	Existing Chemical Substances of China
IP	ionization potential
K _{AW}	air-water partitioning coefficient
KMD	Kendrick mass defect
K _{OA}	octanal-air partitioning coefficient
K _{OW}	octanal-water partitioning coefficient
LC-HRMS	liquid chromatography-high resolution mass spectrometry
LOD	limit of detection
LRT	long-range transporting
LUMO	lowest unoccupied molecular orbital
MD(Q)L	method detection(qualification) limit.
MspA	Mycobacterium smegmatis porin A
N-MetPFOSE	N-methylperfluorooctanesulfonamidoethanol
N-MetPFSM	N-methylperfluorooctane sulfonamide
NTS	non-targeted screening
OP	organic phosphate
P	persistent
PAH	polycyclic Aromatic Hydrocarbons
PBDEs	polybrominated diphenyl ethers
PCA	principal component analysis
PCAs	Polychlorinated n-alkanes
PCTFE	polychlorotrifluoroethylene
PFASs	Per- and polyfluoroalkyl substances
PFCAs	perfluorinated carboxylic acids

PFSM	N-alkylperfluoroalkylsulfonamides
PI	photoionization
POPs	coined persistent organic pollutants
PTFE	polytetrafluoroethylene
PVDF	polyvinylidene fluoride
PXAs	mixed halogenated n-alkanes
QSAR	Quantitative structure-activity relationship
QSPR	quantitative structure-property relationship
REa	adiabatic recombination energy
REACH	the Registration, Evaluation, Authorization and Restriction of Chemicals
RF	radio frequency
RMS	root mean square
SMD	solvation model based on density
SMILES	simplified molecular-input line-entry system
TCDD	tetrachlorodibenzo-p-dioxin
TM	trajectory method
TSCA	Toxic Substances Control Act Chemical Substance Inventory
TOF	time of flight
TW	travel wave
UVCB	unknown or variable composition, complex reaction products or biological materials
Water-HL	half-life in water
α	polarizability
η	hardness
σ	softness
χ	Global electronegativity
ω	electrophilicity index

Chapter 1

Introduction

1.1 Background

A significant number of chemicals are produced, utilized, and eventually released into the environment on an annual basis. To provide an overview of the scale, the Canadian Domestic Substances List (DSL)¹ contains approximately 23,000 existing substances, while the U.S. Toxic Substances Control Act Inventory (US TSCA)² includes over 40,000 active chemicals. Furthermore, the Inventory of Existing Chemical Substances of China (IECSC)³ comprises a list of over 45,000 chemicals, and the Registration, Evaluation, Authorization and Restriction of Chemicals (REACH)⁴ by the European Union lists more than 74,000 chemicals. These inventories reflect the extensive range of chemicals that are currently known and regulated, underscoring the need for robust approaches to assess their potential impacts on human health and the environment. It is not practical to conduct risk assessments of all these chemicals, and this has driven the need to prioritize those chemicals with the greatest potential to harm the environment. At the same time, non-targeted screening (NTS), which refers to the identification of unknown pollutants already in the environment using mass spectrometry, is also a necessity.

Two vital properties needed to evaluate the risk posed by a chemical substance are its persistence and bioaccumulation potential, which describe its resistance to degradation and accumulation in humans and wildlife. Environmental scientists have endeavored to develop various strategies to identify persistent and bioaccumulative organics. Computer modeling methods using partitioning coefficients have successfully predicted a chemical's environment fate. This approach hinges upon the idea that persistent organic pollutants exist in a discrete region of chemical space defined by their intrinsic chemical properties. Complementary experimental techniques, such as HRMS

(high-resolution mass spectrometry), have also revealed the environmental occurrence of chemicals that are persistent and bioaccumulative, but not intentionally produced and thus not in a chemical inventory. Zhang *et al.*⁵ have shown that suspected POPs occupy a discrete region of compositional space defined by properties measured by mass spectrometry. A previously undocumented class of chlorofluoro flame retardants was discovered using this approach⁵.

Halogenated compounds find applications in various fields, including flame retardants, plasticizers, biocides, lubricants, and water/stain-repellents, among others. However, this diverse group of chemicals exhibits diverse side effects on both organism health and the environment, including carcinogenicity and teratogenicity. Many of the persistent organic pollutants (POPs) listed in the Stockholm Convention⁶ are halogenated chemicals, known for their potential to be persistent (P), bioaccumulative (B), and experience long-range transport (LRT), with some also exhibiting toxicity (T). Environmental fate modeling results consistently indicate that a majority of suspected POPs are halogenated. For instance, when screening criteria for P, B, and LRT of the Stockholm Convention are applied to a set of 93,144 organic chemicals, approximately 98% of the prioritized chemicals are found to be halogenated⁷.

Recognizing the environmental and ecosystem hazards posed by chlorine and bromine chemicals, there has been a shift toward the use of fluorine-containing compounds. Fluorinated chemicals are of particular interest in this thesis due to their inertness in the environment, attributed to the stability of the carbon-fluorine (C-F) bond. However, increasing studies have revealed that fluorinated chemicals also pose risks. Among them, per- and polyfluoroalkyl substances, which contain at least a perfluorinated methyl group ($-\text{CF}_3$) or a perfluorinated methylene group ($-\text{CF}_2-$), have

garnered significant concern. PFASs have been widely used due to their resistance to water and stains, owing to their lipophobic and hydrophobic properties. Notorious examples of PFASs include perfluorooctanoic acid (PFOA) and perfluorooctane sulfonate (PFOS). In this thesis, novel models have been developed to prioritize halogenated (specifically fluorinated) chemicals, and a new instrument platform has been employed for the identification of emerging PFAS contaminants.

1.2 Computational and experimental techniques for environmental risk assessment

1.2.1 Quantitative structure-property relationship

Before manufacturing a substance on a large scale, it is crucial to understand its potential environmental risks. Scientists employ quantitative structure-activity relationship (QSAR) models to estimate the environmental behaviors of new chemicals. QSAR, developed over 60 years ago, predicts the activities of new chemicals based on the structure and activity of known chemicals, assuming that similar structures have similar properties. QSAR has expanded to include quantitative structure-property relationship (QSPR) models for predicting chemical properties. There are three types of QSPR models: fragment-based, 3D, and chemical descriptor-based. Partitioning coefficients, such as octanol-water partitioning coefficient (K_{OW}), air-water partitioning coefficient (K_{AW}), and octanol-air partitioning coefficient (K_{OA}), are important parameters that play a significant role in determining the bioaccumulation potential and atmospheric/water transport of a chemical. These parameters contribute to the partitioning space⁸, as illustrated in Figure 1.1. The partitioning space has been previously utilized to prioritize potential chemicals from a dataset comprising over 100,000 distinct industrial chemicals. Chemicals located in different zones within this

space exhibit varying environmental behaviors, reflecting their tendencies towards bioaccumulation and transport in different environmental compartments. By considering the relationships between K_{OW} , K_{OA} , and K_{AW} , valuable insights can be gained into the potential fate and behavior of chemicals in the environment.

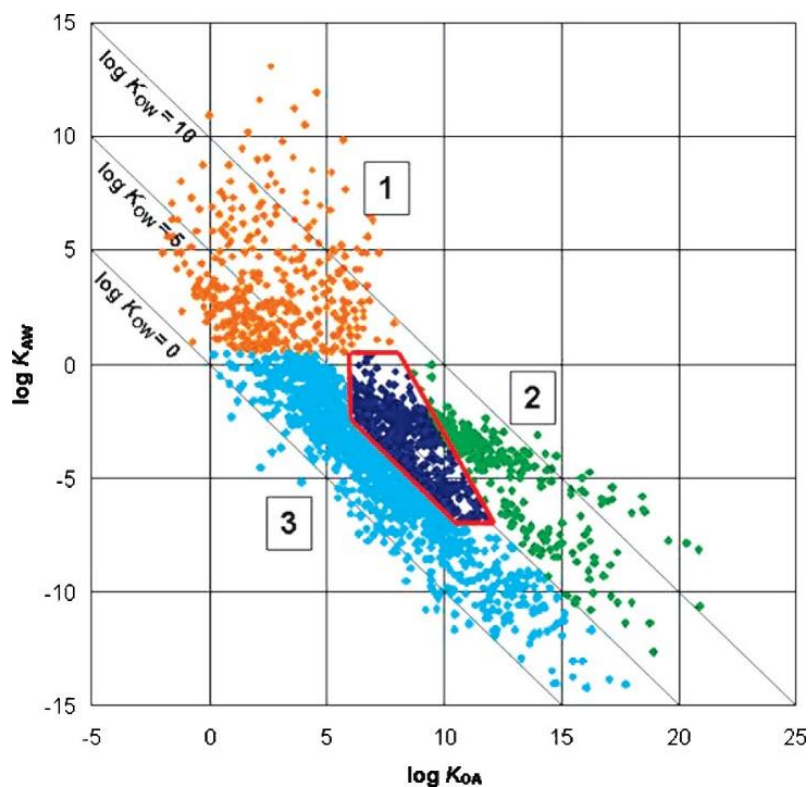


Figure 1.1 Locations of all chemicals in the EPISuite database which match the structural profile of known Arctic contaminants⁸. Type 1: Volatile chemicals. Type 2: Highly sorptive chemicals. Type 3: Small, polar chemicals. Reproduced from Brown and Wania⁸ with permission. Copyright © 2008, American Chemical Society.

Additionally, degradation half-lives (in water and air) and bioconcentration/bioaccumulation factors derived from models help predict the environmental behaviors of chemicals. These partitioning coefficients are closely linked to the structural fragments. As a result, many QSPR models for partitioning coefficient predictions are fragment-based, with the widely used EPI Suite^{TM9} being a

notable example. EPI Suite™ is a user-friendly model series that provides estimates of physical/chemical and environmental fate properties, leveraging a database of over 40,000 chemicals. It utilizes SMILES (Simplified Molecular Input Line Entry System) as the sole input and allows quick batch predictions, making it feasible in dealing with large chemical sets⁹.

1.2.2 Density functional theory

Computational chemistry offers a sophisticated and precise range of techniques for studying chemical phenomena. Through computational chemistry, it is possible to predict molecular geometries, total energies, and thermodynamic properties of various chemical species, including reactants, products, intermediates, and transition states. Additionally, computational chemistry allows for the determination of chemical reactivity indicators such as charge distribution and the calculation of properties that can be measured but sometimes with difficulty using analytical and spectroscopic techniques.

The primary tools employed in computational chemistry can be broadly categorized into two main categories: They are both *ab initio* methods, using traditional wave function based quantum chemistry and relatively new density functional theory, respectively. *Ab initio* methods utilize a fundamental approach to calculate properties based on the laws of quantum mechanics without relying on empirical data. These methods provide highly accurate results but are computationally demanding and require substantial computational resources. DFT is a more efficient approach within computational chemistry. DFT approximates the behavior of electrons in a system by considering the electron density instead of individual electron wavefunctions¹⁰. It offers a good balance between accuracy and computational cost, making it widely used for

investigating chemical properties and reactions. DFT has been employed to provide valuable insight into equilibrium energies (both in the presence and absence of solvent models) to estimate partitioning coefficients in Chapter 3.

Conceptual density function theory (CDFT), which is based on that the electron density is "the fundamental quantity for describing atomic and molecular ground states"¹¹ and provides calculation of many chemical concepts. By calculating the energies of molecules in different environments, such as aqueous or non-aqueous solutions, DFT can provide predictions of the partitioning behavior and aid in assessing the environmental fate of chemicals. In the field of computational chemistry, several key concepts are derived from the ionization potential (IP) and electron affinity (EA) values of molecules, as outlined in Chapter 4. The ionization potential is the energy required to remove an electron from a molecule, while the electron affinity is the energy change associated with adding an electron to a neutral molecule. These properties play a crucial role in determining the chemical reactivity and behavior of molecules, as they govern electron transfer processes and the formation of charged species¹².

These concepts derived from IP and EA include hardness (η), softness (σ ; the inverse of hardness), global electronegativity (χ), and electrophilicity index (ω)¹³⁻¹⁶. Molecules with high hardness values are considered "hard" Lewis acids or bases, characterized by strong ionic or covalent interactions¹⁷. Conversely, molecules with low hardness values are considered "soft" acids or bases, showing a preference for more polarizable interactions. These are fundamental components of Pearson's Hard and Soft Acids and Bases (HSAB) theory¹⁷. These descriptors are relevant for understanding chemical reactivity, bonding, and intermolecular interactions and contribute to a deeper

understanding of the properties and behavior of chemicals¹⁸, aiding in the assessment of their environmental fate and potential impacts.

Indeed, the use of DFT descriptors in assessing the environmental fate of chemicals, particularly their potential to be POPs, is still relatively limited in the existing literature^{19–22}. However, the available reports on this subject demonstrate the promising potential of DFT descriptors in estimating a chemical's likelihood of being a POP. To further enhance prediction accuracy and reduce computational requirements, some QSPR models combine fragment-based descriptors with other chemical descriptors. This combination allows for a more comprehensive representation of the chemical's properties and behavior while also optimizing the computational efficiency of the models^{23,24} (also see Chapter 3). By integrating fragment-based QSAR and DFT approaches, these models can serve as effective prescreening tools for identifying potential POPs and guiding decisions related to the manufacturing, usage, and release of chemicals.

Fluorinated chemicals, known for their stable C-F bond, exhibit distinct properties that can significantly impact their environmental behavior. Therefore, it is important to consider the unique characteristics of fluorinated compounds when developing predictive models. By incorporating the specific properties of fluorinated chemicals into the models, reliable predictions regarding the environmental fate of fluorinated compounds can be achieved.

1.2.3 Gas chromatography atmospheric pressure chemical ionization (GC-APCI)

Gas chromatography (GC) is an analytical technique used to separate heat-stable chemicals in the gas phase based on their partitioning with a liquid stationary phase. Samples can be injected as liquids or gases and are vaporized and carried by a mobile

phase (often nitrogen or helium) through a long column containing the stationary phase. Within the column, the analytes are separated based on their partitioning with the stationary phase. The temperature of the column is controlled to optimize the partitioning coefficient and enhance separation.

GC is particularly suitable for the analysis of medium- to non-polar chemicals, such as POPs, or their derivatization products that can be vaporized at relatively low temperatures (up to 300°C). When coupled with MS, GC-MS enables both quantitative and qualitative analysis. Currently, electron ionization (EI) and chemical ionization (CI) are two common interfaces used to couple GC with MS. However, soft atmospheric pressure ionization techniques, such as atmospheric pressure chemical ionization, have demonstrated unique advantages in POPs analysis (refer to Chapter 2). APCI produces fewer fragmentations compared to EI, resulting in higher sensitivity and selectivity. It also facilitates precursor ion selection in tandem mass spectrometry experiments for compound identification.

Figure 1.2(a) illustrates the GC-APCI source, while Figure 1.2(b) depicts the chemical reaction occurring in the positive mode under dry conditions. The chemical reaction is initiated by the electrons generated by a corona discharge needle. In dry ion source conditions, the reaction is followed by ionization of the make-up gas (usually nitrogen), ultimately forming (quasi) molecular ions that retain their structures. In wet ion source conditions, where water is introduced to the system either from the make-up gas or ambient environment, H₂O promotes protonation, leading to the formation of protonated molecular ions in positive mode. In negative ion mode, O²⁻ produced can assist in structure diagnosis²⁵.

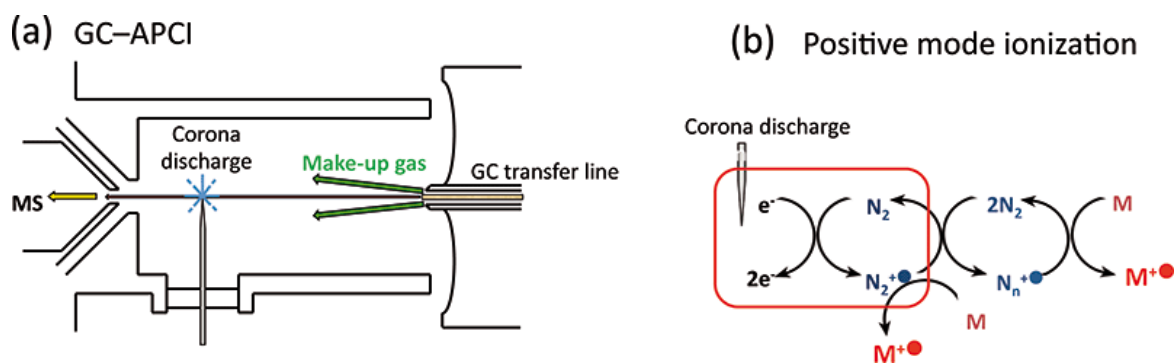


Figure 1.2 (a) The GC atmospheric pressure chemical ion source; (b) general scheme for positive mode ionization in dry ion source²⁵. Reproduced from Jobst *et al.*²⁵ with permission. Copyright @ Springer.

1.2.4 Ion mobility spectrometry mass-spectrometry

The differentiation of isobars and isomers is often crucial in environmental risk assessment, e.g., different structures of tetrachlorodibenzo-p-dioxin (TCDD)²⁶ isomers exhibit different toxicity. Traditional approaches to achieve higher resolution, such as adjusting separation conditions or using high-resolution mass spectrometry, can be laborious and costly, and they may not always provide the desired level of separation. In some cases, the separation is not achievable even with a mass resolution of 1,000,000²⁷. Ion mobility spectrometry combined with mass spectrometry offers a promising solution to overcome these challenges. In this technique, ions are separated based on their mobility in a buffer gas (typically nitrogen or helium) under the influence of an electric field. Ion mobility is influenced by the size, shape, and charge of the ions, allowing for the differentiation of molecules with similar mass-to-charge ratios²⁸.

By coupling ion mobility spectrometry with techniques like liquid chromatography, gas chromatography, capillary electrophoresis, supercritical fluid chromatography, and mass spectrometry, a near-orthogonal separation can be achieved. This means that

compounds can be separated based on their ion mobility in addition to their mass-to-charge ratio, enabling the differentiation of isobars and isomers. As a result, ion mobility coupled with mass spectrometry has demonstrated great potential in non-target screening applications²⁹⁻³².

In the field of IMS, the mobility of ions is typically measured in terms of their drift times and then used to calculate the collision cross section (CCS). In recent years, advancements in data analysis techniques and the combination of IMS-MS have expanded the applications of CCS in the identification of unknown chemicals. IMS-MS has gained significant research attention due to its enhanced identification and characterization for non-target screening in environmental samples^{29,30,33,34}.

IMS instrumentation

Different instrument settings can be employed in IMS-MS experiments to optimize the separation and analysis of unknown chemicals. Three types, *i.e.*, time-dispersive, space-dispersive, and ion confinement with a selective release, of IMS are commercially available in the market³⁵. Linear drift tube IMS (DTIMS) and traveling wave IMS (TWIMS) are categorized as time-dispersive IMS. The space-dispersive IMS includes differential mobility analyzers (DMA) and differential mobility spectrometers (DMS). Confinement and selective release approaches include trapped IMS (TIMS) and cyclic IMS.

1)Time-dispersive IMS

The time-dispersive Ion Mobility IMS instrument generates a time-dependent spectrum wherein all ions traverse a shared trajectory³⁶. The initial commercially available instrument of this kind was the Waters T-WaveTM, employing a traveling wave concept³⁷. This instrument utilizes ion barriers, implemented through voltage

application, to separate ions based on their individual mobilities, akin to surfers navigating ocean waves.

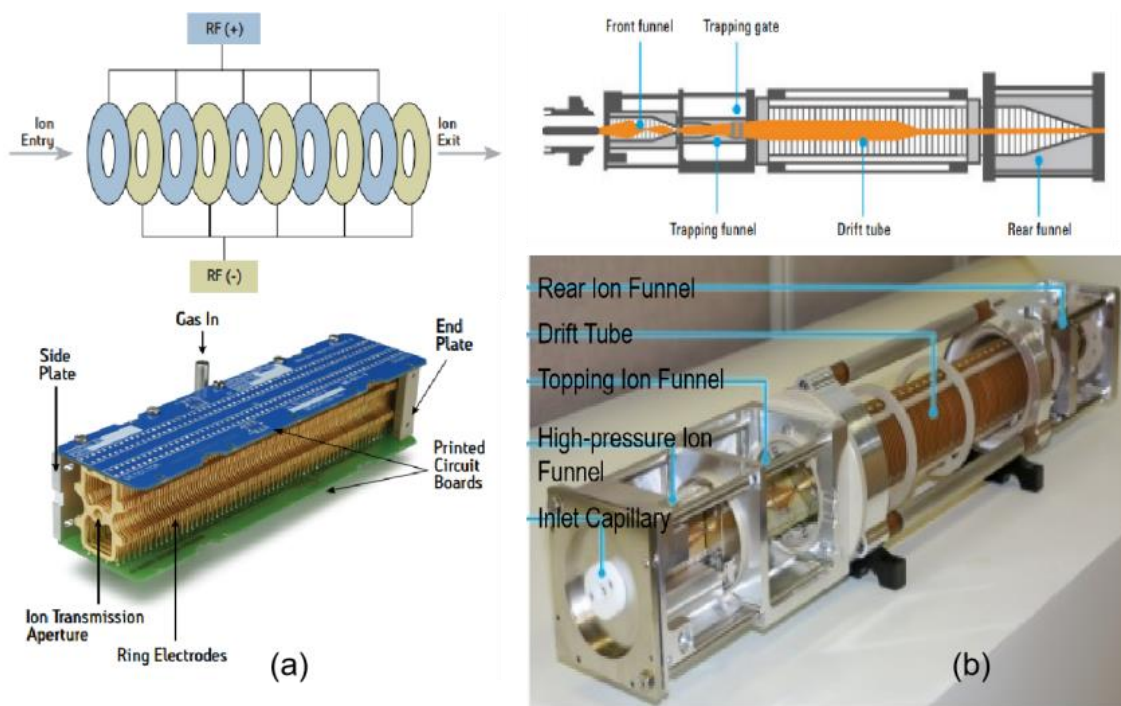


Figure 1.3 (a) Stacked ring ion guide (top) and an actual T-wave collision cell (bottom) of Waters T-wave³⁷; (b) Schematic diagram (top) and real picture (bottom) of the Agilent ion mobility instrument³⁸.

Figure 1.3(a) presents an illustration and actual depiction of a T-wave collision cell. By subjecting ions to a radio frequency (RF) voltage as they traverse a series of stacked rings, the ions are effectively confined, allowing for selective focus and release of the ions of interest. In 2014, Agilent introduced its drift tube IMS instrument (depicted in Figure 1.3(b))³⁸. Within the drift tube, ions traverse while undergoing collisions with the inert gas present. The larger ions with fewer charges, hence possessing greater ion mobility and CCS values, exhibit slower drift compared to smaller ions carrying more

charges. Time-dispersive IMS, commonly combined with a mass spectrometer (typically quadrupole time-of-flight), represents the prevalent IMS configuration.

2) *Space-dispersive IMS*

Space-dispersive ion mobility methods are less common setup compared with the time-dispersive device, and they allow ions to drift along different paths and have no significant separation in time. DMAs can transfer ions with a narrow range of mobility in a fan-shaped trajectory, and when coupled with a mass spectrometer, these ions can be further deconvoluted³⁹. Field asymmetric waveform ion mobility spectrometry (FAIMS), DMS, and differential ion mobility spectrometry (DIMS) are also space-dispersive IMS that can perform analysis under atmospheric pressure³⁵. They share the same mechanism but with different hardware settings. These devices can filter ions by allowing the ions concerned to travel through the drift tube to the mass analyzer by changing the electric field and compensation voltage. Therefore, these IMS devices can remove interferences and thus increase the ultimate method selectivity. Their volumes are small enough to be coupled with existing mass spectrometers easily.³⁵

3) *Ion confinement with selective release IMS*

Ion confinement with selective release IMS is the most advanced IMS technique, in which selected ions (e.g., within specific drift time ranges) are trapped and ejected, producing improved separations.

Trapped ion mobility spectrometry (TIMS) is the first 'true' instrument of this type. It uses a stacked ion trap which provides an opposite field such that the ions are trapped within it, and by scanning the field, ions with different mobility will be selected and analyzed sequentially (shown as Figure 1.4(a))⁴⁰. Since it scans the electric field and allows only ions that have a response to this field to be ejected, the selectivity is greatly

improved. The scan rate can also be slowed for better selectivity. Now, this technique is commercially available by Bruker. Cyclic IMS by Waters (scheme shown in Figure 1.4(b), also see Section 1.2.5 for detail information) is the cyclic TWIMS commercially available⁴². It employs a closed-loop to prolong the ions' travel distance and ion guides that enable injection, ejection, and activation of selected ions with small mobility differences. Each loop traveling along the loop is called one pass. Increasing the number of passes can increase the travel distance and gain better resolving power.

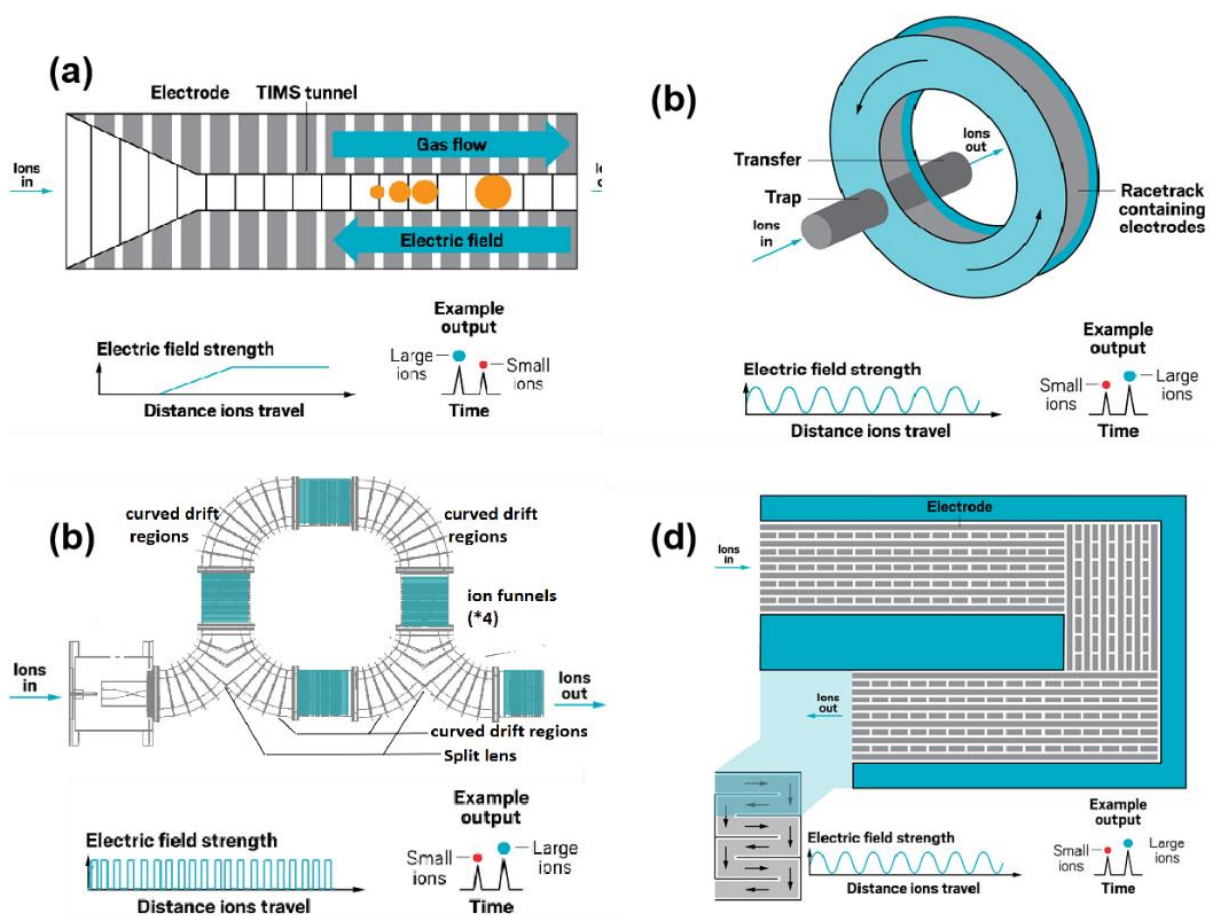


Figure 1.4 Schemes of different ion confinement with selective release IMS. (a) TIMS (b) cIMS (c) cDTIMS (d)SLIM-SUPER IMS. Pictures of (a), (b) and (d) are from⁴⁰; and (c) is reproduced from⁴¹ with permission. Copyright © 2023 American Chemical Society.

This type of experiment is often referred to as multipass experiment. For example, by increasing the number of passes to 16 (Figure 1.5(b)), the TCDD isomers 1,2,3,4- and 2,3,7,8- TCDD which are poorly separated by GC only can be well resolved⁴³.

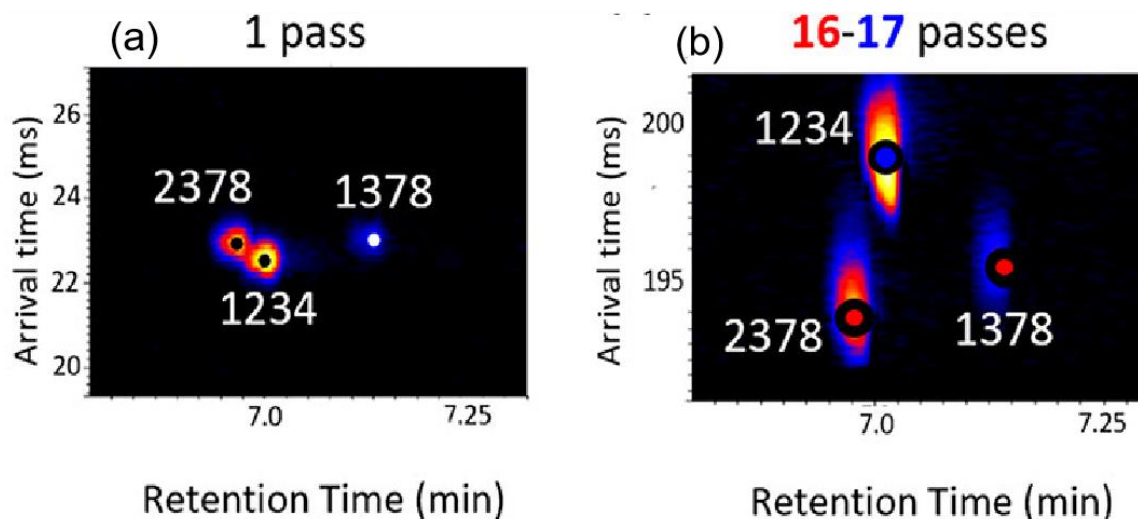


Figure 1.5 Multipass experiment increases the separation of TCDD isomers⁴³. Reproduced with permission. Copyright © 2022, American Chemical Society.

Structures for lossless ion manipulations (SLIM) serpentine ultralong path with extended routing (SUPER) traveling wave (TW) ion mobility (IM) module designed by Deng *et al.*⁴¹ is another set of cTWIMS as shown in Figure 1.4(c). It has a similar drift tube as normal TWIMS but with an ion switch at the end of the drift tube, which can send ions back through the drift tube instead of entering the mass spectrometer. Like cIM, multipass experiments can also be performed using SLIM-SUPER TWIMS platform. The ultra-long route obtained through multiple passes in the serpentine separation enables high resolution capable of separating isotopomers with difference only in the location of heavy isotopes. Another instrument setting, cyclotron IMS⁴⁴ (Figure 1.4(d) is, in fact, a cyclic DTIMS, in which packets of ions accumulated in an

ion funnel are introduced into the cyclic drift tube in a set frequency via an electrostatic gate following the pulse sequence. Each packet of ions is trimmed in the curved drift regions, and the electrostatic gate keeps ions in the drift tube hence increasing the separation power. Cyclic DTIMS was invented before cyclic TWIMS but has not yet been commercialized. Cyclic IMS enlarges the travel distance of ions (cyclic DTIMS) or repeat travel waves (cyclic TWIMS) by allowing ions to cycle within the confining zone; therefore, the resolving power has been greatly improved.

The ion mobility separation happens typically in less than 100 milliseconds (could be n times higher if multipass experiments are conducted); therefore, fast mass analyzers such as time of flight (TOF) is the most common analyzer both DTIMS and TWIMS coupled with e.g., Agilent 6560 Ion Mobility LC/Q-TOF³⁸ and Waters Synapt Series⁴⁵. TOF can also be connected with TIMS (now commercially available as Bruker Daltonics' timsTOFTM⁴⁶) and cyclic IMS (now as Waters cyclic IMS⁴⁵). TIMS experiment can be conducted under different (discrete) ramp rates; therefore, it can also be coupled with slower mass analysis techniques such as Fourier transform ion cyclotron resonance (FTICR)MS⁴⁷. A DTIMS coupled to an orbitrap mass spectrometer has been introduced recently⁴⁸, attracting researchers to explore the possibilities of coupling different types of IMS to all kinds of mass spectrometers.

4) Resolving power

The resolving power in IMS can vary due to the distinct mechanisms employed by different techniques. For instance, TWIMS relies on $CCS/\Delta CCS$, while DTIMS employs $t/\Delta t$ (drift time) to determine resolving power. FAIMS and DMS, on the other hand, use $E_c/\Delta E_c$ (compensation field-based resolving power). Given the prevalence of CCS as a universal measure in ion mobility, it becomes imperative to calibrate or

standardize the various definitions of resolving power to facilitate method comparison and evaluation.

Table 1.1 Resolving power (RP) of different IMS platforms

IMS type	TWIMS	DTIMS	DMAIMS	FAIMS/ DMS/DI MS	TIMS	cDTIMS	cTWIMS	SLIM- SUPER
RP	30~40	50~60	50~60 ⁴⁹	N/A	400-600	>300 ⁴⁴	750 ⁴²	~2000 ⁴¹
Data type	D	C	D	N/A	C	C	C	C

Note: D means 'Direct CCS value', and C means 'calibrated CCS value'. FAIMS/DMS/DIMS works as an ion selector (filter), so they do not provide CCS values.

The CCS value in IMS is not entirely independent of mass. Therefore, when IMS is coupled with MS, the overall resolving power is determined by the combination of the orthogonal factor, IMS resolving power, and MS resolving power. By multiplying these factors together, the overall resolving power of IMS-MS is significantly improved, even with an individual IMS resolving power of 30. The coupling of IMS and MS techniques, along with ion confinement strategies, provides researchers with a valuable tool to overcome the challenges associated with complex sample matrices and the identification of unknown substances.

1.2.5 Gas chromatography cyclic ion mobility mass spectrometer

Gas chromatography coupled with ion mobility spectrometry and mass spectrometry with atmospheric pressure ionization techniques offers unique advantages in the characterization and identification of POPs. In Chapter 5 of our research, we utilized our newly developed platform, GC-cIMS-MS (Figure 1.6), installed at

Memorial University to successfully discover unknown polyfluorinated substances without prior information.

The figure depicts the schematic representation of Waters™ cyclic ion mobility coupled with TOF-MS⁴². In the GC-cIMS-MS setup, following the injection of the sample into the gas chromatograph, the substances (ions) in the analyte sample undergo three consecutive collision-induced dissociation (CID) processes. CID refers to the breaking of chemical bonds or fragmentation that occurs when the gaseous ions collide with neutral gas molecules (e.g., N₂) in the chamber.

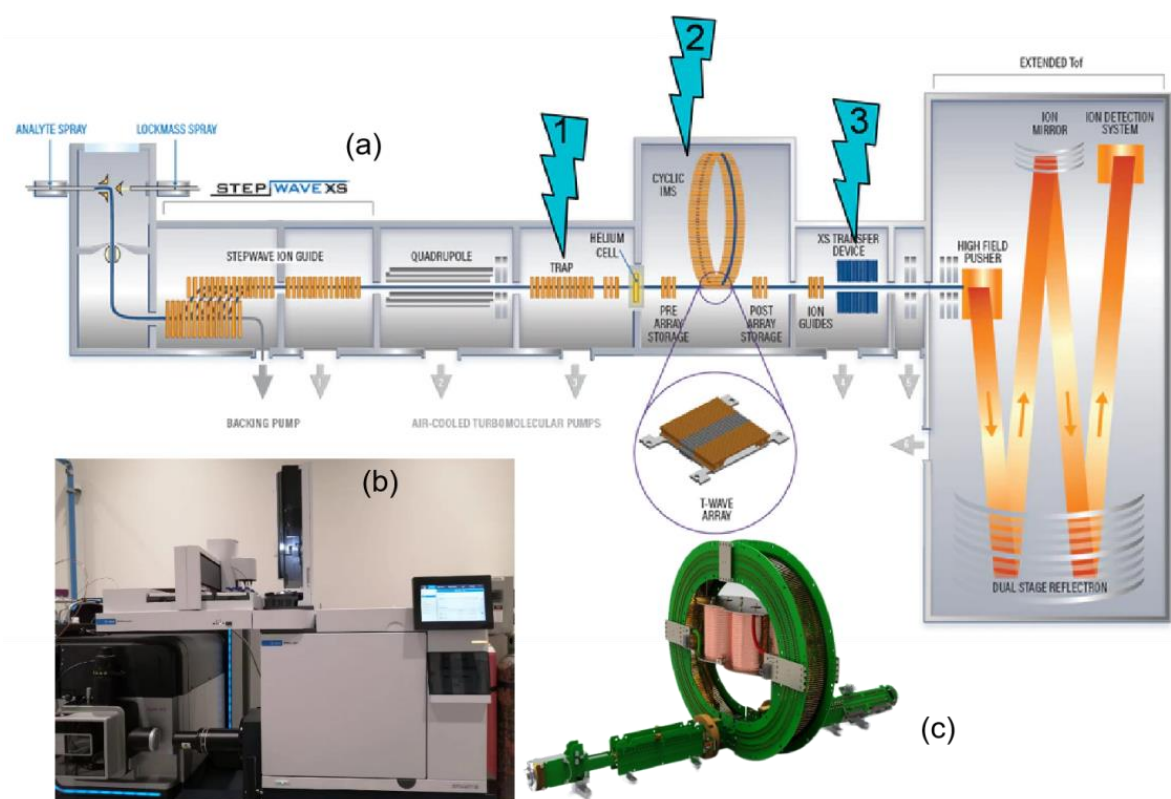


Figure 1.6 (a) Scheme of Waters cyclic ion mobility coupled with time-of-flight mass spectrometry⁴² (b) the GC-cIMS-MS platform used (c) cyclic ion mobility cell. (a) and (c) reproduced with permission. (1) pre ion trap region (2) cyclic ion mobility region (3) post ion transfer. Copyright © 2019 American Chemical Society.

The first collision occurs in the trap region, where pre-ion mobility fragmentation takes place. Subsequently, the analyte ions proceed to the cyclic ion mobility region, where the second collision occurs. Finally, in the transfer region, the ions undergo the third CID process during post-ion mobility collisions. This integrated GC-cIMS-MS approach enables enhanced separation, fragmentation, and identification of POPs. By combining the capabilities of gas chromatography, ion mobility spectrometry, and mass spectrometry, our platform facilitates the comprehensive analysis of complex environmental samples, leading to the discovery and characterization of unknown polyfluorinated substances.

The circular chamber depicted in Figure 1.6(c) allows the ions to travel a lengthened distance through multiple passes and provides precise CCS values. The presence of pre and post-array storage compartments enables the selective retention and guided movement of ions with desired ion mobilities within the chamber. By employing this design, ions that fall outside the targeted range can be ejected without acquisition, ensuring that only the desired ions undergo ion mobility separation. As a result, the mass spectra obtained in targeted analysis exhibit significantly improved clarity. Moreover, the analyte ions can be divided into multiple segments, with one segment undergoing IMS separation within the cyclic tube while the others are stored in the pre-array storage, awaiting their turn for subsequent separation. Additionally, the ions can be stored in the post-array storage and re-injected into the cyclic chamber for further separation if needed. These "trim" strategies often involve multipass experiments, enabling higher-order ion mobility separations (IMSⁿ)⁴². Multipass experiments can also be performed in a non-targeted manner, as discussed in Section 1.3.2, broadening the application of the technique beyond targeted analysis.

1.3 Data analysis technique involved in IMS

1.3.1 Ion-neutral collision cross-section

Mason-Schamp equation^{50,51} (Eq. 1) shows how mobility is related to drift time, where K_0 is the standard ion mobility under standard pressures p_0 (760 Torr) in temperature T_0 (273.15 K), K is the reduced ion mobility under pressure p in temperature T , and N_0 is the buffer gas number density at T_0 and p_0 , L is the drift tube length, t_D is the drift time in the tube, E is the electric field applied to drift tube: $K_0 = K \frac{pT_0}{p_0T} = \frac{v_D p T_0}{E p_0 T} = \frac{L p T_0}{t_D E p_0 T}$ (1), where μ is the reduced mass of the ion-gas interactions, k_B is the Boltzmann constant, z is the absolute value of the ion's nominal charge, and e is the electron's charge.

$$\Omega = \frac{3}{16} \sqrt{\frac{2\pi}{\mu k_B T} \frac{ze}{N_0} \frac{1}{K_0}} = \frac{t_D}{L} \frac{3}{16} \sqrt{\frac{2\pi}{\mu k_B T} \frac{zeE}{N_0} \frac{p_0}{p} \frac{T}{T_0}} \quad (2)$$

In which $\mu = \frac{m_{\text{gas}} m_{\text{ion}}}{m_{\text{gas}} + m_{\text{ion}}}$ (3). Thus, CCS values can be directly generated through calculated (or corrected in ion confinement with selective release IMS) t_D .

However, correction t'_D from observed t_D (or arrival time, t_A) is complicated. In drift tube IMS, the relationship between drift time and Ω seems to be straightforward based on Equation (3): $t_A = t_D + t_0 = \frac{L}{KE} + t_0$ (4), where a transportation time (t_0) for ions to travel from the drift tube to the mass analyzer is considered)⁵². Therefore, $\Omega =$

$$\frac{(t_A - t_0)}{L} \frac{3}{16} \sqrt{\frac{2\pi}{\mu k_B T} \frac{zeE}{N_0} \frac{p_0}{p} \frac{T}{T_0}} \quad (6)$$

Here, t_0 is considered a constant because ions are transferred immediately to the mass analyzer without any further collision. However, collisions that occur after the mobility region are almost inevitable and significant, and will affect t_0 value. In order to construct a more accurate CCS measurement, Marchand *et al.*⁵² proposed including

a t_0 correction term related to the changes in electric field E as voltage difference (ΔV) provided at the entrance and exit of the IMS cell: $E = \frac{\Delta V}{L}$ (7), hence $\Delta V = EL$, therefore $t_A = t_0 + \left(\Omega \frac{\sqrt{\mu}}{Z}\right) \frac{16L^2}{3e} \sqrt{\frac{k_B T}{2\pi}} \frac{NT_0 p}{Tp_0} * \frac{1}{\Delta V}$ (8). This term can be determined using calibrants with known Ω values or derived from step-field experiments.

In TWIMS, t_D is corrected with m/z -dependent flight time: $t'_D = t_D - c \sqrt{\frac{m}{z}}$ (5),

where c is a constant typically between 1.4 and 1.6 and varies slightly from instrument to instrument, and finally, Ω is derived from Equation (2)⁵³. In order to compensate for the difference, TWIMS data analysis usually uses a calibrant ion to correct the arrival time in a given gas, as shown in Equation (6~8). First, the correct drift time is calculated

based on Equation (5), then the correct Ω' using commonly used Ω : $\Omega' = \Omega \frac{\sqrt{\frac{1}{\mu}}}{z} = \frac{\Omega}{z\sqrt{\mu}}$ (6), and plot $\ln \Omega' = X * \ln t'_D + \ln A$ to obtain the values of X and A . Then,

recorrect drift time using: $t''_D = t'_D * \frac{z}{\sqrt{\frac{1}{\mu}}} = t'_D * z\sqrt{\mu}$ (8). Lastly, the equation

derived from re-plotting Ω versus t''_D is used to calculate the Ω value of unknowns. One advantage of DMA is that it provides direct mobility under atmospheric pressure. Still, in the meantime, in order to be comparable with other techniques, the ion mobility needs to be converted back to CCS. Direct CCS determination by DMA-MS is on an empirical basis⁴⁹. It is rare in the non-target analysis, so this review does not cover the CCS calculation procedure involved.

1.3.2 Unwrapping "wrapping around" data in GC-cIMS-MS

In multipass experiments, a phenomenon known as "wrapping around" can occur, wherein slower ions overtake quicker ions⁴³. This can result in the overlapping of ion

information and increased complexity in deciphering the spectra. As a result, cIMS-MS was previously perceived as primarily suitable for targeted analysis.

However, the research conducted by Breen *et al.*⁴³ has demonstrated that a strong linear relationship exists between the number of passes and the arrival time of each ion. Utilizing this relationship, drift times measured in single- and multipass experiments can be used to estimate the number of passes that ions with different retention times will undergo. Figure 1.7 illustrates that the "wrapped" cyclic ion mobility data (a) can be straightforwardly "unwrapped" (b) through this extrapolation method.

As a result, the data obtained using GC-cIMS-MS can be effectively utilized for non-targeted screening applications, overcoming the challenges posed by the "wrapping around" issue and enabling comprehensive analysis of complex mixtures⁴³.

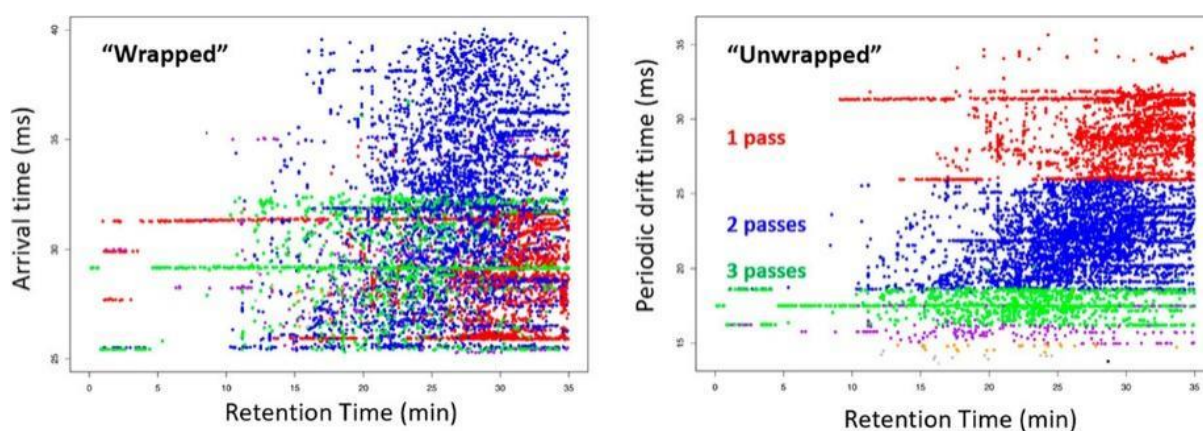


Figure 1.7 Comparison of "wrapping" and "unwrapping" retention time vs. drift time contour plots obtained by GC-cIMS. The horizontal lines bisect populations of ions that travel a different number of passes through the cyclic ion mobility cell⁴³. Reproduced with permission. Copyright © 2022, American Chemical Society.

1.3.3 The potential of CCS in target screening

The terms ^{TW}CCS and ^{DT}CCS are used to refer to the CCS values measured by travel wave and drift time IMS techniques, respectively. $^{TW}CCS_{N_2}$ and $^{DT}CCS_{N_2}$ are commonly used when developing libraries, as nitrogen is the most frequently used drift gas. Hinnenkamp *et al.*⁵⁴ have reported that for most substances (124 in total), $^{TW}CCS_{N_2}$ and $^{DT}CCS_{N_2}$ exhibit a deviation of less than 1%. However, they have also observed a large deviation of up to 6.2% in some chemicals. It is important to note that, similar to molecular mass, CCS is unique to each chemical. The pairing of mass and CCS values can be utilized for the tentative annotation of unknown peaks observed in IMS-MS results, offering a quick and straightforward approach for non-target analysis. This topic will be further discussed in Section 4. Both $^{DT}CCS_{N_2}$ and $^{TW}CCS_{N_2}$ have been reported to possess high reproducibility in interlaboratory evaluations^{55,56}.

However, to fully explore the potential of CCS as a qualification tool, several issues need to be addressed. Firstly, there are relatively large variances among IMS instruments of the same type. For instance, studies have reported a ΔCCS of less than 2% when analyzing mycotoxins using different ^{TW}IMS instruments⁵⁶. Secondly, the discrepancy between $^{DT}CCS_{N_2}$ and $^{TW}CCS_{N_2}$ needs to be resolved due to the different CCS derivation strategies employed. Variances of up to 6.2% have been observed among different IMS instruments⁵⁶. Thirdly, universal CCS libraries that incorporate both $^{DT}CCS_{N_2}$ and $^{TW}CCS_{N_2}$ are necessary for achieving "real" and universal qualification. Currently, a few CCS databases are available, such as ALLCCS⁵⁷, which is primarily based on experimental $^{DT}CCS_{N_2}$ data combined with a small fraction of $^{TW}CCS_{N_2}$. It provides an annotation function where possible formulas and/or structures can be displayed with a confidence level when a mass and CCS value with desired

uncertainty are input. Computational methods for calculating CCS, such as MobCal⁵⁸, based on theoretical principles, are also available and have demonstrated an RMSE of 2.6% in a test set of 162 molecules. These methods can be employed to validate proposed molecule structures.

1.4 Present progress in non-target analysis using IMS-MS

While there are still unresolved issues that need to be addressed for the widespread use of IMS-MS in non-target screening, significant progress has been made by utilizing CCS in conjunction with m/z within results obtained from similar platforms. This approach has led to two main advancements: automated annotation and the discovery of new constituents.

1.4.1 Automated annotation

The direct search against libraries is the most straightforward approach for incorporating CCS values into the annotation framework. Previous studies have shown that for masses up to 500 Da, a high level of confidence in elemental composition determination can be achieved when the mass accuracy reaches around 0.1 mDa⁵⁹. By including CCS values in addition to mass accuracy, the burden on mass accuracy can be significantly reduced. Figure 1.7(a) illustrates that by considering CCS values within $\pm 1\%$ error, the number of possible features for metabolite identification can be reduced by an order of magnitude. Figure 1.7(b) presents a typical workflow that integrates m/z values, CCS values, and MS/MS spectra, resulting in improved confidence in chemical identification.

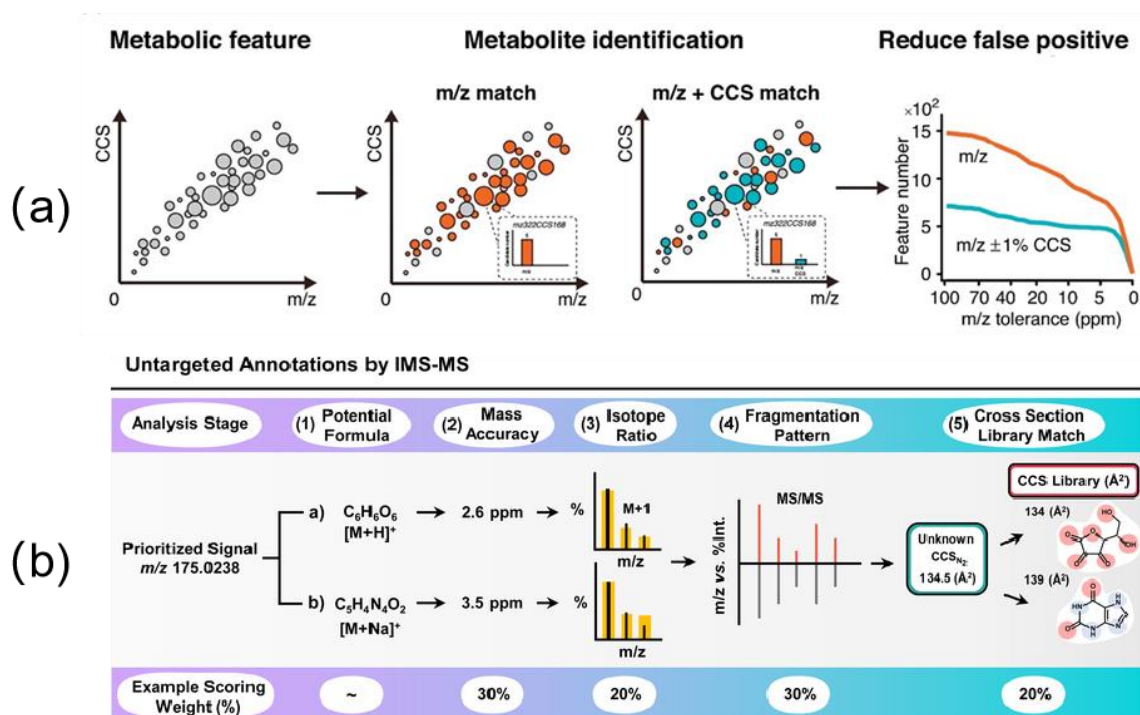


Figure 1.8 CCS as an additional dimension for automated annotation. (a) The CCS value reduces false positives when combined with m/z data; Reproduced with permission from Zhou *et al.*⁶⁰ © 2017 Elsevier Ltd. (b) A typical workflow of untargeted analysis by IMS-MS; cited from Dodds and Baker³⁵ with permission.

However, the impact of CCS value accuracy on reducing the mass resolution requirement is still not well understood. Furthermore, when retention time information provided by liquid chromatography is incorporated, this technique has led to the discovery of unknown metabolites^{57,33,61}, as well as suspected food additives⁶² and contaminants^{63,29} in various sample matrices. This approach has proven effective in identifying unknown compounds and elucidating the presence of potential contaminants or additives in complex samples. Continued research in this area will further refine and expand the capabilities of CCS-based annotation in non-targeted analysis.

1.4.2 CCS and m/z conformation space

Another valuable application of CCS in non-target analysis is the utilization of the multidimensional space formed by m/z and CCS values. CCS has been found to exhibit a significant correlation with m/z, and different chemical groups in the CCS-m/z space tend to occupy distinct trend lines⁶⁴⁻⁶⁶. Figure 1.8 provides examples of the ion mobility (expressed as CCS or drift time/arrival time) and m/z space for various chemical groups. For large molecules such as carbohydrates, peptides, and lipids (depicted in Figure 1.9(a)), their positions cluster in the upper right region of the CCS-m/z space, while small molecules like environmental contaminants (Figure 1.9(c)) predominantly occupy the lower left region due to their high content of halogen atoms.

The regression equation shown in Figure 1.9(e) is a compelling demonstration of the linear relationship observed among small molecules within the same congener group. This relationship suggests that we can utilize it as a screening tool for IMS-MS results to identify potential unknown congeners, as exemplified by the discovery of perfluorinated carboxylic acids (PFCAs) in this case. Similarly, Figure 1.9(d) illustrates the CCS-m/z plotting using 16 polycyclic aromatic hydrocarbons (PAHs) standards, with the red contour plot representing the congener series. By incorporating this approach into the data analysis procedure, fixed distances along both the m/z and CCS axes can aid in elucidating the next possible congeners. This capability proves particularly beneficial in the analysis of pollutants.

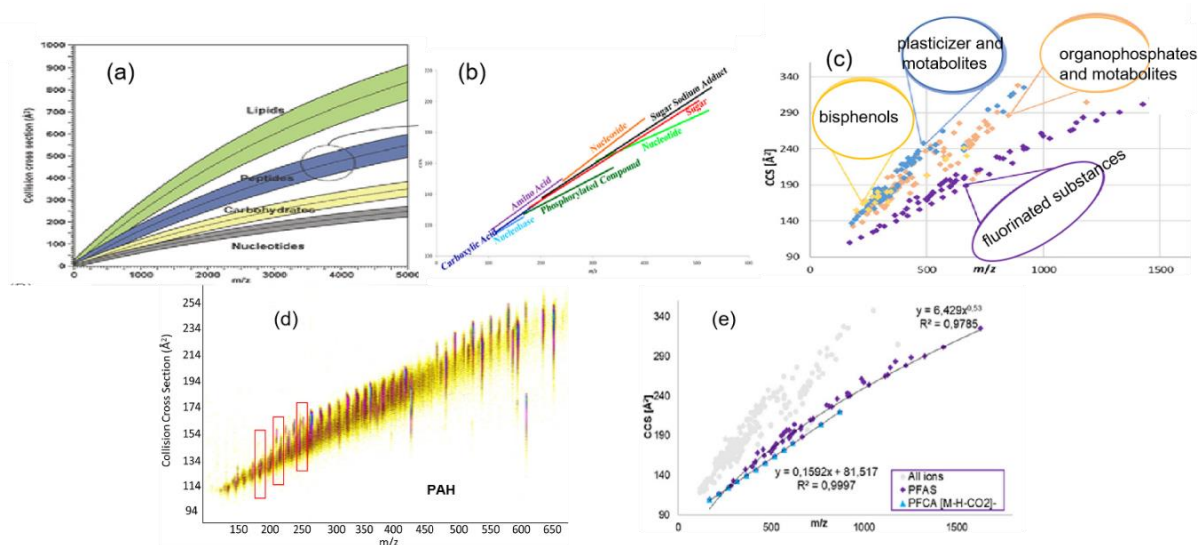


Figure 1.9 Examples of CCS vs. m/z conformation zone. (a) nucleotides, carbohydrates, peptides, and lipids; (b) detailed information below the nucleotides zone shown in (a), cited from⁶⁴; (c) emerging contaminants including bisphenols, plasticizer, and metabolites, organophosphate and metabolites, PFAs⁶⁵; (d) 16 PAHs⁶⁶ (e) PFAs including PFCAs⁶⁵. (c-e) Reproduced with permission. Copyright © 2021, American Chemical Society.

The integration of CCS and m/z information in the analysis process provides additional dimensions to characterize and differentiate chemical species, facilitating the identification of potential congeners and the elucidation of complex sample compositions. The distinct trends observed in the CCS- m/z space for different chemical groups offer valuable insights and contribute to the advancement of non-targeted analysis techniques.

In recent years, significant progress has been made in the field of ion mobility spectrometry coupled with mass spectrometry, with various instrument setups and accessible data analysis techniques available^{41,42,46} (as discussed in Section 2). The integration of IMS with MS has provided enhanced separation capabilities and has

shown great potential in non-target analysis. However, there are still several important questions that need to be addressed for the widespread application of IMS-MS (as discussed in Section 3.2). These questions pertain to issues such as instrument variability, calibration and unification of resolving power definitions, and the establishment of universal CCS libraries. By resolving these challenges, IMS-MS can be further advanced and make significant contributions to the identification and characterization of unknown compounds in various research areas.

1.5 Aims of this research

The primary objectives of this work include 1) to construct predictive models for the environmental behavior of chemicals, with a particular emphasis on fluorinated chemicals leveraging DFT descriptors, QSPR models, and fragment-based QSAR approaches. These models will provide valuable insights into the fate, transport, and potential impacts of these substances in the environment. By understanding their behavior, we can better assess their risks and inform regulatory decisions; 2) to devise innovative strategies for the identification of unknown fluorinated pollutants in environmental samples using our new GC-APCI-cIMS-MS platform. The presence of these unidentified pollutants poses challenges for environmental monitoring and risk assessment. Through the development of new approaches and methodologies, we aim to enhance our ability to detect and characterize these substances, ultimately improving our understanding of their sources, distribution, and potential environmental implications.

Chapter 2

Nontargeted screening using gas chromatography-atmospheric pressure ionization mass spectrometry: Recent trends and emerging potential*

Adapted with permission from Xiaolei, L., Frank, L. D., Paul, A. H., Sonya, K., André, J. S., Myrna, J. S., Karl, J. J. (2021). Nontargeted Screening Using Gas Chromatography–Atmospheric Pressure Ionization Mass Spectrometry: Recent Trends and Emerging Potential. *Molecules*, 26(22): 6911. Copyright 2021 MDPI.

2.1 Introduction

Chemistry is essential to the modern world, producing molecules and materials required in all facets of society. Tens of thousands of chemical substances, representing millions of individual chemical compounds, have now been introduced to the global market, and this number is increasing⁶⁷. Since 1982, the number of substances registered in the U.S. Toxic Substances Control Act Chemical Substance Inventory (TSCA), has grown from 62,000 to over 86,557⁶⁸. According to the United Nations Global Chemicals Outlook⁶⁹, the total volume of chemicals is expected to increase at a rate that outpaces population growth over the next decade. Concerns that some of these chemicals can persist in the environment, bioaccumulate and adversely impact human health have led to international efforts to restrict the (un)intentional release of twenty-eight groups of hazardous chemicals, coined persistent organic pollutants (POPs)⁷⁰. However, the number of unregulated POPs may be much larger: A recent evaluation of substances compiled in the TSCA and other national chemical inventories has resulted in a list of 3421 chemical substances that may be persistent and bioaccumulative, and have so far evaded detection in the environment. The identification of unknown pollutants, most appropriately using mass spectrometry, is the critical first step to evaluating their potential harm to the environment, establishing policies and guidelines to limit exposure, and preventing global contamination. Such experiments have been coined non-targeted screening (NTS)⁷¹.

Gas chromatography- and liquid chromatography-high resolution mass spectrometry (GC-HRMS and LC-HRMS) are powerful, complementary techniques for NTS of persistent and bioaccumulative organic pollutants. The need for both techniques is underlined by the results of a recent interlaboratory study led by Rostkowski *et al.*^{72,73}.

The analysis of an indoor dust sample by over twenty different laboratories using both GC-HRMS and LC-HRMS, resulted in the tentative identification of 2350 compounds. Of these compounds, approximately half were identified by GC-HRMS and only 5% of the compounds were detected using both GC and LC. This is because the compounds amenable to GC or LC separation often have different volatility, polarity and ionization behavior. While LC-HRMS has attracted more recent attention, comprehensive NTS of environmental samples cannot be performed without GC-MS.

Most GC-MS instruments employ electron ionization (EI), which produces highly reproducible, structure-diagnostic mass spectra of organic pollutants whose identities can be established by searching databases of experimental EI spectra such as the NIST Mass Spectral Library⁷⁴. However, extensive fragmentation under EI conditions can also produce mass spectra in which the molecular ion is absent, thereby confounding elemental composition determination and structure elucidation. This drawback can potentially be solved by lowering the electron energy in EI or using other vacuum ionization techniques such as chemical ionization (CI)⁷⁵, photoionization (PI)⁷⁶ and field ionization (FI)⁷⁷, which impart significantly less energy to the analyte molecules. The past thirty years have also witnessed the advent of atmospheric pressure ionization techniques and (hybrid) mass analyzers, whose development was primarily driven by the need for LC-MS and direct analysis applications. An unintended consequence is that the concept of performing aGC-MS on an LC-MS instrument⁷⁸ has attracted renewed interest. GC and comprehensive two-dimensional gas chromatography (GC×GC) have recently been hyphenated with a variety of atmospheric pressure ionization sources, including atmospheric pressure chemical ionization (APCI)⁷⁹, atmospheric pressure photoionization (APPI)⁸⁰, atmospheric pressure laser ionization

(APLI)⁸¹ and electrospray ionization (ESI)⁸². Ionization at elevated pressures offers a number of advantages. Collisional cooling can often minimize fragmentation and increase the yield of (quasi)molecular ions⁸³. The resulting detection limits can be approximately 10~100 times lower than conventional GC-MS experiments⁸⁴. Modifying an LC-MS instrument to perform GC-MS may also reduce costs by minimizing the number of specialized instruments required for analysis. The most attractive benefit however may be the fact that GC-API can be adapted to mass analyzers⁸⁵ and ion mobility-mass spectrometers⁸⁶, resulting in novel configurations that could potentially better tackle complex (environmental) mixtures. GC-APCI has been successfully applied to complex mixtures, such as phenolic compounds in olive oil⁸⁷, metabolites of avocados⁸⁸, and fatty acids in fish⁸⁹, exhaled volatile organic compounds⁹⁰, and steroid hormone profiles in human breast adipose tissue⁹¹.

In this review, we summarize the recent developments and applications of GC-API reported during the last five years, using SciFinder with the keywords ‘GC-APCI’, ‘APGC’, ‘GC-APPI’, ‘GC-APLI’ or ‘GC-ESI’. The ion source designs, geometries and ionization mechanisms have been reviewed elsewhere^{84,92}. Our contribution will instead focus on the application of various GC-API techniques to identify unknown pollutants, as well as the computational techniques being developed to predict mass spectra, and aid in the interpretation of NTS data.

Table 2.1 Recent studies that employ GC-API-MS techniques for (non)targeted analysis of environmental pollutants.

	Sample	Detector	(Non)Targeted chemicals	Method Merits	Ref.
APCI	Food packaging materials	QTOF, HP-5MS	Acrylic adhesives NTS: 2-methyl-1,2-thiazol-3(2H)-one, 5-chloro-2-methyl-1,2-thiazol-3(2H)-one and 1,2-benzothiazol-3(2H)-one		93
APCI	Polyurethane foam disks (PUFs), food, and marine samples	Xevo TQ-S QQQ	Hexabromocyclododecane	IDL: 0.10 pg/ μ L RSD:<7%	94
APCI	Surface water, groundwater, wastewater		Pesticides, polycyclic aromatic hydrocarbons (PAHs), PCBs, PBDEs, fragrances, musks, antimicrobials, insect repellents, UV filters, polychloronaphthalenes (PCNs)		95
APCI	Indoor air sample	QTOF, HP-1-MS			96
APCI	Chinese mitten crab food webs	Xevo TQ-XS QQQ, DB-5MS	PCBs (mono-to deca-) and PCDD/Fs	RSD: PCBs: 3.4%-15.5%; PCDD/Fs: 1.7%-7.9% LOD: PCBs: 0.021-0.150 pg/mL; PCDD/Fs: 0.051-0.237 pg/mL	97
APCI	Standard Reference Material (SRM 2585) of household dust	QTOF	191 POPs including PCBs and agricultural drug residues, such as chlordane and degradation products of DDT and Fentichlor, polychlorinated and polybrominated diphenyl ethers (PCDEs and		5

Sample	Detector	(Non)Targeted chemicals	Method Merits	Ref.
APCI	Electronic waste dust	Q-TOF DB5-HT	PBDEs), other brominated flame retardants such as tetrabromobisphenol A (TBBPA) and bis(2-ethylhexyl) tetrabromophthalate (BEHTBP), chlorine-containing organophosphate flame retardants tris(1,3-dichloro-2-propyl)phosphate (2 isomers), tris(2-chloroisopropyl)phosphate and tris(2-chloroethyl)phosphate. 52 brominated, chlorinated, and organophosphorus compounds identified by suspect screening; 15 unique elemental compositions identified using NTS with 17 chemicals confirmed using standards	85
APCI	Low sulfonate lignin	Q-TOF TOF	59 lignin pyrolysis products were positively identified, with 10 chemicals confirmed using standards	98
APCI	Urine Blood	QTOF DB- 5MS	Illicit psychostimulant drugs	99,100
APGC	Low-temperature coal tar sample and its distillation products	TQ-S DB-35 MS	Phenolic compounds (phenols, indanols, naphthols, and benzenediols)	101
APGC	Human serums	Xevo TQ-S	Organochlorine pesticides (OCPs) and PCBs	RSD: <15% 102
APCI	Urine samples	QTOF	α -pyrrolidinovalerophenone metabolites	103
APGC	Food	FT-ICR, Rtx-	Halogenated flame retardants (HFRs)	Recovery: 59-115%; RSD: 5-15%; 104

	Sample	Detector	(Non)Targeted chemicals	Method Merits	Ref.
APCI	Urine	1614 QQQ, HP Ultra 1	Exogenous androgenic anabolic steroids	IQL: 1-5 pg/g; MQL: 0.002-0.04 ng/g RSD: 15-25%	105
APGC	Seal and egg samples	Xevo TQ-S QQQ, Rtx - 1614	Polybrominated diphenyl ethers (PBDEs), their methoxylated derivatives (MeO-PBDEs) and other emerging (brominated flame retardants) BFRs	Most LOD: below 0.5 ng/ mL RSD: <1. IDL: emerging BFRs, BDE 209 and MeO-PBDEs mixtures: 0.075–0.1 pg/μL; Br1–9 PBDEs mixtures: 0.625–6.25pg/μL	106
APGC	Air fine particulate matter (PM 2.5)	Xevo TQ-S QQQ	Nitro-polyaromatic hydrocarbons	IDL: (0.20-2.18 pg/ mL MDL: 0.001-0.015 pg/m ³ ; Recovery: 70%-120%	107
APGC	Urine samples	Xevo G2-XS QTOF, DB- 17+ custom MXT	1-Hydroxypyrene, hydroxyphenanthrene, hydroxyfluorene	3- 1-Hydroxypyrene LOD: 0.64 ng/L, 9- LOQ 2.16 ng/L; average CV: 11.5%	108
APGC	Simulated burn study samples (household and electronics), Particulate matter coating the firefighter's helmets	Xevo TQ-S, Rtx Dioxin-2	Polyhalogenated dibenzo-p-dioxins and dibenzofurans (PXDD/Fs and PBDD/Fs)	total levels of each halogenated homologue group: parts per billion	109
APGC	Fish, dust	Xevo TQ-S, Rtx Dioxin-2		Soil: MDL: 0.15-1.4 pg/g, RSD<11% Fish: 0.21-2.0 pg/g, RSD<33% S/N: 753 for 40fg on column Average RSD:9.8%	110
APGC	Food and feed	Orbitrap, DB- 5MS	Polychlorinated dioxins and polychlorinated biphenyls		111
APCI	Dust	Xevo G2-XS qTOF, DB-5 HT	40 PBDEs and 25 emerging HFRs	LOD: HFRs: 0.65 (0.016–9.1) pg/ μL; PBDE: 0.17 (0.0123–2.5) pg μL	112

	Sample	Detector	(Non)Targeted chemicals	Method Merits	Ref.
APPI	Drug solutions	HR-LTQ Orbitrap, SLB-5 ms	Pesticide (triazines and organophosphorus), PAH, Drugs (diazepam and methadone)	Pesticide: average 3 pg/mL PAH: 0.1 pg/mL Drugs: average 30 pg/mL	113
APPI	Derivatization	oaTOF	Amines, alcohols, carboxylic acids	LOD: pmol~attmol	114
APPI	River water, tap water	HRMS (Q-Orbitrap)	FTOs, FTOHs, FOSAs and FOSEs (fluorotelomer olefins (FTOs), fluorotelomer alcohols (FTOHs), fluorooctanesulfonamides (FOSAs) and sulfonamidoethanols (FOSEs))	LOD: 0.02-15 ng/L; RSD% < 11, RE% < 12	115
APPI	Fruit and vegetable samples	QTOF	416 pesticides		116
APLI	Human urine	TOF, DB-35	<i>Trans-anti</i> -benzo[<i>a</i>]pyrene-tetraol (BaP-tetraol) (PAH biomarker)	IOD of 0.5 fg	117
APLI	Rocks	HR TOF, RXI-PAH	Triaromatic steroids	LOD: retene: 25 fg on column	118
APLI	Coastal and harbor water	HR TOF, RXI-PAH	48 PAHs (alkylated PAHs in suspected target analysis)	Recovery rate: 60.7% to 157.0%, mean 92.1%	119
APLI	Reference materials (urban dust, organics in marine sediment, fresh water harbor sediment, and contaminated soil from a former gas plant site) and environment samples (bituminous coal, suspended particulate matter from river and pine needles)	HR TOF, RXI-PAH	59 PAHs	Recovery: 34% ~102%, median, 80% mean 78% LODs: 5~50 fg/μL	120

	Sample	Detector	(Non)Targeted chemicals	Method Merits	Ref.
ESI	Human urine	LTQ Orbitrap	Trimethylsilyl (TMS) derivatives of	LOD 0.5-10 ng/mL	121
ESI	Soil	QQQ Ultra-1 QQQ, DB- EUPAH	steroids PAHs	LOD 0.002-10 µg/mL	122

LOD: limit of detection. MD(Q)L: method detection(qualification) limit. ID(Q)L: instrument detection(qualification) limit. CV: coefficient of variance.

2.2 Gas chromatography-atmospheric pressure ionization techniques

Gas chromatography-atmospheric pressure chemical ionization (GC-APCI) was first developed in the 1970s⁷⁹. It saw only limited usage until McEwan & McKay¹²³ and Schiewek *et al.*¹²⁴ adapted the approach to commercially available LC-MS instruments in the early 2000s. The ensuing years witnessed the development of various GC-API ion sources adapted from LC-MS applications. Atmospheric pressure photoionization (APPI), first developed by Robb *et al.*¹²⁵ and Syage *et al.*¹²⁶ as an LC-MS ion source, was later adapted by Revelsky *et al.*⁸⁰ for GC-MS. Schiewek *et al.*⁸¹ developed an atmospheric pressure laser ionization (APLI) source for GC-MS in 2007 and Brenner *et al.*⁸² were the first to employ an electrospray ionization (ESI) emitter to promote ionization of GC effluent. In 2005¹²⁷, Cody introduced Direct Analysis in Real Time (DART), a technique that makes use of Penning ionization, wherein a molecule is ionized through collision with an electronically excited (metastable) atom. In 2008, the DART ion source was first hyphenated with GC¹²⁸, although a similar technique called metastable atom bombardment (MAB) had been developed as a vacuum ion source almost a decade earlier¹²⁹. Dielectric barrier discharge (DBD) ionization is the most recent innovation in GC-MS ion source development¹³⁰. DBD ionization occurs in a low temperature plasma and this approach has been developed in parallel for LC, GC and direct analysis modes of operation. The ion source designs, geometries, and mechanisms of various GC-API techniques have been reviewed elsewhere^{92,76,131}. In the following sections, the techniques are briefly summarized and their advantages and limitations are discussed in light of the results of recent publications that are summarized in Table 1.1.

2.2.1 Atmospheric pressure chemical ionization (APCI)

Ionization under APCI conditions is a seemingly straightforward process. When GC effluent exits the column, a high flow of make-up gas from the transfer line sweeps the GC effluent towards the corona discharge. A plasma consisting of primary ions (e.g., $\text{N}_2^{+\bullet}$ and $\text{N}_4^{+\bullet}$ when using N_2 as the make-up gas) and electrons is generated. Analyte molecules (M) may undergo charge exchange with the primary ions if the adiabatic recombination energy (RE_a) of the primary ions exceeds the ionization energy (IE_a) of M. In the same vein, the formation of radical anions ($\text{M}^{\bullet-}$) will also occur if the electron affinity (EA) of M is sufficiently high. Internal energy in the incipient ions is quickly dissipated by non-reactive collisions with the surrounding make-up gas, thus minimizing fragmentation. This process also depends on the nature of the reagent gas and the presence of other compounds or ions that may be added as dopants.

Nitrogen is the most common reagent gas used in GC-APCI. This is partly because it is conveniently and inexpensively produced (usually by purification of compressed air) at a rate that is necessary for operation of most API ion sources. Although nebulization and desolvation of liquid droplets is not a concern in GC-API, a relatively high volume of nitrogen is still consumed as a skimmer or curtain gas around the orifice of the mass spectrometer to impede neutrals from entering. The ionization energy of N_2 ($\text{IE}=15.6$ eV) also exceeds that of most organic molecules, making N_2 ideal for the analysis of a wide range of compounds as is often required for NTS. In some cases, it may be desirable to select a gas with an ionization energy that lies above that of the analyte, and below that of potential interferents. However, in practice, the high consumption of gases by most API sources discourages the use of alternative gases that are more expensive than nitrogen.

Efforts to control the introduction of reagent gases and dopants have mostly been restricted to placing a small vial containing a volatile liquid into the ion source, sometimes with a short piece of capillary tube inserted in the vial's septum to restrict the flow. For example, when H₂O or other protic solvents (S) are introduced to the ion source, they may undergo charge exchange to form (H₂O^{•+} or S^{•+}), and subsequently self-protonate to form H₃O⁺ or SH⁺ according to the general reaction: S^{•+} + S → [S-H]^{•+} + SH⁺. The protonated solvent molecule SH⁺ may then transfer its proton to an analyte molecule to form [M+H]⁺ if the proton affinity of M exceeds that of S. Promoting the formation of [M+H]⁺ ions by protonation instead of charge exchange may be desirable in cases where the compounds of interest have relatively high proton affinities compared to their potential interferents. Schreckenbach *et al.* used this approach to confirm the identity of the molecular ion of a previously unknown chlorinated amide⁸⁵. However, the unintentional or uncontrolled introduction of H₂O (e.g., from laboratory air humidity) can be a nuisance, especially if the compound of interest has a low PA and thus can be suppressed under those conditions.

In the negative mode, M can form M^{•-} radical anions through electron capture negative ionization. The presence of low concentrations of oxygen (<1%) may also result in displacement reactions between M and O₂^{•-} to form ions [M-X+O]^{•-} (where X=H, Cl, Br)⁹². The negative mode is especially important for the identification of halogenated POPs due to their high electron affinities. Reactions with O₂^{•-} have also been shown to be structure-diagnostic, and this will be discussed in Section 3.4. It is also possible to generate Cl⁻ adducts by placing a vial of chloroform in the ion source, and this reaction appears to be selective towards polyhalogenated alkanes¹³².

As the most popular GC-API technique, a number of publications have recently appeared that demonstrate its advantages over EI or CI. Analysis of hydroxypyrene (a PAH metabolite in human urine) using GC-APCI showed lower detection limits and a wider linear range than LC-MS/MS¹⁰⁸. In the same vein, GC-APCI analysis resulted in >10-fold lower method detection limits (MDLs) for halogenated dioxins and furans in sediments, fish and fire debris as well as 9-nitrophenanthrene and 3-nitrophenanthrene in PM 2.5, as compared to using EI. GC-API techniques may also enable faster analysis. Unlike vacuum ion sources, API is inherently resilient to high flows of both nitrogen and helium carrier gases. For example, Di Lorenzo *et al.* demonstrated that polybrominated diphenylethers (PBDEs) could be separated in less than 7 minutes and 15 minutes, respectively, with helium and nitrogen¹³³ carrier gas. Critical isomers could be separated using nitrogen, which is desirable in the face of looming shortages of helium, a non-renewable resource. A drawback of GC-APCI is increased ion suppression compared to EI. NTS practitioners should be cautious when using APCI to analyze compounds with a wide range of ionization energies. While preserving the sample information is a benefit, interfering matrix could obfuscate unknown pollutants.

2.2.2 Atmospheric pressure photoionization

APPI employs UV light from a Xe, Kr, or Ar lamp, to produce 8.4 eV, 10.1 eV and 11.2 eV photons, respectively, for ionization. A Kr lamp is commonly used because its longevity exceeds that of an Ar lamp, while also providing energetic photons that are capable of ionizing a wider range of compounds than a Xe lamp. The formation of positive ions M^{+} will occur if the energy of the impinging photon exceeds the ionization energy of M, and akin to APCI, negative ions can form by electron attachment or through reactions with $O_2^{\bullet-}$.

Introduction of a suitable dopant (e.g., toluene, acetone, anisole, and chlorobenzene, etc.) whose IE is smaller than the photon energy can promote protonation and/or adduct formation with the analyte and significantly enhance ionization efficiency^{98,134} and broaden the range of chemicals subject to APPI ionization. For example, neutral perfluoroalkyl and polyfluoroalkyl substances¹¹⁵ cannot be directly photoionized into M^{*+} . Instead, negative ions, including adducts with oxygen, were generated with the assistance of a dopant. In this case, the direct ionization of the dopant (D) results in the formation of D^{*+} radical cations, as well as free electrons that can promote negative ionization.

APPI is a more convenient way of selectively ionizing compounds using different photon energies compared to charge exchange reactions with different gases in APCI. For example, it is desirable in some cases to exclude the ionization of H_2O , which drives the formation of $[M+H]^+$ rather than M^{*+} radical cations by charge exchange. Figure 1a shows the partial mass spectra of PBDE-209 and its $^{13}C_{12}$ -labelled analogue obtained under both APPI (top) and APCI (bottom) conditions. Since H_2O cannot be ionized by 10 eV photons, no subsequent protonation occurs and only M^{*+} ions are observed in the APPI spectrum. In contrast, APCI results in a mixture of M^{*+} and $[M+H]^+$ ions, increasing the complexity of the mass spectrum. This contrast is more evident for 1,8-dibromo-2,6-dichloro-9H-carbazole (Figure 2.1 (b)), which belongs to an emerging class of POPs believed to occur as by-products of halogenated indigo dyes¹³³. $[M+H]^+$ ions dominate the APCI spectrum because the presence of nitrogen increases the PA, but the APPI experiments produce M^{*+} ions only. The ability to control the types of (quasi)molecular ions that are generated is an advantage of APPI because (i) the complexity of the mass spectra is reduced; and (ii)

ionization efficiency for a wide range of POPs is more uniform while also excluding potential interfering compounds whose IEs exceed 10 eV.

Excluding the ionization of compounds whose IEs exceed the photon energy of the lamp can also be a drawback. Obviously, the number of compounds that can be identified in such an experiment will decrease, and the use of dopants can also have the same effect. For example, a comprehensive comparison between APPI with and without dopants was performed for 75 EPA priority environmental pollutants. The study showed that the use of dopants increased the ionization efficiency for many compounds, but ultimately decreased the number of compounds detected.¹³⁴

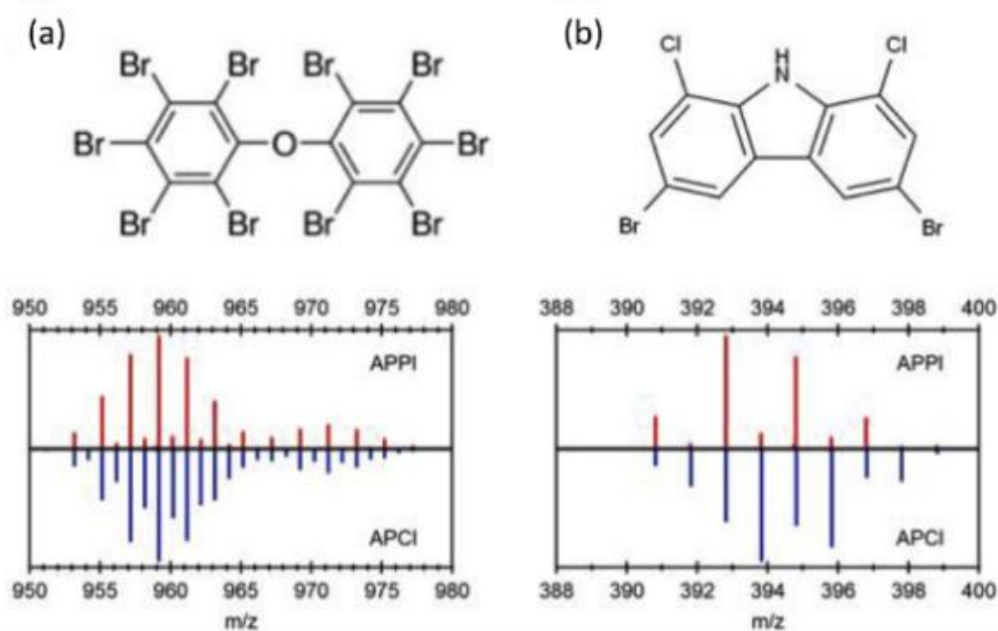


Figure 2.1 Partial mass spectra obtained using GC-APPI (top) and GC-APCI (bottom) for (a) decabromo-diphenylether (BDE-209) and its ¹³C-labelled counterpart, and (b) 1,8-dibromo-2,6-dichloro-9H-carbazole. Reprinted from Di Lorenzo *et al.*¹³³, Copyright 2019, with permission from Elsevier.

2.2.3 Atmospheric pressure Laser ionization (APLI)

APLI is similar to resonance-enhanced multiphoton ionization (REMPI)⁹², wherein two absorption steps are involved in ionization. The absorption of the first photon results in the formation of an excited molecule M^* , which is subsequently ionized by a second photon to form M^+ . This process is favorable if (i) the combined energies of the photons are resonant with the energy required for excitation and ionization; and (ii) the excited state M^* is sufficiently long-lived to absorb a second photon. These two requirements are usually satisfied by π -electron-rich compounds¹³⁵ and most applications of APLI have focused on PAH and other aromatics (see Table 2.1). The high sensitivity of this technique allows sample dilution of up to 1000-fold, resulting in significantly decreased matrix interference, better separation and improved peak shape¹²⁰. To expand the range of compounds that can be analyzed by APLI, Eduard *et al.*¹¹⁴ introduced a series of APLI ionization labels to derivatize amines, alcohols and carboxylic acids. A recent comparison between APPI and APLI revealed that APPI was able to ionize the widest range of analytes (66/77) and halogenated aromatics were much more readily ionized by APPI than by APLI¹³⁴.

2.2.4 Electrospray ionization (ESI)

ESI involves the creation of ions from charged droplets. In LC-MS, the column effluent is delivered through a charged capillary. Gas phase ions are produced as the solvent molecules are stripped away with the aid of a flow nitrogen. ESI produces a wide range of ions that originate from the solvent itself, including protonated molecules and dimers, (sodium and potassium) cationized adducts and cluster ions. In the negative ion mode, ESI produces deprotonated molecules, as well as adducts and clusters bridged by common anions present in the solvent or mobile phase, such as Cl^- or formate. The electrosprayed

droplets ions can also serve as vehicles for protons and other reagent ions that may ionize solid, liquid or gaseous samples. For example, in desorption electrospray ionization (DESI), charged droplets are directed towards a solid, extracting molecules from the surface while transferring charge from the ionized solvent to the analyte. At the same time, the droplet bounces from the surface, propelling the analyte ions towards the entrance to the MS for analysis. Similarly, in extractive electrospray ionization (EESI) the charged droplets collide with and ionize a secondary aerosol spray. In principle the same approach could be used to ionize gaseous molecules exiting a GC column, but to date, GC-ESI has only been attempted by one group^{121,122}. The results of Cha *et al.*¹²¹ showed that GC-ESI could achieve linearity, repeatability, robustness and detection limits that are comparable to standard GC-MS and LC-MS methods. Even non-polar PAHs could be ionized by GC-ESI, and protonated molecules $[M+H]^+$ dominated their mass spectra. GC-ESI is a relatively unexplored means of introducing reagent ions, such as metal cations and anions¹³⁶, that would not be possible using GC-APCI. Whether such ion chemistry will be useful for structure elucidation is a question that deserves more attention.

2.2.5 Penning ionization (PI)

Direct analysis in real-time (DART) was first introduced by Cody and Laramée^{127,137}. Penning ionization is initiated by glow discharge of a gas (commonly helium) resulting in neutral atoms in a metastable excited-state. The internal energy of metastable helium (19.8 eV) exceeds the ionization energies of most common atmospheric gases. While Penning ionization may result in the formation of radical cations M^+ , water from the ambient environment will also ionize, self-protonate and form cluster ions. Akin to APCI, the formation of protonated molecules $[M+H]^+$ will occur when M has a higher PA than H₂O

and its cluster ions. In the vast majority of applications, DART is directly coupled with a mass spectrometer¹²⁷. Penning ionization has also been employed for ionization of GC effluent by Moore *et al.*¹³⁸ and later by Cody *et al.*¹²⁷. In general, the appearance of mass spectra obtained by GC-DART are similar to those obtained by GC-APCI.

2.2.6 Dielectric barrier discharge ionization (DBDI)

The ionization process is initiated by a dielectric barrier discharge (DBD), which involves the creation of a cold plasma (~30°C) that is ignited when a potential is applied between two electrodes separated by a dielectric material. It was first introduced as a GC-MS ion source by Nørgaard and coworkers in 2013¹³⁹. Similar to DART, LTP also produces M^{+} and $[M+H]^{+}$ ions in the positive mode, and $[M-H]^{-}$ and M^{-} ions in the negative mode. As a proof of concept, Nørgaard *et al.* demonstrated that 20 common indoor VOCs, including alkanes, alkenes, alcohols, aromatic compounds, aldehydes, PAHs, phenols, and terpene alcohols, could be detected using this approach¹³⁹. In 2017¹⁴⁰, Hagenhoff and coworkers developed a similar DBD ion source, albeit with electrodes configured in a different geometry. The exquisite sensitivity of the approach enabled detection of femtogram levels of 28 pesticides and 14 illicit drugs. Their ion source also showed promise when applied to NTS: GC-DBD was used to screen semifluorinated n-alkanes (SFAs) in ski wax samples¹⁴¹: SFAs with carbon number of 26, 28, 30, and 32 were tentatively identified and 1-(perfluorooctyl)-hexadecane confirmed with an authentic standard.

2.3 Strategies to identify unknowns by GC-API

2.3.1 Multidimensional chromatography

Recent interlaboratory studies of NTS methods suggest that a combination of complementary chromatography methods and ionization sources are essential to detect and identify all compounds present in a sample.^{72,142} For example, the identification of approximately 1500 organic pollutants in surface and groundwater surrounding a solid-waste treatment plant required the use of multiple techniques, including GC-(EI)TOF, GC-(APCI)QTOF, LC-(ESI)QTOF and LC-(ESI)QqQ¹⁴³. There is also growing interest in developing multidimensional separation techniques that involve multiple separation stages in a single experiment.

Comprehensive two-dimensional gas chromatography (GC×GC) can significantly increase the number of identifiable compounds in a sample compared to using single-dimension GC-MS. Ballesteros-Gomez *et al.*¹⁴⁴ were the first to combine GC×GC with APCI and it has since been applied to characterizing plasma¹⁴⁵ and household dust⁷². The contour plot in Figure 2.2(a) was obtained from a pooled sample of plasma and it may serve to demonstrate the separation power of GC×GC. It is evident from the plot that many compounds can be separated by the 2nd dimension column that would otherwise co-elute in the first dimension. In the interlaboratory study led by Roskowski *et al.*⁷², both GC×GC-APCI and GC×GC-EI were used to tentatively identify approximately >500 compounds, representing a large fraction of the total number of compounds reported by all participants. This is because the improved separation resulted in the collection of higher quality (CID) mass spectra used for identification. Separation is not the only benefit afforded by modulating effluent from the primary column. As shown in Figure 2.2(b), the

width of a GC×GC peak is very narrow and more intense compared to one collected using single-dimension GC. Patterson *et al.*¹⁴⁶ pioneered the approach coined cryogenic zone compression and showed that it could improve the detection limits for trace level contaminants such as polychlorinated dibenzo-p-dioxins. When coupled with GC-API and a full-scanning, high resolution mass spectrometer, the technique could potentially enable the identification of unknown contaminants with volume limited samples, such as dried blood spots¹⁴⁵.

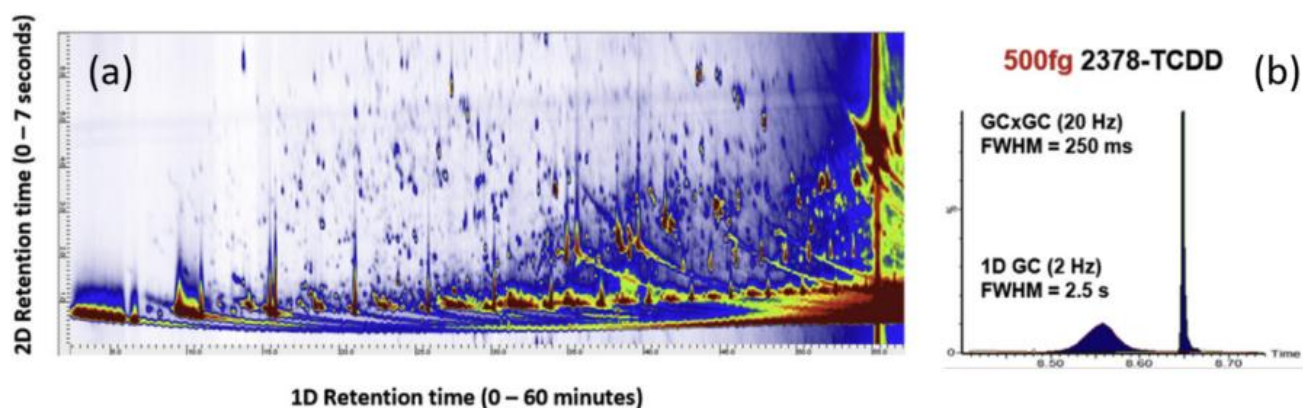


Figure 2.2 (a) Comprehensive two-dimensional gas chromatography (GC×GC) affords unparalleled separation of organic pollutants in plasma; (b) Modulated gas chromatogram obtained from 2,3,7,8-tetrachlorodibenzo-p-dioxin, resulting in 10-fold signal-to-noise (S/N) enhancement. Similar S/N enhancement can be achieved using either thermal or flow modulation. Reprinted from Ref.¹⁴⁵, Copyright 2020, with permission from Elsevier.

Most GC×GC instruments employ cryogenic modulation, whereby the primary column effluent is trapped by a flow of cooled nitrogen gas, and then re-injected into the secondary column by a pulse of heated nitrogen. GC×GC may alternatively be accomplished using a flow modulator, which converts primary peaks to secondary peaks using pulses of gas flow

delivered using one or more valves without cryogenics. Valve-based modulators do not technically zone compress (i.e., focus) the GC effluent, but the width of the secondary peak may still be controlled by the flow, which can exceed the primary flow by 10 times or more. Such a configuration is not compatible with conventional EI and CI ion sources. In contrast, flows in excess of 100 mL/min are well suited to the conditions of GC-API. A multimode flow modulator designed by J.V. Seeley¹⁴⁷ was adapted to a GC-APCI instrument, resulting in significant enhancement in sensitivity²⁵.

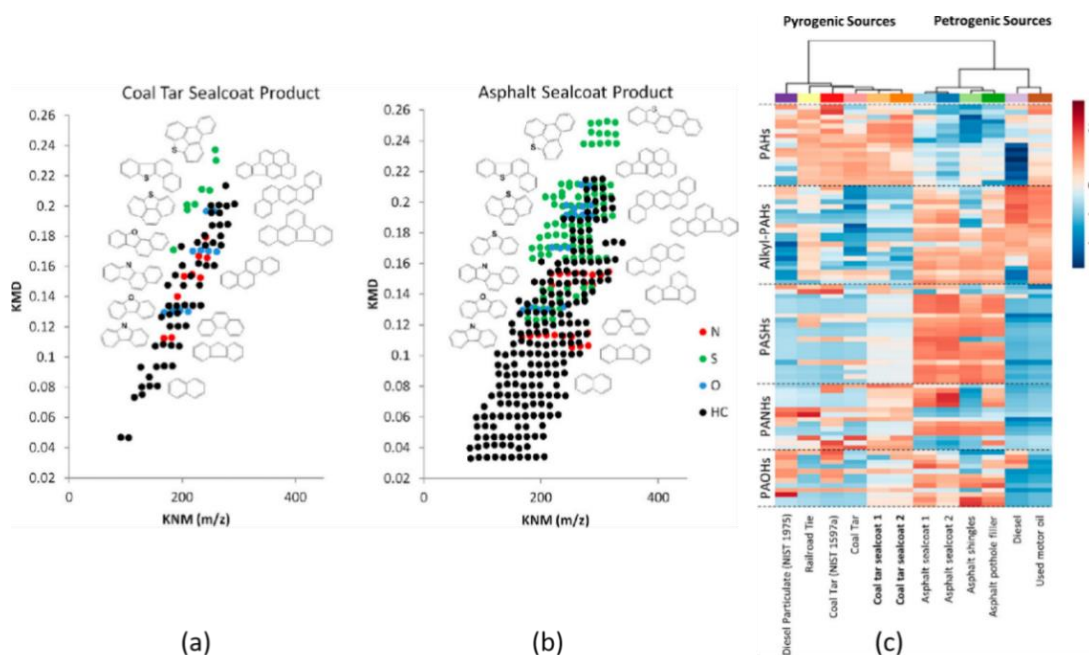


Figure 2.3 Kendrick mass defect (KMD) plots of (a) a coal tar sealcoat product, and (b) an asphalt sealcoat product. (c) Two-dimensional hierarchical cluster analysis with heat map plot of various environmental PAH sources. Red and blue colors represent the most intense and least intense relative abundance values (log scale), respectively. The relative abundances in the heat map plot are presented as an average of 3 replicates. Reproduced from Bowman *et al.*¹⁴⁸

The profile of compounds detected by GC×GC-API, sometimes referred to as a "chemical fingerprint", has proven to be vital for identifying potential sources of pollution. For example, Bowman *et al.*¹⁴⁸ used GC×GC-APCI to characterize the components of coal tar-based sealcoat products in comparison to those in other sources of polycyclic aromatic compounds (PACs). The results revealed that there was a clear difference in the composition of PACs across different types of sealcoat products and sources of PAHs. Figures 2.3(a) and 2.3(b) display the Kendrick mass defect plots obtained from coal tar and asphalt sealcoat products, respectively. They show that the petrogenic asphalt sealcoat is characterized by a greater range of alkylated PAHs compared to the pyrogenic coal tar sealcoat. Individual components were also identified by accurate mass measurements in combination with 1st dimension retention indices. Hierarchical clustering analysis led to the identification of signature compounds that could distinguish coal tar from other pyrogenic sources of PAHs pollution, such as creosote (from a railroad tie), and diesel particulate.

2.3.2 Data-independent identification

In NTS, an important benefit afforded by "soft" ionization techniques like GC-APCI is the abundant formation of (quasi)molecular ions whose accurate mass can be used to determine the elemental composition of an unknown. However, a major drawback is the loss of structure-diagnostic fragmentation normally obtained by EI. Instead, the structural identity of newly discovered contaminants is typically achieved using tandem mass spectrometric techniques, such as collision-induced dissociation (CID). One strategy that has emerged for automated collection of CID mass spectra during GC(×GC) separation, viz. data-dependent acquisition (DDA) and data-independent acquisition (DIA).

Data-independent acquisition (DIA)¹⁴⁹ was first introduced for the analysis of peptide mixtures in combination with LC-MS separation. It was only recently applied to GC-APCI for suspect screening and NTS of organic pollutants⁸⁵. Compared to data-dependent acquisition (DDA), which selects ions based on predefined criteria such as mass, intensity or isotopic ratios, the DIA approach enables the automated, unbiased selection and acquisition of the precursor and CID mass spectra of all ions detected in the sample⁸⁵. By cycling between low and high-collision energy, precursor and product ions can be identified by changes in their intensities: precursor ions will decrease in intensity when subjected to high collision energy, whereas the opposite is true for fragment ions. A computer algorithm then deconvolutes the CID mass spectrum of each compound by grouping together precursor and product ions that share the same GC retention time. A drawback of this approach is its inability to deconvolute CID mass spectra of compounds that co-elute. For example, Figure 4a shows the CID mass spectrum of the flame retardant PBDE-47 that was collected using DIA during a short 15 minute GC separation⁸⁵. Numerous interfering peaks (m/z 206, 253 and 340) are observed that are absent when a longer GC \times GC separation is performed, see Figure 4c. However, it is not always possible to separate co-eluting compounds and in this case the time requirement for the GC \times GC separation exceeded that of the single-dimension experiment by four-fold⁸⁵!

One way to obtain a better-quality CID mass spectrum is to use the quadrupole analyzer to cycle through narrow isolation windows (typically c. 20~50 amu segments) and sequentially subjecting the selected ions to CID. For example, a mass spectrum with a range of 20~1000 amu can be subdivided into 49 segments or *swaths*, which are isolated and fragmented. This was pioneered by Gillet *et al.*¹⁵⁰ who coined the approach sequential

windowed acquisition of all theoretical fragment ion mass spectra (SWATH-MS). Scanning quadrupole DIA (SQDIA) is closely related to SWATH-MS, but instead of cycling the quadrupole between *swaths*, it is scanned continuously across the mass range.¹⁵¹

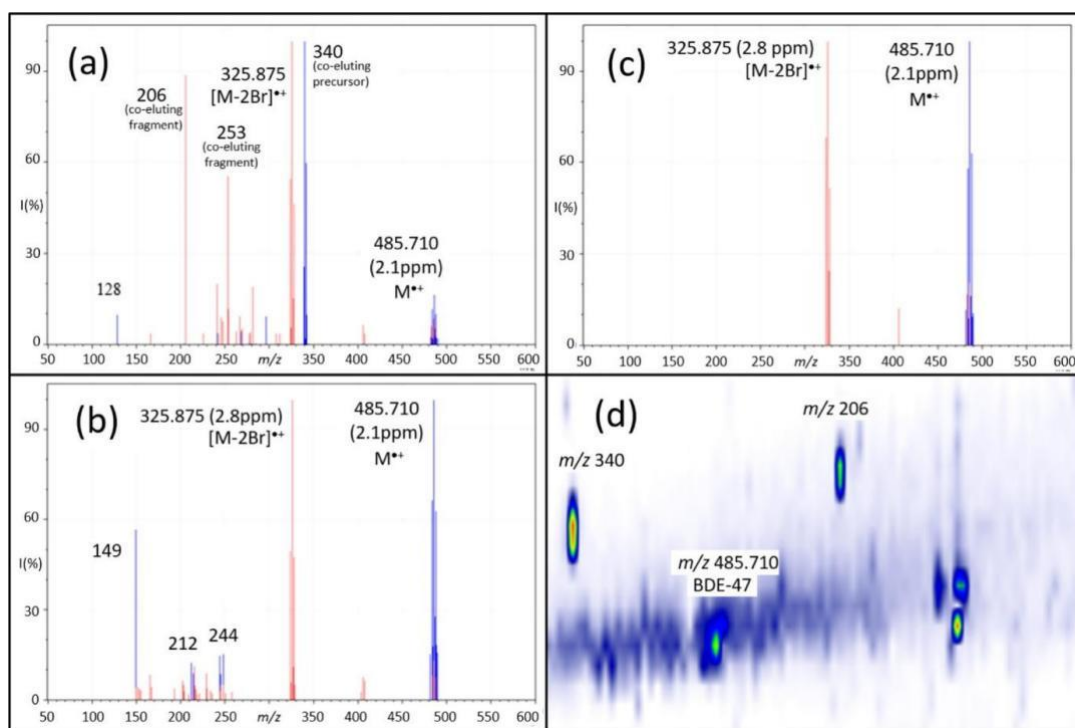


Figure 2.4 Comparison of (a) GC-DIA, (b) GCxGC-DIA, and (c) deconvolved GC-SQDIA spectra of a tetrabromodiphenyl ether. In all spectra, the low-energy channel is shown in blue and the high-energy channel is shown in red. (d) GCxGC-DIA chromatogram showing separation of compounds that coeluted in one-dimensional GC-DIA (as seen in (a)). Greater separation in both GCxGC-DIA and GC-SQDIA resulted in spectra with fewer interferences than those obtained using GC-DIA; this separation can be obtained chromatographically, as in GCxGC, or utilizing the quadrupole, as in SQDIA. Adapted with permission from Schreckenbach *et al.*⁸⁵ Copyright 2021 American Chemical Society.

This significantly reduces co-eluting interferences in the resulting CID mass spectra, as illustrated by comparing the DIA and SQDIA mass spectra obtained for PBDE-47 shown in Figure 4a and 4b respectively. SQDIA can produce CID mass spectra without sacrificing the time required for a more rigorous chromatographic separation. The gain in selectivity and speed provided by SQDIA however also comes with a cost in sensitivity: while the quadrupole is scanning, only a small subset of the ions proportional to the isolation window (IW) are transmitted to the detector and the remaining ions are lost. The theoretical transmission can be calculated using the equation: $IW \text{ (amu)} / \text{mass range (amu)} = \text{transmission (\%)}$.

GC-SQDIA has been used to screen 2542 suspected organic contaminants listed in the AMAP (Arctic Monitoring and Assessment Programme) 2016 Chemicals of Emerging Arctic Concern in a dust sample collected from an electronics recycling facility. The procedure for structure assignment involved comparing the measured mass of the (quasi)molecular ions with the theoretical masses of the 2542 suspected pollutants. Then, a software tool (MassFragment¹⁵²) was used to predict the possible fragments from each of the structures in the library. The structure that produced the greatest number of fragments that match with those observed in the CID mass spectrum was then assigned. In this case, the software tool was part of a commercial software package (UNIFI¹⁵³), but in principal the same structure assignment procedure could be applied using open source software such as MetFrag¹⁵⁴, CSI (Compound Structure Identification):FingerID¹⁵⁵, CFM (competitive fragmentation modeling)-ID¹⁵⁶, and QCEIMS¹⁵⁷. A more detailed discussion on the prediction of mass spectra will be presented in Section 2.3.6. The results of this suspect

screening experiment showed that SQDIA significantly lowers the rate of false structure assignment.

Ion mobility can also be used to disentangle the CID mass spectra of co-eluting compounds¹⁵⁸. One requirement of this approach is that compounds that co-elute from the GC column must be separable according to their mobility, which can be approximated by an ion's collisional cross-section (CCS). At elevated pressures, non-reactive collisions impede the ions akin to an aircraft in flight such that large, bulky ions tend to have larger CCS values and lower mobilities than small, compact ions. CCS values can also be used as confirmatory evidence of a structure assignment⁸⁶. Lipok *et al.* were the first to combine GC×GC with ion mobility-mass spectrometry. They used an in-house database consisting of 800 CCS values to screen for drug-like compounds and pesticides⁸⁶. Recently, Olanrewaju *et al.*¹⁵⁹ have analyzed PAHs and related petroleum hydrocarbons in crude oil using a trapped ion mobility-mass spectrometer hyphenated with GC. In this study, the identification of isomeric PAHs and related unknown aromatic hydrocarbons was accomplished with the aid of CCS measurements. The results also raise the intriguing possibility of separating small contaminant molecules by ion mobility alone. For example, the difference in collisional cross-sections (ΔCCS) of the isomers triphenylene and chrysene is only $\sim 2 \text{ \AA}^2$. Using the formula $R = \text{CCS} / \Delta\text{CCS}$, it is anticipated that an ion mobility resolution of ~ 73 would be sufficient to resolve isomers that closely elute by GC. Commercially available ion mobility-mass spectrometers capable of $R > 200$ are now available⁴², but it has yet to be shown that this separation is fast enough to be compatible with GC(×GC).

2.3.3 Evaluating confidence in structure assignments

According to Schymanski *et al.*¹⁴², structure assignments based on accurate mass and isotopic measurements of their (quasi)molecular ions may be considered tentative at best, corresponding to structure confidence levels 4 and 5 on their 5-level scale. The highest confidence score, level 1, requires confirmatory evidence obtained using authentic standards. While meaningful study of the occurrence and fate of organic pollutants will require authentic standards⁷¹, it is also recognized that this is not always practical at the earliest stage of a contaminant's discovery. In the absence of authentic standards, acquiring complementary information such as CID mass spectra, retention time(s) and CCS can increase the confidence in a tentative identification.

The time-honored approach to identify an unknown pollutant involves comparing its EI mass spectrum with those compiled in spectral libraries. There are databases containing hundreds of thousands of EI spectra (e.g., the NIST Mass Spectral Library), but equivalent libraries compiling CID mass spectra are orders of magnitude smaller, especially for odd-electron ions that are often generated by GC-API. For example, Mesihää *et al.*¹⁰⁰ have developed an in-house GC-APCI-QTOFMS library that includes 29 psychoactive substances. However, creating spectral libraries is time-consuming and costly. To bridge this gap, practitioners of GC-API can take advantage of workflows that were originally conceived for LC-MS. Instead of relying on spectral libraries, one could search structure libraries (e.g. PubChem and ChemSpider) and then compare the experimental CID mass spectra with those predicted by *in silico* methods¹⁶⁰. This approach involves comparing the measured mass of the (quasi)molecular ions with the theoretical masses of all compounds in the structure library. Then rules-based or combinatorial fragmentation predictors are

used to predict the possible fragments from each of the structures in the library whose molecular ions fall within a preselected mass range (usually 1~5ppm) of the experimental mass. The structure that produces the greatest number of fragments that match with those observed in the CID mass spectrum is then assigned.

Su *et al.*¹⁶¹ have suggested a modified version of the confidence scale proposed by Schymanski *et al.*¹⁴². Their approach hinges on comparing results obtained by GC-APCI-MS and GC-EI-MS, taking advantage of both structural and spectral libraries¹⁶². Briefly, the criteria for a level 3 identification are: (i) a compound's EI spectrum must match that of a library spectrum with a match factor >700; and (ii) the mass of the compound's (quasi)molecular ion peak must fall within 5ppm of the theoretical mass. Confidence in the proposed structure increases to level 2 when complementary evidence, such as retention index, or CCS is used. In the absence of a good quality spectral library match, a structure library search can also be used in combination with careful interpretation of the CID mass spectrum. This requires a firm understanding of the dissociation chemistry of organic ions and their reactivity with gas molecules used in the ion source and collision cell. Ultimately, a tentative identification must be confirmed with an authentic standard.

2.3.4 Ion-molecule reactions for separation and structural elucidation

The conditions of the GC-APCI ion source can promote ion-molecule reactions that are structure-diagnostic and in some cases can differentiate between toxic and non-toxic isomers. A prime example is the reaction between dioxygen and (mixed) halogenated dibenzo-*p*-dioxins in the negative ion mode. Quasimolecular ions $[M-Cl+O]^-$ can be generated by reactions between the analyte molecules and $O_2^{\cdot-}$. Mitchum and Korfmacher *et al.*¹⁶³⁻¹⁶⁵ showed early on that the reaction between 2,3,7,8-tetrachlorodibenzo-*p*-dioxin

(2,3,7,8-TCDD) and $O_2^{\bullet-}$ also results in cleavage at the ether bonds of 2,3,7,8-TCDD, as shown in Figure 5a. This specific reaction was shown to distinguish 2,3,7,8-TCDD from many other common interfering species, including its isomers. For example, the negative ion APCI mass spectrum of 2,3,7,8-TCDD displays an intense peak at m/z 176, corresponding to the ether cleavage product shown in Figure 2.5a. In contrast, 1,2,3,4-TCDD cannot produce a peak at m/z 176 because all four of its chlorine atoms are present on the same ring. As shown in Figure 2.5(b~e), this difference can be exploited to reduce the burden on GC to separate TCDD isomers.

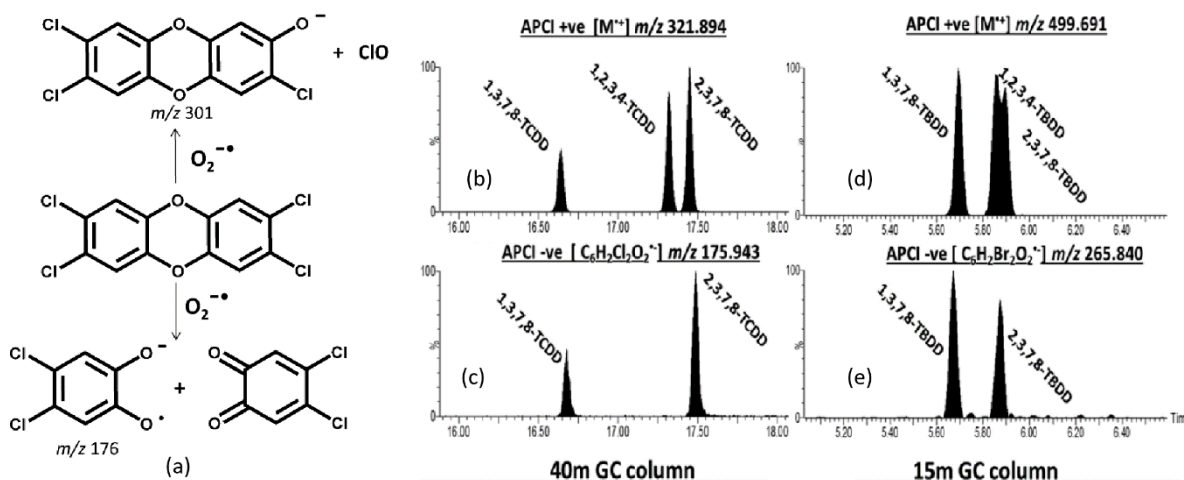


Figure 2.5 (a) Scheme of reaction between 2,3,7,8-TCDD and $O_2^{\bullet-}$; (b~e) APCI⁻ spectra of 2,3,7,8-TCDD, 2,3,7,8-TBDD, and 2,3Br-7,8Cl-DD. Ether cleavage products (ECPs) are observed at m/z 176 and 266 for the 2,3,7,8-TCDD and 2,3,7,8-TBDD species. Both of these ECPs are observed for the 2,3Br-7,8Cl-DD. Reproduced with permission from Ref.¹⁶⁷, Copyright 2016 American Chemical Society.

The ubiquity of brominated flame retardants in everyday household items increases the likelihood that brominated dibenzo-p-dioxins (PBDDs) will be formed during

(accidental) fires¹⁶⁶. Highly brominated contaminants, including the PBDDs are challenging to analyze by GC-MS because of their thermal lability. To minimize thermal decomposition during chromatographic separation, a relatively short (~15m) GC column is used along with a relatively thin (0.1 μm) stationary phase. Therefore, separating toxic from non-toxic isomers is a major challenge that cannot be solved using GC alone, as witnessed by the co-eluting isomers 2,3,7,8-TBDD (toxic) and 1,2,3,4-TBDD (non-toxic) in Figure 5d. Fernando *et al.*¹⁶⁷ showed that ion-molecule reactions with oxygen could be exploited to separate the co-eluting isomers because 2,3,7,8-TBDD reacts with oxygen to produce the ether cleavage product $\text{C}_6\text{H}_2\text{BrO}_2^+$ (m/z 265.840), whereas 1,2,3,4-TBDD cannot. When applied to samples collected from a major industrial fire, this ion chemistry could differentiate isomers of PXDDs (where X=Cl, Br) that would not be feasible using EI.

Structure-diagnostic reactions have also been observed in the positive ion mode¹³³. For example, Di Lorenzo *et al.*¹³³ observed that the PBDE flame retardants can undergo isomer specific photooxidation in a GC-APPI source, viz. that PBDE 71 produces an $[\text{M}-\text{Br}+\text{O}]^+$ ion in its APPI mass spectrum that is absent in that of PBDE 49. According to EPA method 1614, the separation of isomers PBDE 49 and PBDE 71 is a requirement, but the observation that GC-APPI can differentiate isomeric PBDEs raises the possibility that this requirement may be relaxed. The group of R.G. Cooks¹⁶⁸ has shown that corona discharge under solvent-free conditions can promote oxidation reactions of alkanes that would otherwise require catalysis. Megson *et al.*¹⁶⁹ have also observed similar reactions under GC-APCI conditions: the ubiquitous plasticizer and flame retardant, tricresyl phosphate (TCP) undergoes uncatalyzed oxidative transformation into the metabolite 2-(ortho-cresyl)-4H-1,3,2-benzodioxaphosphoran-2-one (CBDP), which is responsible for the

neurotoxicity of TCP. This ion-molecule reaction is specific to ortho substituted triarylphosphates, which are toxic, unlike the non-toxic meta and para substituted isomers. The reaction also mirrors the microsome/enzyme promoted transformation that occurs *in vivo*. There is currently little fundamental understanding of this reactivity, but the implications for NTS are significant: Substituted arylphosphates are widespread environmental contaminants and an indoor dust sample may contain hundreds of (unknown) homologues. GC-APCI could potentially be used to selectively identify the neurotoxic isomers in such a mixture.

2.3.5 Retrospective analysis and compound discovery

A key advantage of all HRMS techniques is that full scan results can be digitally archived and exploited retrospectively. Lai *et al.*¹⁷⁰ recently developed a prescreening and identification workflow implemented as an R package to support regulatory environmental monitoring. One of the challenges of retrospective analysis is developing a strategy to recognize pollutants from among the many thousands of chemicals detected by HRMS. Zhang *et al.*⁵ recently developed an approach to identify unknown persistent and bioaccumulative organics using mass spectrometry and applied this approach using GC-APCI. Most POPs contain three or more Cl or Br atoms; making them easy to recognize based on their isotope patterns. Even polyfluorinated compounds can be recognized based on a relatively weak ¹³C-isotopic peak compared to non-fluorinated compounds, see Figure 2.6.

Data collected using GC-APCI is ideally suited for retrospective analysis because the molecular ion is preserved. Using their prioritization strategy, Zhang *et al.*⁵ identified 191 isotopic clusters from a housedust standard reference material. The identified chemicals

included polychlorinated biphenyls (PCBs) and agricultural drug residues, such as chlordane and degradation products of DDT and Fentichlor, polychlorinated and polybrominated diphenyl ethers (PCDEs and PBDEs), other brominated flame retardants such as tetrabromobisphenol A (TBBPA) and bis(2-ethylhexyl) tetrabromophthalate (BEHTBP), chlorine-containing organophosphate flame retardants tris(1,3-dichloro-2-propyl)phosphate (2 isomers), tris(2-chloroisopropyl) phosphate and tris(2-chloroethyl)phosphate. Previously unknown chlorofluoro flame retardants were also discovered in this study, including thermal decomposition products of 2,3,4,5-Tetrachloro-6-((3-(trideca-fluorohexyl)sulfonyloxy)phenylaminocarbonyl)benzoic acid.

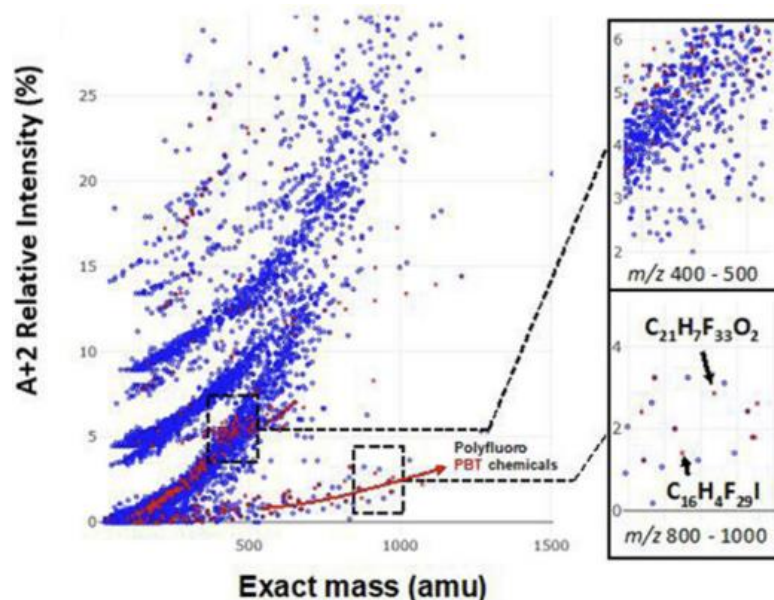


Figure 2.6 Distribution of 610 prioritized persistent, bioaccumulative (P, B) compounds (in red) and commercial chemicals (in blue) from the North American chemical inventories in the compositional spaces defined by m/z of the molecular ion and the ratio of its isotopic peaks $(A + 2):A$, where "A" is the most intense isotopic peak. Adapted from Zhang *et al.*⁵, Copyright 2019, with permission from Elsevier.

2.3.6 Computational tools to predict mass spectra

Libraries of experimental CID mass spectra are much smaller than those compiled for EI. To bridge this gap, novel computational tools have emerged to predict CID spectra. These tools may be broadly classified into three types that have been reviewed by Scheubert *et al.*¹⁶⁰ and have been widely used for the prediction of CID mass spectra collected during LC-MS experiments. The most common type utilizes either a rules-based or a combinatorial approach to predict the fragmentation of an ion. Examples include MetFrag¹⁵⁴, MassFragment¹⁷¹, and Mass Frontier¹⁷². These methods do not technically predict the spectrum, but rather identify the number of experimentally observed peaks that can be explained by a given structure. This approach is popularly used for suspect screening and structural database searching, but one limitation is the fact that an unknown's structure must be present in the database in order for a search to be successful. Another limitation is the absence of peak ratios, which could be used to more reliably assign a structure. In contrast, recently developed machine learning methods, such as CFM-ID¹⁵⁶ can predict whole mass spectra, including relative intensities, but their accuracy depends on the size of the training set used. This is problematic for GC-API because there are few experimental CID spectra available. CSI: FingerID¹⁵⁵ combines fragmentation tree computation and machine learning to predict the molecular fingerprint of the unknown compounds. Another spectra prediction tool is based on computational chemistry. Quantum chemical electron ionization mass spectrometry (QCEIMS)¹⁵⁷ employs semiempirical quantum mechanical and/or density functional theory (DFT) methods, and Born-Oppenheimer molecular dynamics to predict the dissociation behaviour of radical cations. While this approach is the most accurate way to predict a mass spectrum, it is also the most resource demanding.

CSI: Finger ID, CFM-ID and QCEIMS have all been used to predict CID spectra and guide the interpretation of GC-MS data. CSI: Finger ID was used by Larson *et al.* to identify products of lignin pyrolysis.⁹⁸ QCEIMS was evaluated by Schreckenbach *et al.*¹⁷³ to predict the mass spectra of selected halogenated and organophosphorous flame retardants. While QCEIMS is designed for EI spectral prediction, it can also be informative when predicting the CID mass spectra of ions M^{+} generated by charge exchange (GC-APCI) or photoionization (GC-APPI). This is because the unimolecular dissociation behavior of an ion is largely determined by the potential energy surface that does not depend on the ionization technique.

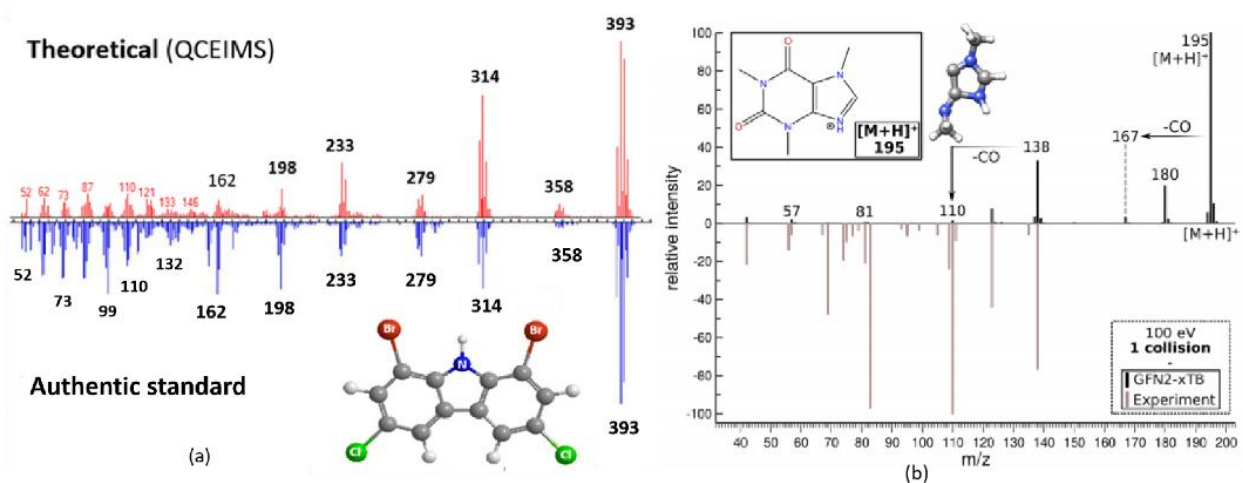


Figure 2.7 (a) EI mass spectrum calculated by QCEIMS and experimental EI mass spectrum of 3,6-dichloro-1,8-dibromo-carbazole, Reproduced from Ref¹⁷³. Copyright 2021 American Chemical Society. (b) calculated spectrum and 40 eV literature spectrum of the most populated caffeine protomer at 600 K, single collision at 100 eV ELAB, Reprinted from Ref¹⁷⁴, Copyright 2021 American Chemical Society.

The results showed that QCEIMS predicted the mass spectra of 35 organic pollutants as accurately as the less computationally demanding CFM-ID method. QCEIMS is best

suited for compounds that are truly unknown and thus not present in any library or training set. For example, QCEIMS accurately predicted the EI mass spectrum of the dioxin-like compound 1,8-dibromo-3,6-dichlorocarbazole (shown in Figure 2.7), an emerging contaminant of the Laurentian Great Lakes. A recent study¹⁷⁴ reports on the development of QCxMS, which extends QCEIMS for the prediction of both EI and CID spectra prediction. A test with six standards showed the calculated data was in reasonable agreement with the experiment (see Figure 2.7(b)). These methods can help guide the analyst in selecting authentic standards.

2.4 Summary and outlook

GC-API techniques generally minimize fragmentation and preserve the (quasi)molecular ion, resulting in simplified mass spectra and improved detection limits. It is relatively facile to modify an existing LC-MS instrument and increase its analytical power. The conditions of the ion source are compatible with high flows that enable faster analysis as well as ion-molecule reactions that can aid in structure analysis. Moreover, spectacular advances in mass spectrometry have led to the development novel mass analyzers and ion mobility-mass spectrometers that have not previously been coupled to GC, enlarging the scope of GC-MS analysis. It is now possible to use techniques and workflows, such as data-independent acquisition, which can significantly decrease the false-positive rate for unknown structure assignment.

GC-API may eventually supplant EI as the *de facto* GC-MS ion source used to identify unknowns, but to achieve this, a number of challenges will need to be surmounted. First, the absence of libraries of CID mass spectra is the most obvious challenge. However, EI mass spectra can still inform the interpretation of GC-API experiments, considering both

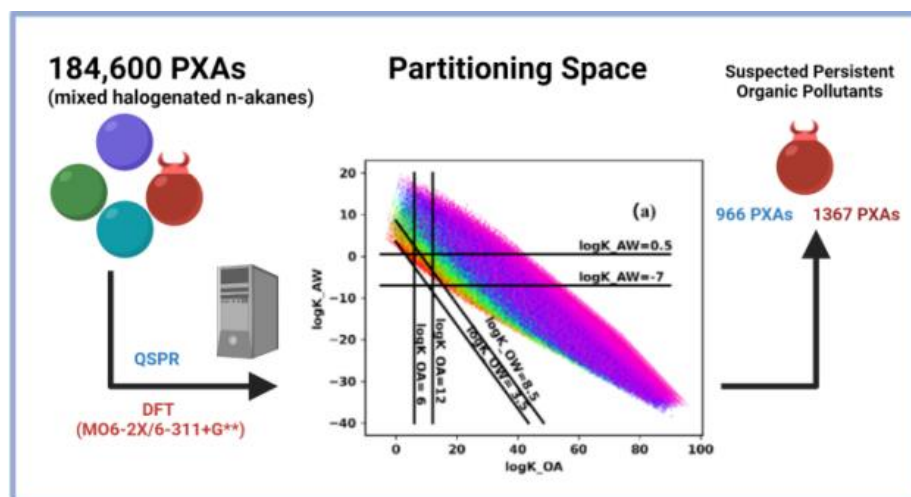
GC-API and EI can produce the same types ions. The dissociation chemistry of a radical cation M^+ is only partly dependent on how it is formed, and it is likely that the low energy reactions will be observed in both experiments. There are also emerging computational techniques that promise to reliably predict CID mass spectra and construct *in silico* spectral libraries.

Second, the ion chemistry is not fully understood yet. Studies have shown that uncatalyzed reactions occurring in the ionization source can have further applications for structure analysis, e.g. oxygen or nitrogen insertion can happen when air is fed to APCI source, which can be beneficial for molecular mass determination because few fragment and adduct ions are produced¹⁶⁸. More knowledge of the complex mechanism happening in ionization region can aid in structure elucidation.

Finally, due to the fact that API can produce molecular ions to a large extent, the constitute information of samples is largely preserved; therefore, new strategies are required to prioritize data from the rich database for further interpretation and retrospective analysis. Also, automated annotation methods specified for GC-API are required for a wider range of users.

Chapter 3

Which of the (mixed) halogenated n-alkanes are likely to be persistent organic pollutants? *



*Adapted with permission from Li, X.; Chevez, T.; De Silva, A. O.; Muir, D. C. G.; Kleywegt, S.; Simpson, A.; Simpson, M. J.; Jobst, K. J. (2021). Which of the (mixed) halogenated alkanes are persistent organic pollutants? *Environ. Sci. Technol.* 2021, 55, 23, 15912–15920. Copyright 2021 American Chemical Society.

3.1 Introduction

Polychlorinated n-alkanes (PCAs) are highly complex mixtures that have been extensively used in industry as lubricants, plasticizers and additives in paints, sealants and adhesives¹⁷⁵. PCAs can remain in sludge during wastewater treatment¹⁷⁶, enter the environment, and pose a risk to aquatic ecosystems. Short-chain ($C_{10\sim 13}$) and medium-chain ($C_{14\sim 17}$) PCAs have been detected in waters impacted by industries, such as municipal incineration, landfills, textile mills and manufacturers of electronics, furniture, and plastics¹⁷⁷. They are also ubiquitous flame retardants in vehicle¹⁷⁸ and household items ranging from kitchen appliance¹⁷⁹ to children's toys¹⁸⁰. Concerns have been raised that humans are exposed to these industrial chemicals as evidenced by the detection of PCAs in household dust samples collected in many countries¹⁸¹, as well as in human blood¹⁸² and breast milk¹⁸³. Due to their persistence and long-range transport potential, these chemicals have become distributed worldwide, even in remote regions like the Arctic¹⁸⁴ and will remain in the environment for decades after their production has ceased. Consequently, short-chain PCAs that contain between 10 and 13 carbon atoms ($C_{10\sim 13}$) have been designated for elimination in Annex A of the Stockholm Convention¹⁸⁵. While medium-chain ($C_{14\sim 17}$) and long-chain ($C_{>17}$) PCAs have been suggested as replacements for their short-chain homologues, recent studies indicate that they too exhibit similar bioaccumulation potential¹⁸⁶, cytotoxicity and metabolic effects¹⁸⁷.

A common albeit questionable strategy to replace chlorinated industrial products is to incorporate other halogens, particularly fluorine or bromine, into the same core structure. For example, bromochloro alkanes are listed in several national chemical inventories, incorrectly labeled as "alkenes" (CASRN 68527-01-5), and they have been in use for

decades. A recent experimental study¹⁸⁸ showed that a flame retardant product described as 97.5% C₁₂₋₃₀ bromochloro alpha-alkenes consists of mixed halogenated n-alkanes (PXAs) containing C₁₈ alkanes substituted with 3-7 chlorine atoms and 1-3 bromine atoms. Chlorofluorocarbons (CFCs) with between 1 and 3 carbon atoms are infamous ozone-depleting substances, but longer chain oils and waxes continue to be produced as metalworking fluids and engineered lubricants¹⁸⁹. Polymers, such as polychlorotrifluoroethylene (PCTFE, [-CClF-CF₂]_n), have been manufactured since the 1950s, and PCTFE has found modern applications in printed circuit boards¹⁹⁰ and as transparent coatings on electronic display panels¹⁹¹ of computers and smartphones. While PCTFE (CASRN 9002-83-9) is listed as a high production volume chemical in the Canadian Domestic Substances List (DSL) and the U.S. Toxic Substances Control Act (TSCA) inventory, both low molecular weight oils and high molecular weight polymers of PCTFE share the same CASRN. Therefore, information on the production volumes of the low molecular weight analogues is not available. Polybromotrifluoroethylene oils (CASRN 598-73-2) have been used as flotation agents and damping fluids for gyroscopes and accelerometers in inertial guidance systems¹⁹². Still, there is less information on their use compared to other halogenated alkanes such as polytetrafluoroethylene (PTFE)¹⁹¹ and polyvinylidene fluoride (PVDF)¹⁹³. Despite the obvious similarities between some of these substances and their chlorinated counterparts, the environmental impact of the (mixed) halogenated n-alkanes (PXAs) is a major knowledge gap.

There are 184,600 elemental compositions corresponding to PXAs that contain between 10 and 25 carbon atoms and incorporate all possible combinations of fluorine, chlorine, bromine and hydrogen. Their synthesis by direct radical halogenation of alkane

feedstocks results in low positional selectivity, yielding myriad isomers that cannot yet be resolved using standard chromatographic separations. This challenge is exacerbated by the paucity of authentic standards, and consequently, it is impractical to monitor all possible PXAs. Studies by Howard and Muir^{67,194} Brown and Wania⁸, Rorije *et al.*¹⁹⁵ and Scheringer *et al.*⁷ have prioritized anthropogenic chemicals using properties such as partitioning coefficients, bioconcentration/bioaccumulation factors, and half-life in water/air predicted by quantitative structure-property relationships (QSPR) that describe a chemical's fate in the environment. In the present study, QSPR and density functional theory (DFT) are applied to a set of 184,600 representative PXA structures to obtain a prioritized list of elemental compositions that exhibit the greatest potential to be persistent organic pollutants (POPs). This knowledge will help guide environmental analytical chemists to develop methodologies capable of accurate determination of the PXAs, most appropriately using mass spectrometry. We also estimate the mass resolving power required to distinguish the prioritized PXAs from other elemental compositions that likely interfere.

3.2 Experimental methods

3.2.1 Generating representative SMILES structures of the PXAs

MOLGEN 5.0¹⁹⁶ was used to create a list of elemental compositions that correspond to C₁₀₋₂₅ n-alkanes substituted with all possible combinations of fluorine, chlorine, bromine and hydrogen. Then for each PXA elemental composition, the SMILES (simplified molecular-input line-entry system) string of a single randomly selected isomer was generated using a script developed in Python 3.7, which is included in the SI. The script generates unique strings with randomly substituted halogenated n-alkane configurations, with no branching or rings. Not all possible isomers of the PXAs are likely to exist¹⁹⁷.

However, for the purpose of this study, it was assumed that the partitioning coefficients (and thus environmental fate) of isomeric PXAs would be similar and this assumption is discussed in the Results and Discussion.

3.2.2 Persistence, bioaccumulation potential and chemical fate modeling

EPISuite⁹ was used to predict the physical-chemical properties of the PXAs, including the partitioning coefficients between octanol and water (K_{OW}), octanol and air (K_{OA}), air and water (K_{AW}) as well as bioconcentration factor (BCF), bioaccumulation factor (BAF), half-life in the atmosphere (Atm-HL), and half-life in water (Water-HL). The results of Gawor and Wania¹⁹⁸ indicate that a linear relationship exists between the K_{OW} data computed from EPISuite and from experiment for short-chain PCAs: $EPISuite \log K_{OW} = 0.67 \times \text{experimental } \log K_{OW} + 3.30$. We used the same relationship to correct our EPISuite derived $\log K_{OW}$ data and then calculated the octanol-air partitioning coefficient ($\log K_{OA}$) using the relationship $\log K_{OA} = \log K_{OW} - \log K_{AW}$.

A computational chemistry approach¹⁹⁹ using density functional theory (DFT) developed by Nedyalkova *et al.* was used to predict the partitioning coefficients of selected PXAs. Briefly, a random 3D structure (coordinates) is generated for each SMILES string using the software package OpenBabel²⁰⁰. This 3D structure was then optimized, and its free energy was calculated at the M06-2X/6-311+G** level of theory in combination with the continuum solvation model based on density (SMD) in Gaussian 16 (Version C.01)²⁰¹. The optimized structures and Gaussian output files are available upon request.

Table 3.1. Summary of the number of persistent and bioaccumulative PXAs identified in this study using the criteria developed by Muir and Howard⁶⁷, Howard and Muir¹⁹⁴, Brown and Wania⁸, Rorije *et al.*¹⁹⁵ and Scheringer *et al.*⁷

Reference	Criteria X=	PXAs class [a]							
		F	Cl	Br	Br Cl	ClF	BrF	BrCl F	Total
Muir and Howard, 2006	BCF>5000 Atm-HL≥2 d	48	3	2	32	187	142	352	766
Howard and Muir, 2010	Atm-HL≥2 d -1>logK _{AW} >- 5 logK _{OW} >3	0	60	5	179	1822	1271	1996 2	23299
Brown and Wania, 2008 Czub <i>et al.</i> 2008 ²⁰²	12≥logK _{OA} ≥6 0.5≥logK _{AW} ≥- 7 8.5≥logK _{OW} ≥ 3.5	0 (+25)	27 (+2 6)	23 (+1 3)	119 (+1 5)	83 (+383)	127 (+264)	587 (+641)	966 (+136 7) [b]
Rorije <i>et al.</i> , 2011	BAF>5000 Atm-HL≥2 d Water-HL> 1440h(60d)	41	22	0	67	523	97	1113	1863
Rorije <i>et al.</i> , 2011	BCF>5000 Atm-HL≥ 2 d Water- HL>1440h (60d)	46	3	2	32	187	139	352	761
Scheringer <i>et al.</i> , 2012	BAF>20,000 Atm-HL>10 d water- HL>180 d	127	2	0	9	699	318	1416	2541

Note [a]: The PXAs have been categorized according to the halogens present in each class, where X is equal to various combinations of F, Cl, and Br; [b] All numbers were obtained using EPISuite derived properties, except those in parenthesis, which were obtained by correcting the EPISuite data with DFT results from a training set of n=207 PXAs.

The partitioning and degradation properties of a chemical play a crucial role in determining its fate in the environment. In the present study, five different chemical fate models were used to prioritize the PXAs^{7,8,67,194,195}. The criteria proposed by Howard and Muir¹⁹⁴ were developed to identify potential persistent and bioaccumulative organics based on their predicted BCF and Atm-HL. Brown and Wania⁸ observed that persistent organic pollutants occupy a discrete region of chemical space enclosed by $\log K_{OA}$, $\log K_{OW}$, and $\log K_{AW}$. Gawor and Wania¹⁹⁸ later suggested that complex mixtures, such as PCAs and PXAs, can be assessed by graphing the predicted $\log K_{OA}$ and $\log K_{AW}$ values of each constituent in partitioning space. The criteria developed by Rorije *et al.*¹⁹⁵ and Scheringer *et al.*⁷ are also used in Annex D of the Stockholm Convention, and include predicted Water-HL. Scheringer *et al.*⁷ used higher BAF and longer atmospheric half-life criteria to prioritize the most persistent and bioaccumulative compounds. The criteria used in all five models and the number of PXA elemental compositions identified by these methods are summarized in Table 3.1.

3.2.3 Prediction of PXA mass spectra

PXAs likely behave similarly to their chlorinated analogues that can ionize by negative mode chemical ionization²⁰³ to yield $M^{\bullet-}$ or $[M+X]^-$ ($X=Cl, Br$) adducts. The isotopic masses and peak intensities of the $M^{\bullet-}$ ions of all 184,600 elemental compositions were calculated using the EnviPat package²⁰⁴ in R. The full-width-half-maximum mass resolution ($R= m/\Delta m$) required to resolve individual PXA elemental compositions was computed using a Python script developed in-house. The script is described in the SI. Briefly, the script determines the minimum mass difference (Δm) between the intensoid

peak (i.e., the most intense isotopic peak) of a selected PXA elemental composition and all other (isotopic) peaks produced by the 184,600 PXAs.

3.3 Results and Discussion

3.3.1 Development of a set of representative PXA structures

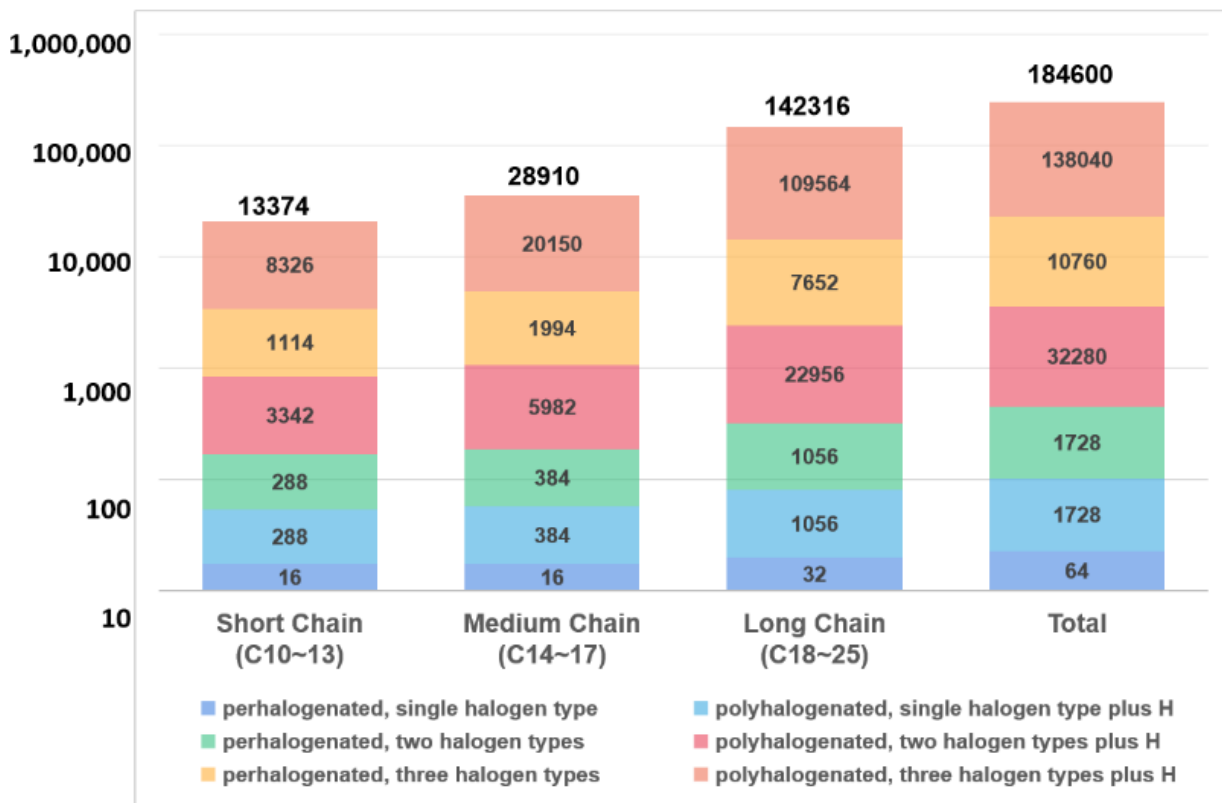
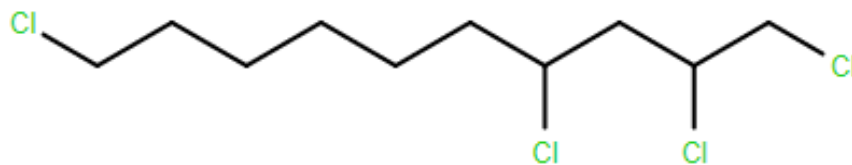


Figure 3.1 Distribution of elemental compositions corresponding to (mixed) halogenated n-alkanes (PXAs) of varying carbon length.

The number of elemental compositions corresponding to PXAs of varying carbon length (C_{10-25}) and halogen composition are summarized in Figure 3.1. The number of PXAs rapidly increases with carbon-chain length and the inclusion of additional types of halogens. As shown in Figure 3.1, there are 288 polyhalogenated elemental compositions

corresponding to short-chain PXAs that incorporate hydrogen and a single halogen type, where X = F, Cl, or Br. The PCAs fall within this category. Similarly, up to 288 *per*halogenated alkane compositions consisting of two halogens (e.g., Cl and F, or Br and F) are also possible. Polychlorotrifluoroethylene oil^{189,192} is an example of this type of PXA. When two halogen types are included in the presence of hydrogen, up to 3,342 elemental compositions become possible. Doverguard 8207A, a flame retardant mixture characterized by Chibwe *et al.*¹⁸⁸, falls within this family of compositions. If all three halogens, F, Cl, and Br, are included, up to 9,440 short-chain elemental compositions are possible, adding up to 13,374 short-chain PXA elemental compositions. Additionally, there are up to 28,910 medium-chain (C₁₄₋₁₇) and 142,316 long-chain (C₁₈₋₂₅) PXA elemental compositions, yielding a total of 184,600.



Scheme 3.1

The number of potential (stereo) isomers is enormous. We have not attempted to compute every possible structure because doing so is impractical and may be unnecessary for the purpose of assessing environmental fate. In order to minimize the number of calculations, a single structure was selected at random using an in-house script for each of the 184,600 elemental compositions in this study. For example, the results obtained using

MOLGEN 5.0 indicate that the short-chain PCA formula $C_{10}H_{18}Cl_4$ produces 19,226 structures. However, as might be expected, the $\log K_{OW}$ values predicted from EPISuite for all possible isomers are similar, ranging between 5.8~7.5, with a mean value of 6.4. Sophisticated quantum mechanical calculations by Endo *et al.*^{23,24} also showed that there is a similarly narrow range of $\log K_{OW}$ values for short-chain PCAs isomers. These values reflect the uncertainty that is introduced when a single randomly selected isomer is used to represent the behavior of the entire elemental composition group. For example, when applied to the $C_{10}H_{18}Cl_4$ family of isomers, the in-house script returns the SMILES structure shown in Scheme 3.1, corresponding to $\log K_{OW}=6.1$, $\log K_{OA}=6.3$ and $\log K_{AW}=-0.2$, which deviate by -0.2, -0.1 and 0 from the mean values of all isomers. The distributions of $\log K_{OW}$ and $\log K_{OA}$, are also relatively narrow with standard deviations of ~ 0.4 . EPISuite employs a QSPR model that produces the same $\log K_{AW}$ value, regardless of isomeric structure.

However, the results of Endo *et al.*^{23,24} suggest that the distribution of $\log K_{AW}$ values of isomers is also quite narrow, with standard deviations of ~ 0.4 for all short-chain PCAs considered in their study. All computed parameters, ranges, means and standard deviations (errors) of all the possible structures of $C_{10}H_{18}Cl_4$ are summarized in Table 3.2. For the partitioning coefficients, $\log K_{OW}$, $\log K_{OA}$ and $\log K_{AW}$, we suggest that this uncertainty is relatively small compared to the criteria ranges summarized in Table 3.2.

Table 3.2 The physical-chemical properties and statistics of all C₁₀H₁₈Cl₄ isomers predicted by EPISuite.

	logK _{OW}	logK _{OA}	logK _{AW}	Water_H L (days)	Water_H L (hours)	BCF	Fish_H L	BAF	Atmos_HL
Min	5.82	6.047	-0.227	92.2	2212.5	202.7	6.48	4757	0.94
Max	7.46	7.687	-0.227	913.6	21927.2	14000.0	48.70	1162598	14.51
Mean	6.23	6.45	-0.227	291.5	6997.1	6589.4	12.50	60536	2.36
SD	0.361	0.361	0	109.2	2620.1	3631.5	5.42	93125	1.04

	slope	intercept	R ²	R	MAE	MSE	RMSE	MAPE
logK _{OW} , logK _{OA} , & logK _{AW}	1.15250		0.9498	0.974577	0.7026	0.7397	0.8600	0.7343
logK _{OW}					0.5046	0.3911	0.6254	0.2284
logK _{OA}					0.9532	1.2694	1.1267	0.3618
logK _{AW}					0.9763	0.6136	0.7833	0.6018

3.3.2 Screening PXAs that are potential POPs using chemical fate models and partitioning space

The concept of partitioning space to assess a chemical's environment fate was first introduced by Wania³⁶ in 2003 and then later applied to the PCAs by Gawor and Wania¹⁹⁸. Partitioning space is a two-dimensional coordinate system formed by the partitioning coefficients, logK_{OA} and logK_{AW}. Brown and Wania⁸ showed that chemicals characterized by the following criteria exhibit the greatest potential to persist, bioaccumulate and undergo long-range transport to remote regions, such as the Arctic: logK_{OW} ≥ 3.5; logK_{OA} ≥ 6.0; 0.5 ≥ logK_{AW} ≥ 3.5; logK_{AW} ≤ -1.78 × logK_{OA} + 14.56. By plotting the predicted logK_{OA} and logK_{AW} values for each of the representative constituents of a complex mixture, one can

identify chemical compounds that pose the greatest risk. A drawback of this approach to screening is that it does not account for possible (bio)transformation, which may result in the formation of products that are more persistent and bioaccumulative than their precursors²⁰⁵.

Figure 3.2 displays this partitioning space overlaid with 184,600 representative PXAs. The criteria of Brown and Wania is enclosed by the magenta line shown in Figure 3.2(b). It is expected that the PXAs occupying this region will have ~10% of the maximum potential to persist, bioaccumulate and undergo long-range transport. PXAs with partitioning coefficients outside the constrained criteria are either too volatile to bioaccumulate (e.g., short-chain highly fluorinated n-alkanes) or too involatile to undergo long-range transport (e.g., long-chain highly brominated PXAs)⁸.

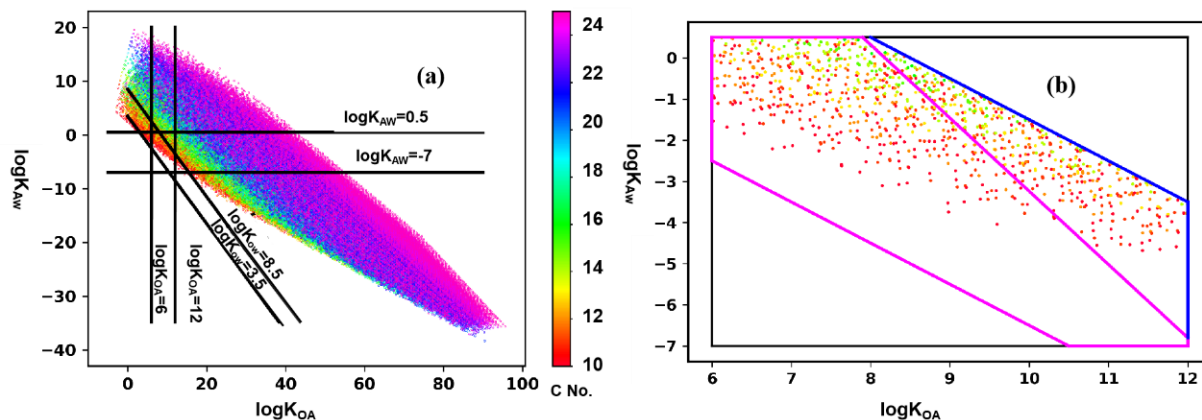


Figure 3.2 (a) Partitioning space for 184,600 PXAs. The colour bar indicates the number of carbon atoms present; (b) Expanded view of partitioning space in the region identified by Czub *et al.*²⁰² The magenta line encloses the region with PXAs that are expected to exhibit in excess of 10% of the maximum bioaccumulation and long-range transport potential. This region expands to the blue line for compounds continuously released for at least 10 years²⁰².

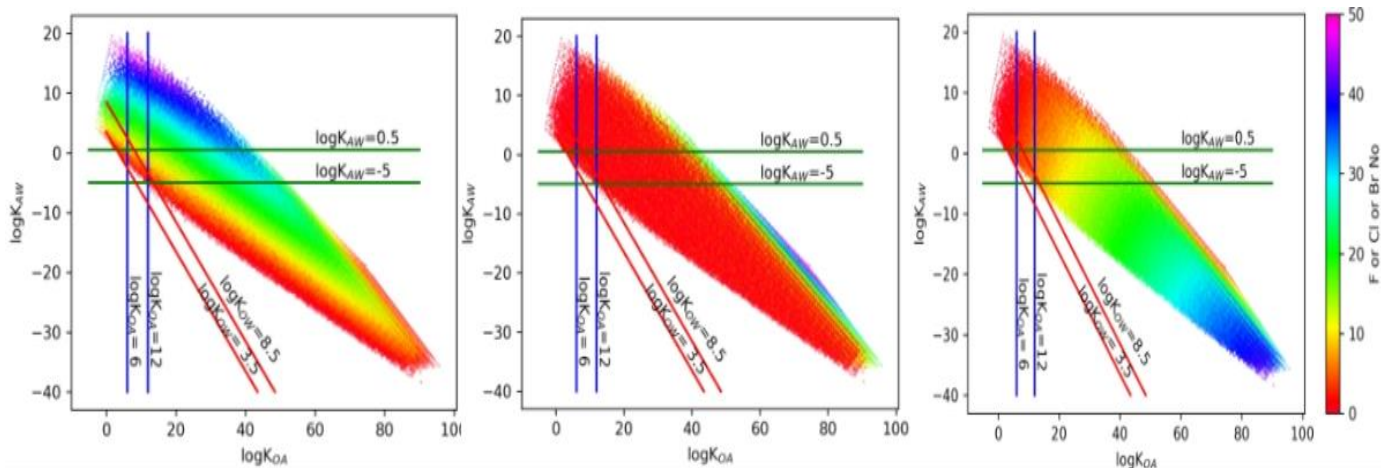


Figure 3.3 Partitioning space for 184,600 PXAs using DFT correction. (a) Color bar: the number of fluorine atoms in the composition; (b) Color bar: the number of chloride atoms in the composition; (c) Color bar: the number of bromine atoms in the composition.

Note: blue line: the $\log K_{OA}$ range in Brown and Wania criteria; Green line: the $\log K_{AW}$ range in Brown and Wania criteria; Red line: the $\log K_{OW}$ range derived from $\log K_{OW} = \log K_{OA} + \log K_{AW}$ in Brown and Wania criteria.

We note that the ratio of $\log K_{AW} : \log K_{OA}$ tends to be larger in polyfluorinated n-alkanes (Fig. 3.3(a)), reflecting their increased volatility. In contrast, PXAs with a large number of Cl and/or Br atoms are characterized by negative $\log K_{AW}$ values and large $\log K_{OA}$ values (see Fig. 3.3(c)).

Among the 184,600 elemental compositions, the EPISuite calculations indicate that only 560 are expected to fall within the criteria first defined by Czub *et al.*²⁰² and later used by Brown and Wania⁸ to screen chemical inventories for potential POPs in the Arctic. The boundaries of this space can also change as a function of the number of years during which the chemical is emitted to the environment²⁰², with compounds emitted in more recent years characterized by greater $\log K_{OW}$ values. When the Brown and Wania criteria is expanded

to capture compounds emitted up to 10 years ago, as indicated by the blue line in Figure 3.2(b), the number of PXAs of concern increases to 966. While this model assumes perfectly persistent chemicals that are not degradable whatsoever, we estimate that 752 out of the 966 elemental compositions have significant atmospheric half-lives > 2 days. It is expected that biological transformation of the PXAs will result in the formation of the corresponding carboxylic acids and other oxygen-containing products. While these biotransformation products may also be POPs²⁰⁶, we have not further considered them in this study.

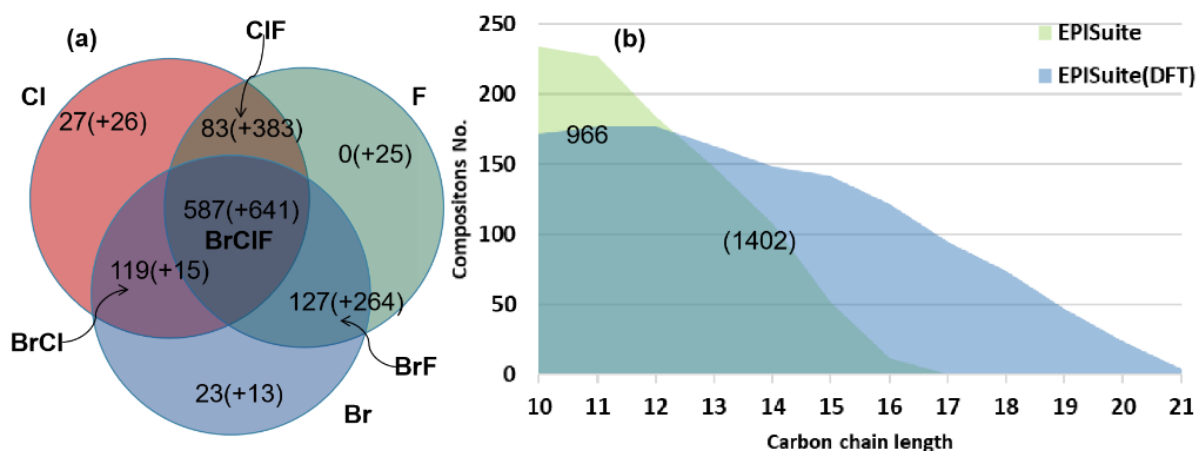


Figure 3.4 Breakdown of the PXAs identified using partitioning space based on (a) the types of halogens present; and (b) the carbon chain length. The numbers in round brackets are obtained when the EPI Suite data is corrected using DFT results from a training set of n=208 PXAs.

A breakdown of the 966 prioritized PXA elemental compositions is shown in Figure 3.4(a). There are 27 chlorinated n-alkanes, 23 brominated n-alkanes, 127 bromofluoro PXAs, 119 bromochloro PXAs, 83 chlorofluoro PXAs and 587 bromochlorofluoro PXAs

identified as potential POPs using the Brown and Wania criteria. Greater than 82% of these elemental compositions correspond with short- to medium-chain PXAs having between 10 and 16 carbon atoms, see Figure 3.4(b).

There are other chemical fate models that could potentially be used to screen the PXAs for potential POPs. Table 3.1 summarizes the number of PXA elemental compositions that meet the criteria proposed by Muir and Howard⁶⁷, Howard and Muir¹⁹⁴, Brown and Wania⁸, Rorije *et al.*¹⁹⁵ and Scheringer *et al.*⁷. There is overlap between the resulting lists of priority PXAs. While only 11 elemental compositions are selected by all five chemical fate models, 4264 compositions are identified using more than two; 934 are selected by three and 157 were identified by four. The largest number of compositions were identified using the criteria proposed by Howard and Muir in 2010. However, with over 20,000 compositions selected, the list is somewhat impractical as a means to prioritize compounds for future analytical monitoring. Further, the prescribed criteria also capture PXAs with large $\log K_{OA}$ values that are less likely to undergo long-range transport as semi-volatiles, although these compounds could potentially transport adsorbed to particles. Similarly, compounds with $\log K_{OW} > 8$ are less likely to bioaccumulate. The models reported in references^{67,7,195} all use BCF or BAF as an important criterion.

However, we note that the methods used to predict BCF may be less reliable when applied to the PXAs due to the absence of experimental data. Even for the short-chain PCA elemental composition $C_{10}H_{18}Cl_4$, the uncertainty in the QSPR-predicted BCF was extremely large, see Table 3.2. The discussion below focuses on the PXAs prioritized using partitioning space, in part because this model relies on partitioning coefficients (K_{OW} , K_{OA} , K_{AW}) that are easier to predict. However, the question remains as to whether current QSPR

models²³, including EPISuite, are appropriate for PXAs. This question is addressed in the next section using density functional theory.

3.3.3 Prediction of partitioning coefficients using density functional theory

EPISuite is a free tool that provides rapid, batch predictions of physical-chemical properties for a wide range of chemicals. However, EPISuite is less accurate in predicting the properties of the PCAs compared to COSMOtherm or SPARC²⁰⁷. For example, the deviation between the calculated and the experimental logK_{OW} values of the short-chain PCAs are on average 1.5, 0.8 and 0 for EPISuite, SPARC and COSMOtherm, respectively. To partially address this issue, we have used the linear relationship that exists between the logK_{OW} data computed from EPISuite and from experiment, as reported by Gawor and Wania²⁷. The experimentally corrected logK_{OW}^{*} was obtained using the equation: $\log K_{OW}^* = 1.5 \times (\log K_{OW} - 3.30)$. However, it is also reasonable to assume that there is at least some uncertainty in the experimental logK_{OW} values of the PCAs used to train these models. To our knowledge, no models have yet been created to accurately predict the properties of the *mixed* halogenated PXAs due to a paucity of experimental data that could be used as a training set. One way to circumvent this problem is to perform density functional theory calculations to predict a chemical's properties¹⁹⁹.

Figure 3.5 compares the logK_{OW}, logK_{OA} and logK_{AW} partition coefficients computed using the MO6-2X/6-311+G** level of theory with experimentally determined values for 22 available chlorinated (16), brominated (2), bromochloro (2) and chlorofluoro (2) n-alkanes. The MO6-2X/6-311+G** level of theory was selected because it proved to be the most accurate of the three methods evaluated by Nedyalkova *et al.*¹⁹⁹ The complete list of PXAs used in our evaluation of this method can be found in Table 3.3.

A good linear correlation was observed between experimental and computational results. The results also demonstrate the accuracy of the DFT method, with root mean square (RMS) errors of 0.6, 1.1, and 0.8 when predicting $\log K_{OW}$, $\log K_{OA}$ and $\log K_{AW}$. Therefore, this approach appears to be capable of estimating the partitioning coefficients of the PXAs, with only the input of a molecular structure.

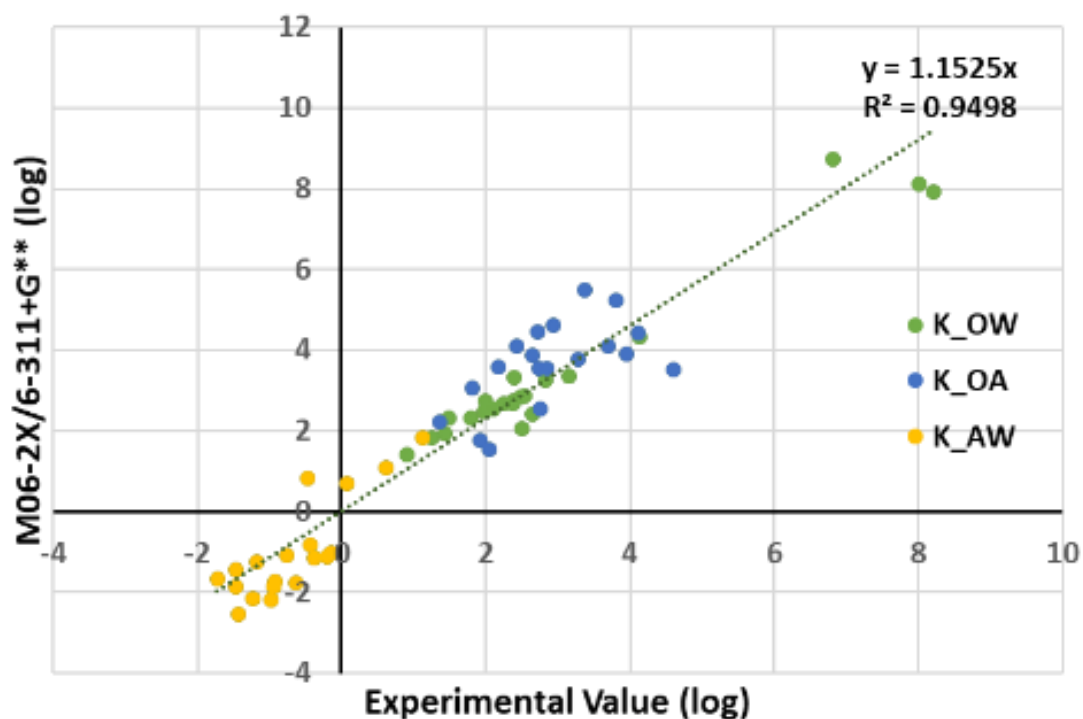


Figure 3.5 Comparison of the experimental $\log K_{OW}$, $\log K_{OA}$ and $\log K_{AW}$ partitioning coefficients with those computed using the MO6-2X/6-311+G**¹⁹⁹. The experimental values are from ref.²⁰⁸⁻²¹¹

Table 3.3 Partitioning coefficients computed using DFT(MO6-2X/6-311+G**) and experimental determined values of available halogenated n-alkanes, with the statistics shown below.

SMILES	logK _{ow} _{Experimental}	logK _{oa} _{Experimental}	logK _{aw} _{Experimental}	logK _{ow} _{Gaussian}	logK _{oa} _{Gaussian}	logK _{aw} _{Gaussian}
<chem>C(CC(CC(CC(CC(C(C(C(C(C(C)Cl)Cl)Cl)Cl)Cl)Cl)Cl)Cl)Cl)Cl)Cl</chem>	6.81			8.74	19.01	-10.28
<chem>C(C(CC(CCCC(C(CC(CCC(C)Cl)Cl)Cl)Cl)Cl)CC</chem>	8.21			7.93	13.07	-5.14
<chem>C(C(C(C(CCCC(C(CC(CCC(C)Cl)Cl)Cl)Cl)Cl)Cl)Cl)Cl)Cl)Cl)Cl</chem>	8.01			8.10	15.63	-7.52
<chem>ClC(F)(F)C(Cl)(Cl)F</chem>	3.16	2.04	1.12	3.36	1.55	1.82
<chem>C(Br)Br</chem>	2.5	3.96	-1.46	2.06	3.91	-1.85
<chem>C(Br)(Br)Br</chem>	2.38	4.11	-1.73	2.75	4.41	-1.68
<chem>C(Br)(Cl)Cl</chem>	2.1	3.28	-1.18	2.55	3.79	-1.23
<chem>C(Br)(Br)Cl</chem>	2.24	3.70	-1.46	2.66	4.10	-1.44
<chem>C(Cl)(Cl)(Cl)F</chem>	2.53	1.91	0.62	2.86	1.78	1.08
<chem>C(Cl)</chem>	0.91	1.35	-0.44	1.40	2.22	-0.83
<chem>C(Cl)(Cl)</chem>	1.25	2.17	-0.92	1.83	3.58	-1.74
<chem>C(Cl)(Cl)(Cl)</chem>	1.97	2.73	-0.76	2.46	3.56	-1.10
<chem>C(Cl)(Cl)(Cl)(Cl)</chem>	2.83	2.75	0.08	3.25	2.54	0.71
<chem>CC(Cl)</chem>	1.43	1.81	-0.38	1.93	3.07	-1.14
<chem>CC(Cl)(Cl)</chem>	1.79	2.43	-0.64	2.31	4.09	-1.78
<chem>C(Cl)C(Cl)</chem>	1.48	2.72	-1.24	2.32	4.46	-2.14
<chem>CC(Cl)(Cl)(Cl)</chem>	2.49	2.64	-0.15	2.85	3.86	-1.01
<chem>C(Cl)(Cl)C(Cl)</chem>	2.38	3.81	-1.43	2.67	5.23	-2.56
<chem>C(Cl)(Cl)C(Cl)(Cl)</chem>	2.39	3.37	-0.98	3.33	5.50	-2.18
<chem>C(Cl)(Cl)(Cl)C(Cl)(Cl)(Cl)</chem>	4.14	4.61	-0.47	4.33	3.52	0.82
<chem>C(Cl)C(Cl)C</chem>	2	2.94	-0.94	2.74	4.61	-1.87
<chem>C(Cl)CC</chem>	2.64	2.85	-0.21	2.42	3.53	-1.12

It is not currently practical to use DFT to calculate 184,600 PXAs with limited computational resources. Instead, in addition to the PXAs with known experimental values, we randomly selected a subset of 200 PXAs that fall with the EPISuite predicted $\log K_{OA}$ and $\log K_{OW}$ ranges of 4~12 and 3~11 using Python command "random". These ranges capture a slightly larger area surrounding the partitioning space boundaries shown in Figure 3.4(b). Figure 3.6 shows a comparison of the DFT and EPISuite derived partitioning coefficients obtained from this subset of PXAs. The correlation between EPISuite and DFT predicted partitioning coefficients appears to be linear ($p < 0.05$). We hypothesize that by using this relationship, a more accurate estimate of the partitioning coefficients of the *mixed* halogenated n-alkanes can be inferred from the EPISuite data. $\log K_{AW}$ was obtained using the relationship: $K_{OA} = K_{OW} / K_{AW}$ or $\log K_{AW} = \log K_{OW} - \log K_{OA}$. Indeed, the RMS errors for $\log K_{OW}$ and $\log K_{OA}$ using this approach, 0.6 and 1.9 respectively, are acceptable. When applied to the larger data set of 184,600 elemental compositions, the PXAs shift such that a new group of 1402 PXAs comes into focus within the partitioning space boundaries defined by Brown and Wania (Figure 3.3(b)). DFT calculation on 113 compositions which were randomly chosen from these 1402 PXAs showed that 63 out of 113 (56%) remained within the boundaries.

A breakdown of the 1402 PXA elemental compositions selected after the DFT correction is shown in round brackets in Figure 3.3(a). These include 25 fluoro, 14 bromo, 28 chloro, 389 chlorofluoro, 16 bromochloro, 270 bromofluoro and 660 bromochlorofluoro PXAs. Interestingly, this correction brought into focus the short-chain PCAs with chlorine content (28~50% wt.) below the 48% threshold prescribed by the Stockholm Convention, and this result is mirrored by the COSMO-RS calculations reported elsewhere³⁴. We also

note that the DFT correction significantly increased the number of fluorinated elemental composition groups (F, ClF, BrF), but not the non-fluorinated groups. This is consistent with the observation that the DFT predicted $\log K_{OW}$ and $\log K_{AW}$ values appear to be lower than the EPISuite results (see Figure 3.6), reflecting the increased polarity of carbon-fluorine bond.

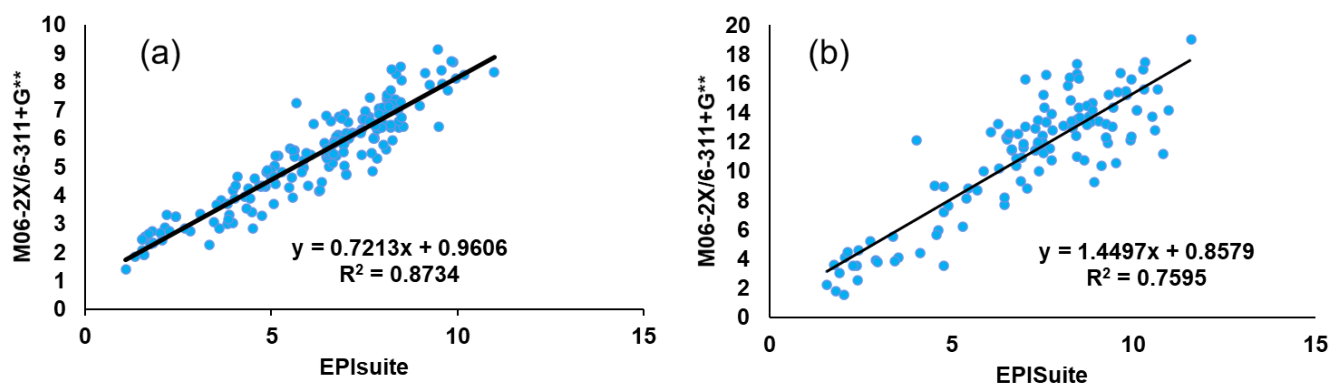


Figure 3.6 The relationship between DFT and EPISuite values obtained for (a) $\log K_{OW}$; and (b) $\log K_{OA}$.

Figure 3.7 displays the carbon chain length and halogenated weight distributions of the entire set of PXAs screened using both EPISuite (in green) and DFT corrected data (in blue). This data is also summarized in Table 3.4. While the EPISuite data suggests that the total halogen content of the priority PXAs generally exceeds 40% (see Figure 3.6(d)), this number decreases significantly when the DFT correction is applied.

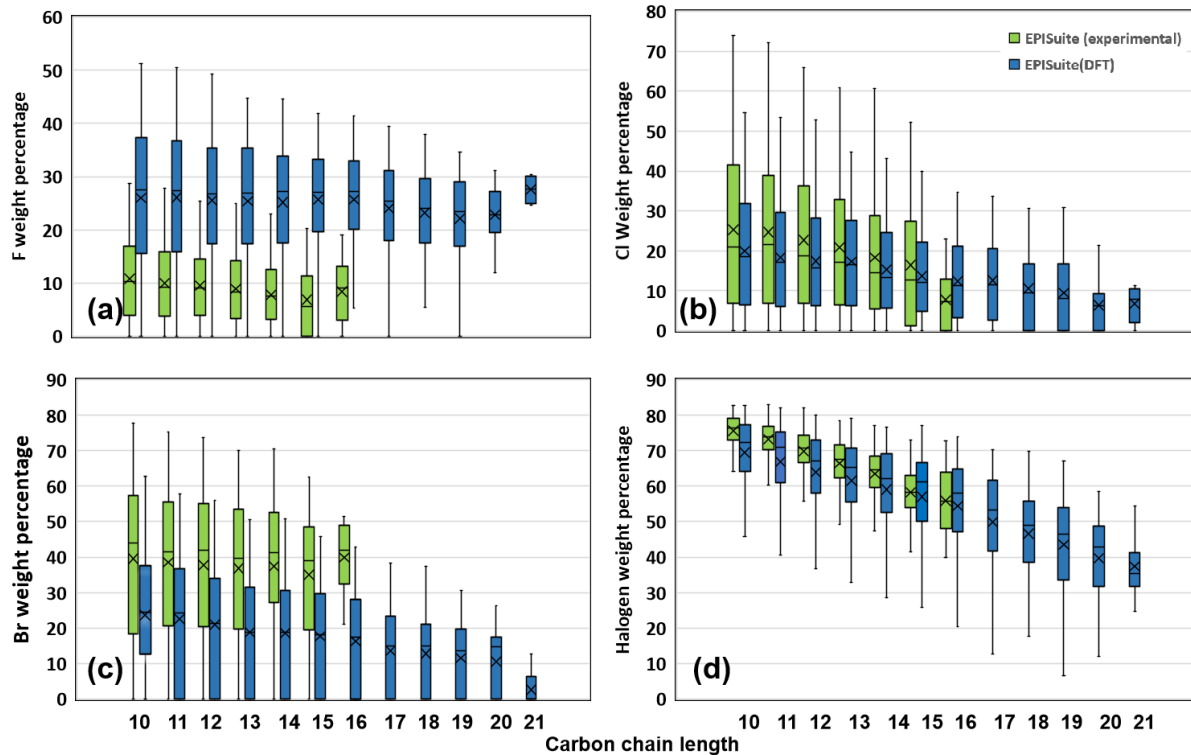


Figure 3.7 Distributions of (a) fluorine; (b) chlorine; (c) bromine; and (d) total halogen content by weight. The data shown in green was obtained from EPISuite; and the data shown in blue was obtained by correcting the EPISuite partitioning coefficients using the DFT training set (see Figure 3.5).

Note: × marks the mean value of the halogen percent in the compositions with certain carbon chain length; - marks the median value; the whiskers indicate the range.

This is because there are many more (mixed) fluorinated compounds identified as potential POPs using the DFT correction. Fluorine is less massive than chlorine or bromine, meaning that more fluorine atoms can be incorporated into a molecule while contributing less to the %weight. As shown in Figures 3.7(a-c), the DFT corrected list of PXAs is characterized by a decrease in Cl and Br content, and an increase in F content.

Table 3.4 The breakdown of screened compositions using experimental and DFT correction.

Note: $n_c=10$ and Cp. No. (Compositions No.)=172 mean that there are 172 compositions that have a carbon-chain length of 10 is screened in the partitioning space. The weight percent is reported as to the nearest half unit. The halogen atom number range in the compositions with certain carbon chain length is shown in bracket. The median value of weight percent is shown in bold.

nc	Experimental corrected EPISuite data					DFT corrected EPISuite data				
	Cp. No.	F w% (No.)	Cl w% (No.)	Br w % (No.)	Halo w% (No.) Median v alue	Cp. No.	F w% (No.)	Cl w% (No.)	Br w % (No.)	Halo w% (No.) Median v alue
10	235	0-28.5 (0-11)	0-74 (0-11)	0-77.5 (0-7)	55.5-83 (4-16) 76.36	193	0-51.5 (0-17)	0-54.5 (0-7)	0-62.5 (0-5)	20-83.5 (1-21) 75.89
11	227	0-28 (0-11)	0-72 (0-11)	0-75.5 (0-7)	58-83 (3-16) 73.89	192	0-50.5 (0-17)	0-53.5 (0-7)	0-55 (0-4)	11-82 (1-21) 71.39
12	184	0-25.5 (0-10)	0-66 (0-10)	0-73.5 (0-7)	51-82 (3-16) 70.85	190	0-50 (0-17)	0-45.5 (0-7)	0-58 (0-4)	10-80 (1-21) 67.75
13	148	0-25 (0-10)	0-61 (0-9)	0-70 (0-7)	43.5-78.5(3-16) 67.68	171	0-45 (0-17)	0-44.5 (0-7)	0-50 (0-4)	9.5-79 (1-21) 65.74
14	108	0-23 (0-9)	0-60.5 (0-10)	0-70.5 (0-6)	41.5-77 (2-15) 64.34	153	0-44.5 (0-17)	0-43 (0-6)	0-47 (0-4)	9-77 (1-20) 62.10
15	52	0-20.5 (0-8)	0-52 (0-7)	0-62.5 (0-6)	40-73 (2-15) 58.27	145	0-42 (0-16)	0-40 (0-7)	0-46 (0-4)	8.5-77 (1-21) 61.07
16	12	0-8 (0-19)	0-4 (0-23)	21-51.5(1-5)	40-73 (2-14) 55.75	124	0-41.5 (0-17)	0-34.5 (0-6)	0-43 (0-4)	8-74 (1-21) 57.97
17						97	0-39.5 (0-14)	0-33.5 (0-6)	0-38 (0-3)	7.5-70 (1-18) 53.40
18						76	5.5-38 (1-15)	0-31 (0-5)	0-37.5 (0-3)	7-70 (1-20) 49.05
19						49	6-34.5 (1-13)	0-31 (0-5)	0-30.5 (0-3)	6.5-67 (1-17) 46.52
20						26	12-31 (2-10)	0-21.5 (0-3)	0-26.5 (0-2)	12-58.5 (2-13) 42.81
21						4	24.5-30.5(5-10)	0-11 (0-2)	0-12.5 (0-1)	24.5-54.5(5-13) 35.41

The Stockholm Convention is directed at short-chain PCAs that contain >48% chlorine by weight¹⁸⁵. An important question is whether this threshold needs to be adjusted to capture other (mixed) halogenated n-alkanes that may also persist, bioaccumulate and undergo long-range transport. The findings of this study suggest that it would be regrettable to substitute the short-chain PCAs with PXAs that contain 14~21 carbon atoms and a total halogen weight of 10~40%. The DFT results also suggest that PXAs containing fluorine may also pose a greater risk than previously assumed, akin to their better-known chlorinated and brominated analogues.

3.3.4 Potential sources of PXAs to the environment

Not all of the PXAs identified as potential POPs are likely to be synthesized. While mixtures of Cl and Br/Cl alkanes can be synthesized by direct radical halogenation, incorporation of fluorine may require a separate electrochemical fluorination step. A few bromochlorofluoro methanes are used as synthetic precursors and previously as refrigerants, but to our knowledge, no commercial mixtures corresponding to the over 500 BrClF compositions identified in the present study have been introduced to the global market. On the other hand, the chloro, bromo, fluoro, bromochloro, bromofluoro, and chlorofluoro n-alkanes (Cl, Br, F, BrCl, BrF, and ClF groups) are more likely to be constituents of industrial chemical mixtures currently in use.

Of the 36 brominated n-alkanes identified above, two compositions are likely produced in high volume. For example, 1,10-dibromodecane (C₁₀H₂₀Br₂) appears to be used as a starting material for synthesis, and it is listed on the U.S. TSCA. The C₁₂H₂₀Br₆ isomer, 1,1,4,7,10,10-hexabromododecane, is also listed in the TSCA. While its use is

unclear, we note that its cyclic analogue, hexabromocyclododecane (HBCCD) is a widely used flame retardant.

The EPISuite data suggests that none of the fluorinated n-alkanes are POPs. However, when the DFT correction is applied, 25 compositions were flagged. The screening results reported by Muir and Howard⁶⁷ also identified 48 fluorinated n-alkanes on the basis of BCF and atm-HL. The ubiquitous polymer PTFE (Teflon) may well be a source of fluorinated alkanes. Myers *et al.*²¹² have shown that a wide range of saturated and aromatic compounds are generated by thermal degradation of fluoropolymers, which may occur during municipal waste incineration or electronics waste recycling. Similarly, Nakajima *et al.*²¹³ have identified C₁₁₋₂₇ fluorohydrocarbons during the pyrolysis of co-polymers of ethylene and tetrafluoroethylene. There is also evidence that PTFE microplastic particles can transport to the Arctic²¹⁴, but via a different mechanism than is considered in the present study. Fluorinated n-alkanes are used as ski wax. C₁₂H₁₇F₉, C₁₃H₁₇F₁₁, C₁₅H₁₇F₁₅, and C₁₆H₁₉F₁₅ elemental compositions have been identified in snow and soil in Sweden as well as in ski wax samples²¹⁵, but their long-range transport and bioaccumulation potential have not been confirmed.

Commercially available PCTFE is used as a lubricant, but its molecular weight range has not been reported. Its polymer is also widely used and shares the same CAS registry number. Therefore, a comparison between the elemental compositions screened in the present study is not possible. Polybromotrifluoroethylene is also listed in the Canadian DSL and U.S. TSCA. The compositions of these mixtures have not been reported, and they are used in small volumes in the aerospace sector¹⁹². C₁₂₋₃₀ bromochloro alkanes (CAS RN 68527-01-5) have been used as flame retardants for over 30 years¹⁸⁸. Chibwe *et al.*¹⁸⁸

characterized a commercial mixture and determined that its main components are C₁₈ alkanes substituted with 5~8 halogen atoms. For this range of elemental compositions, EPISuite predicted an average logK_{OW} of 11.5. Using the relationship shown in Figure 5a, an estimated logK_{OW} value of 9.2 was obtained, which is in good agreement with the average (logK_{OW}=8.6) measured experimentally. Note that because the experiments of Chibwe *et al.*¹⁸⁸ were performed using octanol saturated with water, the logK_{OW} (wet) measurements were converted to logK_{OW} (dry) values using the relationship described by Beyer *et al.*²¹⁶ Both our calculations and those of Chibwe *et al.* agree that the C₁₈ n-alkanes substituted with 5~8 Cl or Br atoms reside outside the boundaries in Figure 2b. We estimate that the C₁₀₋₁₆ n-alkanes substituted with 2~5 halogen atoms are more likely to behave as POPs.

3.3.5 Is it possible to identify the PXAs using high-resolution mass spectrometry?

Many of the priority PXAs are likely produced in large volumes in industrial processes or from polymer degradation, but their environmental impacts have not been investigated. Analytical methods are urgently needed to identify these chemicals and two mass spectrometry-based strategies have emerged that could potentially be used for this purpose. First, the accurate mass of the molecular ion could be used as an identifier, but it may well be masked by interfering compounds, such as the ubiquitous chlorinated paraffins, which have similar masses. The second approach involves monitoring the loss of halogen atoms that are specific to a PXA class. For example, one can potentially distinguish a bromochloro n-alkane from an isobaric chlorinated n-alkane by monitoring the formation of bromide ions or the loss Br in its collision induced dissociation (CID) mass spectrum. In the

following section, we discuss the potential for mass spectrometry to identify the PXAs confidently.

The full-width-half-maximum mass resolution ($R = m/\Delta m$) required to resolve each of the 966 priority PXAs from all 184,600 elemental compositions, including their isotopic masses, was computed, and this information is summarized in Table 3.5. The results show that only 339/966 (35%) priority PXA elemental compositions can be distinguished from all other possible PXAs with a resolving power 1,000,000. Such experiments may be possible using Fourier transform ion cyclotron resonance mass spectrometry (FT-ICR), but at the same time, the low concentrations of contaminants would make this approach impractical.

However, it is unlikely that all classes of PXAs are present in the environment as potential interferences. The first step to establishing the presence of *mixed* halogenated n-alkanes must be to show that they can be distinguished from the PCAs, which are already ubiquitous.

The calculations show that 714/966 (74%) of the priority PXAs can be distinguished from the most possible interferences, PCAs, at $R=60,000$, a resolving power that is achievable by modern time-of-flight and fourier transform mass spectrometers. This requirement may be relaxed by using chromatographic separation and by confirming the presence of halogens by CID. Of the 714 elemental compositions that can be resolved, 283 belong to the chloro, bromo, chlorobromo, bromofluoro classes, which are the more likely to be present in industrial chemical mixtures currently in use.

Table 3.5 Different category of screened PXAs number separated against category of 184,600 PXA under different resolution. Numerator: the composition number separated; denominator: the total number in the screened category.

		Categories in 184,600 PXAs									
		F	Cl	Br	ClF	BrF	BrCl	BrClF	All*	w/o* BrClF	R (10 ⁴)
Cl	24/27	27/27	18/27	0/27	9/27	1/27	1/27	0/27	0/27	0/27	1
	27/27		23/27	16/27	23/27	18/27	20/27	6/27	6/27	6/27	6
			23/27	27/27	25/27	18/27	21/27	11/27	14/27	14/27	10
			23/27		27/27	18/27	22/27	11/27	14/27	14/27	20
			27/27			21/27	23/27	18/27	21/27	21/27	50
						21/27	26/27	20/27	21/27	21/27	80
					21/27	26/27	20/27	21/27	21/27	100	
Br	22/23	6/23	23/23	0/23	3/23	3/23	0/23	0/23	0/23	0/23	1
	23/23	17/23		11/23	7/23	8/23	4/23	0/23	1/23	1/23	6
		17/23		13/23	9/23	8/23	6/23	2/23	3/23	3/23	10
		23/23		15/23	23/23	8/23	6/23	3/23	8/23	8/23	20
				16/23		8/23	16/23	8/23	8/23	8/23	50
				18/23		8/23	16/23	8/23	8/23	8/23	80
			18/23		8/23	16/23	8/23	8/23	8/23	100	
ClF	83/83	1/83	48/83	0/83	9/83	0/83	0/83	0/83	0/83	0/83	1
		68/83	76/83	40/83	47/83	53/83	34/83	7/83	16/83	16/83	6
		68/83	76/83	54/83	47/83	67/83	37/83	13/83	28/83	28/83	10
		83/83	79/83	83/83	55/83	75/83	37/83	20/83	47/83	47/83	20
			79/83		73/83	76/83	48/83	44/83	66/83	66/83	50
			79/83		73/83	80/83	57/83	45/83	66/83	66/83	80
		79/83		73/83	80/83	59/83	45/83	66/83	66/83	100	
BrF	122/1	1/127	55/12	0/127	3/127	0/127	0/127	0/127	0/127	0/127	1
	27		7								
	127/1	89/12	117/1	15/12	41/12	38/12	0/127	0/127	2/127	2/127	6
	27	7	27	7	7	7					
		105/1	117/1	22/12	41/12	59/12	0/127	0/127	7/127	7/127	10
		27	27	7	7	7					
		119/1	126/1	41/12	116/1	92/12	0/127	0/127	28/127	28/127	20
		27	27	7	27	7					
	127/1	127/1	74/12	127/1	115/1	14/12	14/12	65/127	65/127	50	
	27	27	7	27	27	7	7	7	7		
			96/12		127/1	14/12	14/12	96/127	96/127	80	
			7		27	7	7	7	7		
			96/12			14/12	14/12	96/127	96/127	100	
			7			7	7	7	7		
BrCl	116/1	20/11	71/11	1/119	14/11	16/11	5/119	0/119	0/119	0/119	1
	19	9	9		9	9					

Categories in 184,600 PXAs									
F	Cl	Br	ClF	BrF	BrCl	BrClF	All*	w/o* BrClF	R (10 ⁴)
119/19	82/119	112/19	48/119	91/119	63/119	33/119	6/119	23/119	6
	82/119	112/19	57/119	110/19	63/119	43/119	6/119	31/119	10
	109/19	112/19	69/119	115/19	71/119	46/119	8/119	39/119	20
	109/19	119/19	73/119	115/19	85/119	48/119	14/119	50/119	50
	110/19		100/19	117/19	85/119	62/119	45/119	72/119	80
	119/19		101/19	117/19	85/119	63/119	48/119	80/119	100
BrC IF	587/87	19/87	256/87	0/587	9/587	0/587	1/587	0/587	1
	431/87	532/87	62/87	345/87	223/87	44/87	6/87	23/87	6
	501/87	560/87	120/87	466/87	307/87	56/87	10/87	70/87	10
	565/87	570/87	284/87	494/87	466/87	106/87	25/87	212/87	20
	587/87	584/87	335/87	558/87	566/87	149/87	62/87	307/87	50
		584/87	429/87	579/87	584/87	177/87	153/87	423/87	80
		584/87	482/87	580/87	587/87	189/87	180/87	472/87	100
			87/87	87/87	87/87	87/87	87/87	87/87	

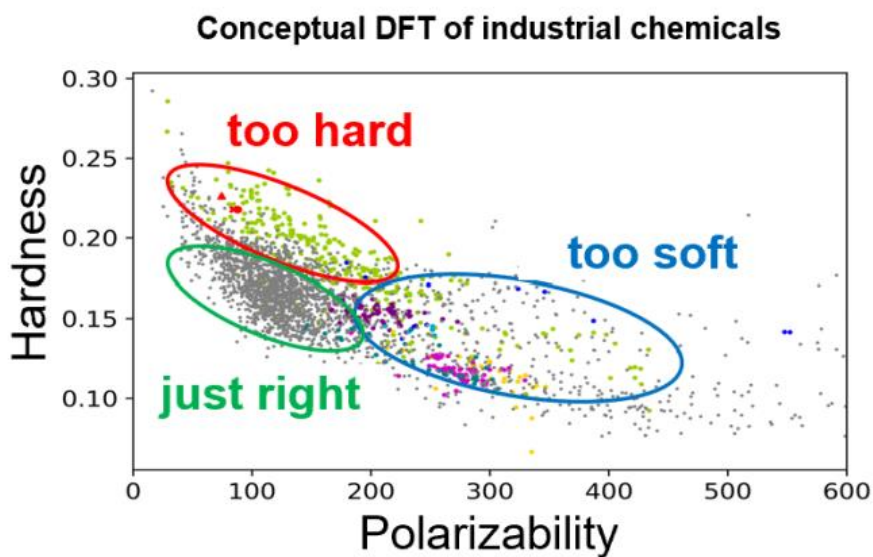
*all: all the 184,600 PXAs; w/o BrClF: BrClF PXAs not included in the pool.

In summary, guided by quantitative structure-property relationship models and DFT, a list of 2333 PXA elemental compositions is prioritized from among 184,600. Armed with a more manageable suspect screening list, environmental chemists are encouraged to search for the PXAs, but they are advised to be cautious about reporting their identification, especially considering authentic standards may not be available. While our study is limited to the PXAs defined as short (C₁₀₋₁₃), medium (C₁₄₋₁₇) and long chain (C_{>17}), we note that very short chain halogenated n-alkanes are also quite important, with compounds

containing between C₆₋₉ reported in 94% of wildlife samples from the Yangtze River Delta²¹⁷. We also expect that the behaviour of many of the chlorinated and brominated n-alkanes prioritized in the present study will be akin to that of the PCAs, and thus the sampling, extraction and analysis strategies designed for PCAs may well be effectively repurposed²¹⁸. Adipose tissue is an ideal sample type when searching for most POPs. Some may question whether fluorine-containing compounds will accumulate in lipid because the inclusion of fluorine has the effect of increasing a compound's lipophobicity. However, we note that all PXAs identified in the present study fall between logKow 3.5 and 8.5. Blood may be a more attractive sample type to search for fluorine-containing PXAs. The pioneering work by Yeung *et al.*²¹⁹ has shown that known per- and polyfluorinated compounds account for only a small fraction of the total organofluorine contaminants in human blood. Semifluorinated alkanes are extractable from aqueous matrices using cyclohexane-water extraction and the same approach may be used to test the hypothesis as to whether fluorine-containing n-alkanes are present in blood⁴⁷.

Chapter 4

"Forever chemicals" chemicals are either too hard or too soft: Conceptual density functional theory as a screening tool for emerging pollutants



4.1 Introduction

Global chemical production is accelerating and is expected to double by 2030²²⁰, and the number of new chemical substances being introduced to the global market is also increasing²²¹. Sustainable strategies are increasingly being adopted to design safer, more sustainable chemicals²²¹. Inventories of anthropogenic chemical substances have been created to help manage the risks of chemical pollution. Nevertheless, challenges such as incomplete or confidential information on their manufacture/use and unknown transformation products from (a)biotic processes have hindered the identification of anthropogenic chemicals present in the environment²²².

Parties to the Stockholm Convention have agreed to ban or limit the release of 31 groups of persistent organic pollutants (POPs) that have the potential to be persistent (P), bioaccumulative (B), toxic (T), and undergo long-range transport (LRT) to remote regions far from their source²²³. However, computational studies of environmental fate have shown that the actual number of PBT-LRT chemicals is likely in the thousands^{7,205,224,225}. In the same vein, emerging contaminants continue to be discovered using nontargeted screening^{5,225,226}. Perfluorooctanoic acid (PFOA), Perfluorooctane sulfonic acid (PFOS), and Perfluorohexane sulfonic acid (PFHxS), are examples of pollutants targeted by the Stockholm Convention, while >14,735 structurally similar per- or polyfluoroalkyl substances (PFAS)²²⁷ have yet to be investigated for their potential impacts on the environment and human health.

The development of proactive regulations that identify chemical hazards before they become global pollutants is essential in order to solve this problem. Consequently, there is

an urgent need to gain new insight into the fundamental chemical properties that determine a chemical's environmental fate, which can guide the development of better, more comprehensive environmental monitoring and risk assessment strategies. Previous studies^{7,8,205,228} have focused on prioritizing chemical hazards using models based on partitioning coefficients between air, water, and octanol, as well as bioaccumulation /bioconcentration factors and half-lives in the atmosphere and/or water. These properties are often predicted through quantitative structure-activity relationships (QSAR), but a limitation is the paucity of experimental data used to train these models. As a result, significant uncertainties are introduced when trying to predict the behaviour of novel chemicals when similar structures are absent from the training set.

One way to circumvent the absence of experimental data is to employ computational methods such as density-functional theory (DFT)²²⁹⁻²³¹, which allow accurate prediction of chemical properties ab initio. A prime example²⁷ concerns the halogenated n-alkanes, ubiquitously used as flame retardants, lubricants, plasticizers, and additives in paints, sealants, and adhesives. Standard risk assessment approaches to inform current regulations suggest that such compounds having >48% by weight of chlorine and between 10 – 13 carbon atoms are hazardous. DFT analysis of the halogenated n-alkanes revealed that compounds with >13 carbon atoms and 10-48% by weight of halogens, including bromine and fluorine, may be equally harmful to the environment.

DFT hinges on the idea that electron density is the fundamental quantity that determines the energy and structure of a molecular species²²⁹⁻²³¹. The Hohenberg-Kohn theorem and extensions show that all properties of a chemical system can be determined from the electron density. In 1983, Parr and Pearson²³² bridged the gap between DFT and

classical chemical concepts with the realization that the first derivative of the energy with respect to the number of electrons (N) corresponds to the Mulliken electronegativity (χ). Thereafter, quantitative measures of hardness (η), and its inverse softness (σ), that underlie the hard-soft acid-base principle were determined from the second derivative of the energy with respect to N . These discoveries heralded the birth of conceptual DFT (CDFT)^{11,13,233,234}, which provides mathematically rigorous chemical insight into the behaviour of chemical systems; the prediction of molecular properties; and the discovery of general "rules of thumb" applicable to a broad range of chemical reactions across inorganic and materials chemistry, organic and polymer chemistry, physical chemistry, and biochemistry²³⁵.

CDFT reactivity descriptors could potentially be used to determine a chemical's environmental fate. Electrophilicity measures the second-order energy of an electrophile saturated with electrons²³⁶, and it can reflect a molecule's structural and bonding properties, and its stability. Electrophilicity has been recently used for toxicity and biological property prediction¹⁹. The polarizability (α) of a molecule, i.e., the linear response of a molecule acquiring an electric dipole moment (three-dimensional electron density distribution) in an applied electric field, is proportional to its softness²³⁷. The work of Hati and Datta provide a cube root relationship¹⁶. The work of Vela and Gazquez²³⁸ along with the work of Ghanty and Ghosh²³⁷ suggests that softness and polarizability are related through the Fukui function as was also suggested in the work of Stott and Zaremba²³⁹. The Fukui function is the CDFT generalization of Frontier Molecular Orbital Theory (FMO)^{18,20,240-242}. In other words, it is the valence electrons, particularly the behaviour of the highest occupied molecular orbital (HOMO) and the lowest unoccupied molecular orbital (LUMO), that can

cause two molecules with the same hardness/softness to have different polarizabilities. According to the Maximum Hardness Principle, as hardness increases, the stability of the molecule increases. Polarizability is important in predicting intermolecular and molecule-field interactions, and it has been used to predict the subcooled vapor pressure²²⁷, octanol-air partitioning coefficient^{229, 23}, and octanol-water partitioning coefficient²².

4.2 Computational methods

4.2.1 Chemical lists

In order to evaluate the potential for CDFT descriptors to predict P, B, and LRT potential for various chemicals, values for substances with high and low environmental hazard levels were computed and compared in this study. Two chemical databases were selected, viz. the Canadian Domestic Substances List (DSL)¹ and the U.S. Toxic Substances Control Act (TSCA) inventory². The DSL and TSCA lists contain the substances manufactured in or imported into Canada or the United States on a commercial scale, respectively. Together, the DSL and TSCA consist of ~17,400 chemical substances with duplicates removed, and these chemicals are referred to as the "DT" list hereafter. Among these chemicals, previous environmental fate modeling studies²²⁵ have identified 3,360 substances that may be persistent, bioaccumulative, and undergo long-range transport using QSAR-based models. These include chemicals prioritized by the Arctic Monitoring and Assessment Programme (AMAP) and the Stockholm Convention. The prioritized chemicals are hereafter referred to as the "POPs" list.

4.2.2 Chemical property calculations

To conserve computing resources, 2624 chemicals were randomly selected from the DT list based on the mass distribution, and all the substances in the POPs list were calculated. A guess geometry of each compound was generated using OpenBabel²⁴³. Density functional theory was used to optimize ground state geometries of the neutral molecule and compute its total energy (E_N) at the B3LYP²⁴⁴⁻²⁴⁷/6-311+G**²⁴⁸⁻²⁵¹ level of theory using Gaussian 16²⁰¹. Total energies of the radical anion (E_{N+1}) and radical cation (E_{N-1}) were then computed using the optimized structure obtained at the B3LYP/6-311+G** level for the neutral molecule (E_N). According to Koopmans' theorem²⁵², the adiabatic ionization energy (IE) is approximately the negative energy of the highest occupied molecular orbital (E_{HOMO}), and the negative of electron affinity (EA) is approximately equal to the lowest unoccupied molecular orbital energy (E_{LUMO})²³⁵. While the Fukui function can be used to approximate the HOMO-LUMO gap²⁵³, we chose to use the fundamental gap for descriptor calculation because the accuracy of the B3LYP/6-311+G** method is well characterized for IEs and EAs²⁵⁴⁻²⁵⁶. The IEs and EAs were computed from the following equations:

$$IP = E_{N-1} - E_N \quad (1)$$

$$EA = E_N - E_{N+1} \quad (2)$$

The DFT descriptors were then derived as follows:

$$\text{hardness } (\eta) = (IP - EA) / 2 \quad (3)$$

$$\text{softness } (\sigma; \text{ the inverse of hardness}) = 1 / \eta \quad (4)$$

$$\text{electronegativity } (\chi) = - \text{ chemical potential } (\mu) = (I + A) / 2 \quad (5)$$

$$\text{electrophilicity index } (\omega) = \chi^2 / 2\eta \quad (6)$$

$$\text{Polarizability } (\alpha) = (\alpha_{xx} + \alpha_{yy} + \alpha_{zz})/3 \quad (7)$$

(α_{xx} refers to the x components of polarizability, i.e., the perturbation in the x- coordinates when a coordinate system is put at a molecule's original position. The averaged three-dimensional polarizability is calculated with the assumption that the molecule is spherical.). 2363 and 2825 chemicals were successfully calculated in DT and POPs lists, respectively. The calculations that failed were excluded from this study. The complete data set is available from the authors upon request.

The CDFT approach is more computationally demanding than QSAR-based models, but it does not require previous experimental data to evaluate the risk of novel chemicals. It is also less demanding than predicting partitioning coefficients using DFT¹⁹⁹. Whereas the latter requires geometry optimization of three structures, the CDFT approach only requires one. Overall, the 5188 compounds computed in this work required approximately 1 core hour per compound. Such calculations are ideally performed in parallel using a computing cluster.

4.2.3 Data analysis

In order to investigate the major variations between POPs and those with no or less persistent potential, a T-test was performed using Microsoft office EXCEL with two-tailed distribution and heteroscedastic variance. The two-dimensional spaces formed by the above parameter couples were drawn to differentiate between the two lists. DFT descriptor combinations were plotted and compared to visualize the difference. 100 chemicals randomly selected from each list (not included in space plotting) were used as a validation set for the thresholds derived from these parameters. A principal component analysis (PCA) was also performed to better assess the potential of DFT descriptors in environment

behavior prediction. 70% of chemicals in the two lists were used as training sets, and the left 30% were used as test sets. Precision, accuracy, and F1 score were calculated. The PCA and its result merits were performed using the Python Scikit-learn package.

4.3 Results and discussion

Differences between suspected POPs and chemical substances not prioritized by standard environmental risk assessment methods were evaluated using a heteroscedastic T-test performed with a two-tailed distribution. The distribution of hardness, global electronegativity, electrophilicity index and polarizability are shown in Figure 4.1. (Softness and chemical potential are not discussed here since they are inversely related to hardness and global electronegativity). Most known and suspected POPs contain electronegative halogens, but there was no significant difference between the mean global electronegativity values of the POPs and DT lists (P-value of 0.08). On the other hand, there are significant differences in hardness, electrophilicity and polarizability, with t-test P-values approaching zero ($p < 0.0001$). In other words, known and suspected POPs appear to be characterized by high polarizability and electrophilicity, and are relatively "soft". This is consistent with most compounds on the POPs list containing polarizable atoms such as Br and Cl.

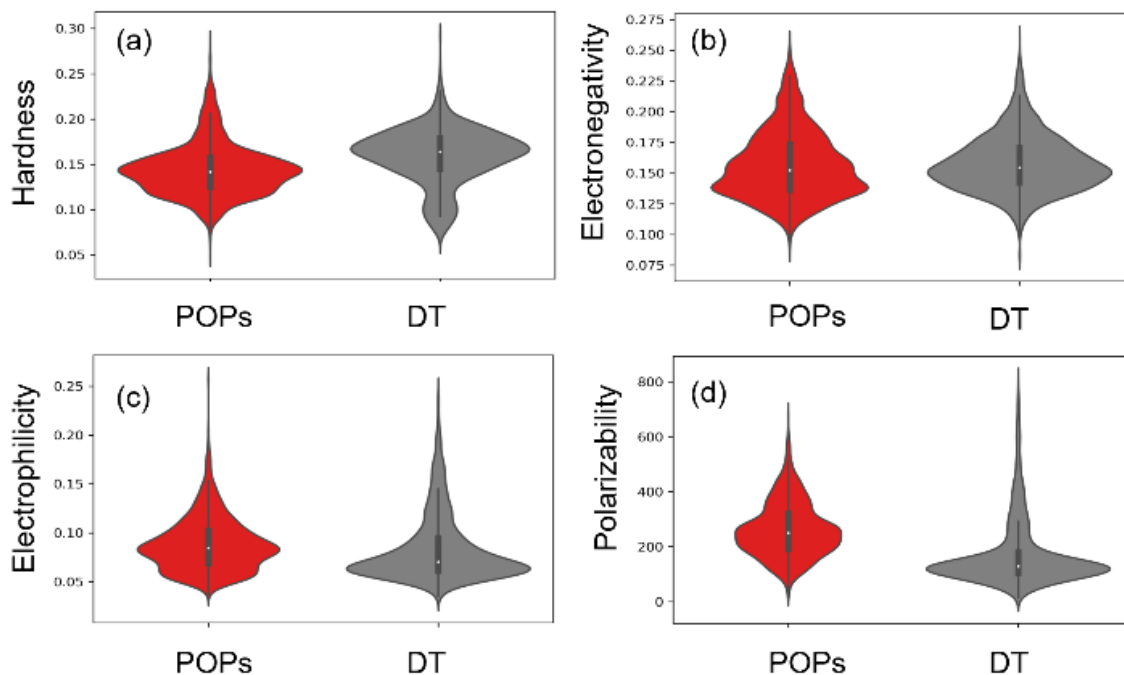


Figure 4.1 Distribution of CDFT descriptors among suspected POPs (red) and all industrial chemicals (grey): (a) Hardness; (b) Global electronegativity; (c) Electrophilicity; (d) Polarizability. The white dot indicates the median value. The 1st and 3rd quartile values are indicated by the grey box, and the vertical line indicates the 95% confidence interval.

The two-dimensional spaces formed by pairs of CDFT descriptors were graphed to differentiate between the two lists, see Figure 4.2. A persistent chemical is unreactive, and thus one might assume that many would be characterized by a relatively large E_{HOMO} and E_{LUMO} gap, which would also correspond with high hardness. However, as shown in Figure 4.2(a), the POPs span the entire range of hardness, and we were unable to find a clear relationship between persistence and CDFT metrics. Greater insight is provided when the POPs are categorized into different classes, including polybrominated diphenylethers

(PBDEs), polychlorinated biphenyls (PCBs), per-/polyfluoroalkyl substances (PFAS), polycyclic aromatic hydrocarbons (PAH), and organophosphate esters (OP).

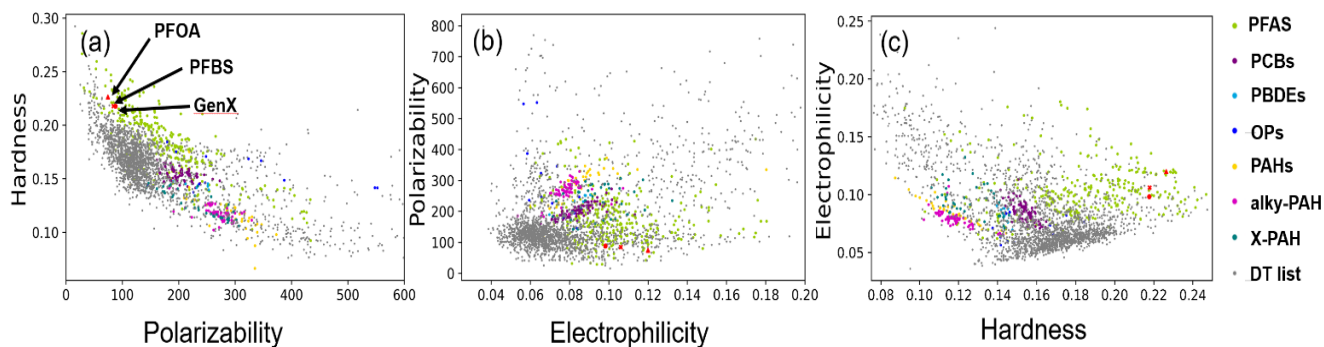
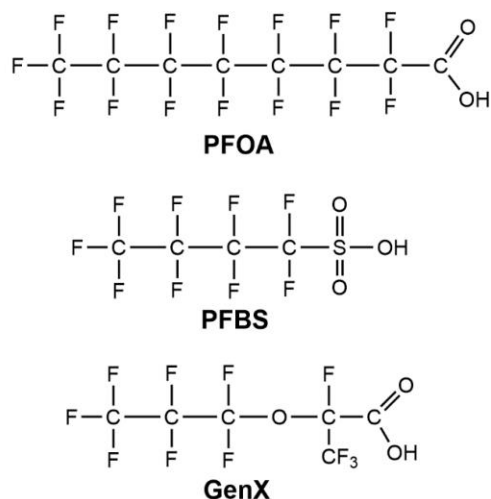


Figure 4.2 Chemical space defined by CDFT properties: (a) Polarizability and Hardness; (b) Electrophilicity and Polarizability (c) Electrophilicity and Hardness. Known or suspected POPs over various classes are coloured. All remaining compounds on the DT list are in grey.

One observes that PFAS are characterized by high hardness, low polarizability, and high electrophilicity. In contrast, all other classes of chlorinated, brominated and non-halogenated POPs are characterized as relatively soft and polarizable. These observations are consistent with the work of Damoun *et al.*²⁵⁷, which demonstrated that the softness of the fluorinated methyl group will decrease with the increase of fluorinated atoms incorporated. In contrast, they observed the reverse trend with increased chlorine substitution.

In the present study, among the 226 chemicals with hardness >0.20 Ht, 109 (48%) are known or suspected POPs, and 165 (73%) contain fluorine atoms. We therefore suggest as a general rule of thumb that compounds characterized by a hardness value that exceeds

0.20 Ht are likely per/polyfluorinated POPs. Only 106 (49%) fluorinated compounds that exceed this threshold have been previously prioritized as known or suspected POPs.



Scheme 4.1 Selected PFAS with hardness value > 0.20 Ht

The perfluorocarboxylic acid PFOA shown in Scheme 1 is a prototypical example. The remaining 59 include concerning compounds like perfluorobutane sulfonic acid (PFBS)²⁵⁸ and hexafluoropropylene oxide dimer acid, which is known by its trade name GenX²⁵⁹ see Scheme 4.1. That GenX and PFBS are recognized as potential POPs based on their hardness may serve to illustrate the drawback of relying on QSAR-based risk assessment.

The position of a compound in Figures 4.1(a-c) may also reflect the mechanism by which it bioaccumulates. Hard PFAS are more likely to accumulate on proteins instead of lipids in organisms, and the serum albumin protein plays a primary role in transporting PFAS within the human body²⁶⁰. This implies that the hardness of a PFAS could partly explain its affinity for a protein. To our knowledge, there is no report on the overall

hardness of natural proteins, but hard-soft acid-base theory has been used to rationalize ion-amino acid interaction in (engineered) proteins²⁶¹. Zhang *et al.*²⁶² have shown that binding of (PFCAs depends not only upon hydrogen bonding interactions with the carboxylate, but also intermolecular forces between the fluoroalkyl chain and the non-polar side-chain of surrounding amino acids, *viz.* Leu, Ile, Met, and Phe. This is why the binding affinity of PFCA homologues to serum albumin increases with the number of CF₂ units, until the number of carbons exceeds 11 and the molecule can no longer easily fit in its binding pocket^{263,264}. Within the binding pocket, the fluorocarbon chain will make contact with a range of protein atoms. Zhou *et al.*²⁶⁵ estimate that interactions between C-F and protonated nitrogen atoms are among the most frequent, and the resulting hydrogen-bridged fluorine bond, C-F---NH₂⁺-R, is among the most stable, enjoying ~10 kcal/mol stabilization. The underlying strength of this non-covalent fluorine²⁶⁵ bond is likely electrostatic in nature, involving the C-F dipole interacting with the positive charge on NH₂⁺-R. This interaction may explain the preference for some PFAS to accumulate on proteins and not in lipid. We also note that the binding affinity between PFAS and proteins also depends a protein's structure, which may explain why PFAS bind to certain proteins and not others²⁶⁶.

When constrained to a narrow range of polarizability values (between 75 and 125 Å³), one observes a positive correlation between hardness and bioconcentration factor (BCF), a metric often used to prioritize suspected POPs^{7,205}, see Figure 4.3. We note that most compounds above our suggested threshold of 0.2 Ht are also characterized by logBCF values greater than 3.7.

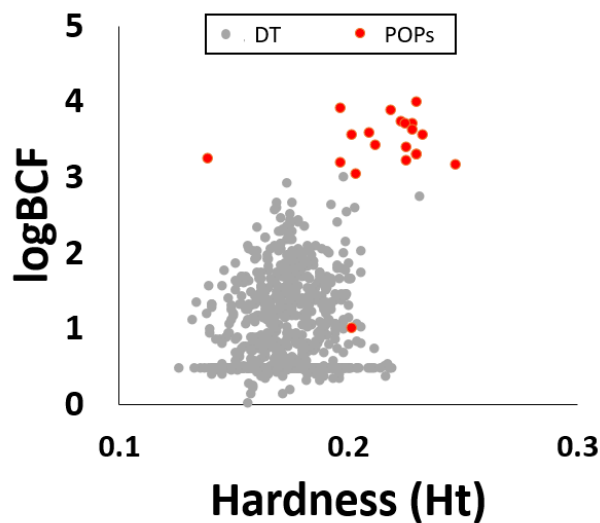


Figure 4.3 Hardness (Ht) vs. the logarithm of the Bioconcentration Factor (BCF) predicted by EpiSuite. Known or suspected POPs are coloured red. All remaining compounds on the DT list are in grey.

That the remaining classes of POPs are characterized by low hardness and high polarizability is also consistent with how they bioaccumulate. Since lipophilicity is positively related to polarizability⁵¹, POPs with larger polarizability tend to be lipophilic and have a preference for lipid fractions of organisms. For a lipophilic compound to bioaccumulate, it must adapt to both aqueous environments that facilitate exposure and consumption of the toxicant, as well as the non-polar environment of lipid tissue. We observe that 86.0% (1636/1903) of lipophilic POPs are characterized by a polarizability value greater than 200 \AA^3 . In the same vein, 65.9% (781/1186) of non-halogenated chemicals suspected of PBT-LRT behaviour are also characterized by computed polarizability values larger than 200 \AA^3 (Figure 4.2). Unlike the fluorinated compounds, few of the non-halogenated compounds exceed hardness values of 0.20 Ht.

PCA (principal component analysis) was employed to obtain a more refined prediction model. 70% of chemicals in the DT/POPs lists were randomly selected and used as training sets, and the remaining 30% were used as test sets. This analysis was performed using the Python Scikit-learn package. The results showed that principal components 1 and 2 account for 48.7% and 43.3% of the variance, respectively. Principal component 1 is mainly determined by hardness, the negative of polarizability and global electronegativity; principal component 2 is primarily due to global electronegativity and electrophilicity index, as shown in Figure 4.4 (b). The covariance matrix showed that the two principal components are uncorrelated but don't have unit variance. When applied to a randomly selected test set, the statistics yield a training accuracy of 88.8%, a validating accuracy of 83.3% and an F1-score of 0.86. While the PCA model is promising, its accuracy (c. 80%) is only marginally better than when the polarizability $>200 \text{ \AA}^3$ and hardness $>0.20 \text{ Ht}$ thresholds are used, which result in a training accuracy of 75.0% and a validating accuracy of 75.2%.

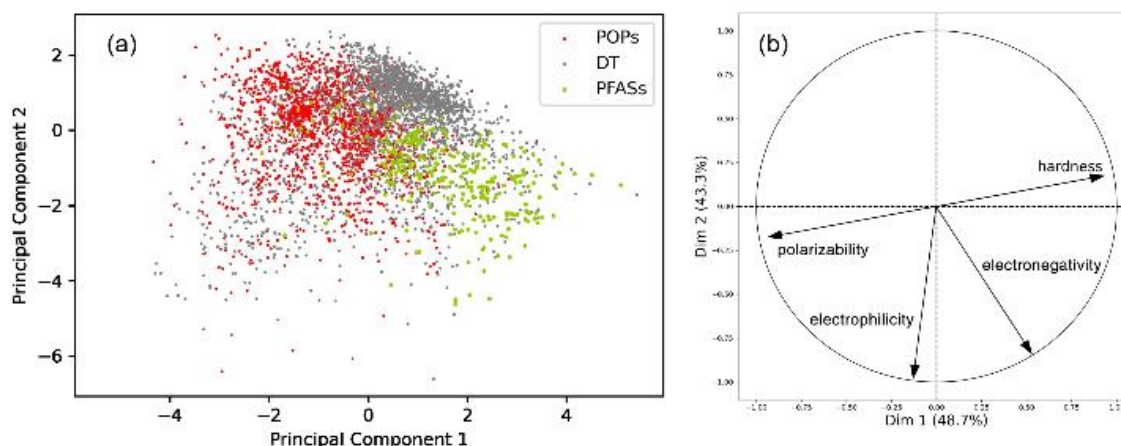


Figure 4.4 (a) Scores plot and; (b) loadings plot obtained by PCA. Note: POPs have been split into PFAS and all remaining POPs.

In summary, we calculated polarizability, electrophilicity index, global electronegativity and hardness for a wide range of industrial chemicals and linked these descriptors with environmental fate. The results show that different classes of pollutants occupy discrete regions in the spaces formed by polarizability, hardness and electrophilicity. The PCA analysis showed that these parameters could be good indicators of the PBT potential of a chemical. However, a threshold of polarizability $> 200 \text{ \AA}^3$ and/or a hardness $> 0.21\text{Ht}$ can work as preliminary assessment criteria.

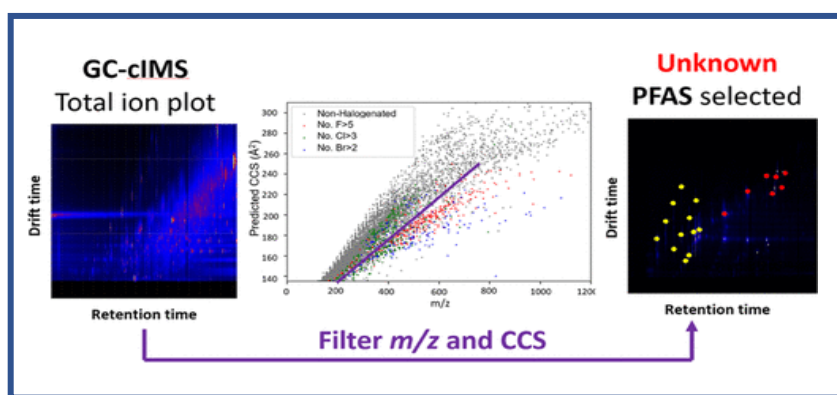
These parameters can be employed to establish other predictive models aimed at determining the future persistence and environmental consequences of chemical and can serve as a preventive measure to discourage the development of novel chemicals with inherent high-risk properties within the industry. The utilization of similar modeling techniques and machine learning approaches could potentially be expanded to address other environmental challenges, including long-distance transport. We note that these values may shift if a different level of level of theory, or if frontier molecular orbitals were used to compute the HOMO-LUMO gap. The deviation between experimental and computed $\text{IE}/\text{EA}^{254}$ is expected to be on the order of 0.01-0.02 Ht, and we suspect that the uncertainty of our proposed hardness threshold (0.20 Ht) will be similarly small [± 0.01 Ht ($\pm 5\%$)]. However, the conclusion that bioaccumulative chemicals are either too hard or too soft would not change.

The purpose of this study was to explore the potential of CDFT in environmental fate prediction of a chemical, and the results have provided us with a new "rule of thumb" to guide risk assessment of chemical hazards. These intriguing results appear to align with the bioaccumulation mechanism of suspected POPs, namely that "soft" chemicals

accumulate in lipids, whereas "hard" chemicals are more likely to accumulate via a different mechanisms, such as protein binding. Based on the study's findings, it is crucial to exercise caution while designing, manufacturing, or using chemicals that are excessively hard or soft. These chemicals are suspected persistent organic pollutants and may pose potential risks to the environment and human health.

Chapter 5

Gas chromatography-(cyclic) ion mobility mass spectrometry: a novel platform for the discovery of unknown per-/polyfluoroalkyl substances



*Adapted with permission from MacNeil, A.[#]; Li, X.[#]; Amiri., R.; Dorman, F. L.; Kleywegt, S.; Simpson, A.; Simpson, M. J.; Jobst, J. K. Gas chromatography-(cyclic) ion mobility mass spectrometry: a novel platform for the discovery of unknown per-/polyfluoroalkyl substances. *Analytical Chemistry* 2022 94 (31), 11096-11103. Copyright 2022 American Chemical Society.

5.1 Introduction

Non-targeted screening (NTS) is a contemporary name used to describe experiments designed to identify unknown organic pollutants⁷¹. This is not a new question as some of the earliest NTS experiments were performed over 40 years ago²⁶⁷. The first detection in human blood of perfluorooctanoic acid (PFOA), a ubiquitous and infamous persistent organic pollutant (POP), is a prime example. In 1976, Guy *et al.*²⁶⁸ reported on their pioneering nuclear magnetic resonance (NMR) experiments that revealed the presence of PFOA and at least two more structurally similar compounds, *viz.* perfluorooctane sulfonic acid (PFOS) and its perfluorohexane homologue PFHxS. A drawback of this approach however is the enormous sample size required for NMR analysis, which exceeded 10 L of blood at that time. Targeted monitoring of PFOA and PFOS with practical quantities of biological and environmental media would eventually be achieved using liquid chromatography-tandem mass spectrometry (LC-MSMS)²⁶⁹ and this ultimately led to the realization that PFOS and PFOA contamination is widespread. These so-called "forever" chemicals are present in the blood of virtually every human and animal²⁷⁰. Consequently, signatories of the Stockholm Convention²²³ have imposed restrictions on the emission and production of PFOA, PFOS and PFHxS in 2004, 2009 and 2017 respectively, and these efforts are reflected by the steady decline of their blood concentrations more recently. Despite this success, the number of structurally similar perfluoroalkyl substances (PFASs) introduced to the global market has rapidly outpaced research on their potential health and environmental impacts and there are still over 12,000 other PFAS of interest to researchers that have evaded study and regulation²²⁷. This knowledge gap has driven analytical chemists to create new NTS strategies to identify unknown POPs and PFASs²⁷¹.

A renaissance in NTS has in part been enabled by increased accessibility to high resolution mass spectrometry (HRMS)²²², with modern instruments capable of sensitive detection of (tens of) thousands of chemical compounds. The wealth of data collected in an HRMS experiment will undoubtedly help accelerate the pace of contaminant discovery, but the challenge of recognizing an undocumented POPs from among the many thousands of co-extracted matrix ions is daunting, akin to finding a needle in a haystack²⁷². Inspired by the work of Kendrick and Hughey *et al.*²⁷³ practitioners of NTS now routinely use mass defect plots²⁷⁴ to help disentangle highly complex mass spectra and guide the search for homologous fluorinated²¹², brominated²⁷⁵, and chlorinated²⁷⁶ POPs, characterized by a negative mass defect. This has led to the identification of previously unknown (mixed) halogenated POPs in a wide range of environmental media, including freshwater²⁷⁶ and marine biota^{277,278}, air²⁷⁹, and dust²⁸⁰. Unlike chlorinated and brominated compounds that display characteristic isotope patterns, polyfluorinated compounds ions are more difficult to recognize because ¹⁹F exists as a single stable isotope. Zhang *et al.*⁵ suggest that the ¹³C/¹²C ratio could be diagnostic as a PFAS will always have fewer carbon atoms compared to non-halogenated compounds of similar mass. However, this method hinges on the detection of ¹³C isotopic peaks that are of relatively low abundance.

A promising approach for the discovery of PFASs and other halogenated compounds harnesses ion mobility^{30,65,281}. During its travel through an ion mobility cell, an ion will undergo non-reactive collisions with nitrogen (or helium), impeding its mobility and increasing its drift time and relative separation to other ions. An ion's mobility is related to its size, shape, and charge, which may be approximated by its collision cross section (CCS)²⁸². Compared to non-halogenated organic molecules of similar mass, PFASs

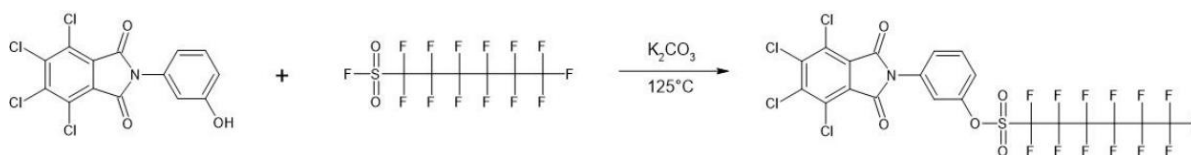
are relatively compact, consisting of fewer atoms and consequently having relatively small CCSs and high molecular density³⁰. We hypothesize that this difference is sufficiently universal to distinguish PFASs from non-halogenated compounds on the basis of the ratio of an ion's mass and CCS, which correlates to its density. In this work, we have modeled the CCSs of approximately 20,000 industrial chemicals listed on the Canadian Domestic Substances List (DSL) ¹ and the U.S. Toxic Substances Control Act Inventory (TSCA)² with the aim of creating a method that can select unknown PFASs. To evaluate this approach, we have applied this method to a well characterized standard reference material of indoor dust (SRM 2585) in which the occurrence of PFASs has been characterized by several NTS methods. With few exceptions^{5,212}, virtually all NTS studies of PFAS have been performed using liquid chromatography²⁷¹. In the present study, we demonstrate that gas chromatography, hyphenated with a novel cyclic ion mobility mass spectrometer (GC-cIMS)⁴² is complementary to traditional efforts to identify PFASs that are less polar than PFOA and PFOS. When applied to 20 indoor dust samples, we show for the first time that polyfluorochloro n-alkanes are contaminants of the indoor environment.

5.2 Experimental Methods

5.2.1 Chemical Standards

8:2 fluorotelomer alcohol (8:2 FTOH), N-methylperfluorooctane sulfonamide (N-MetPFSM) and N-methylperfluorooctanesulfonamidoethanol (N-MetPFOSE), were obtained from Wellington Laboratories (Guelph, Ontario). Zhang *et al.* reported the tentative identification of a series of mixed chlorofluoro flame retardants in NIST SRM 2585. To confirm their identities, one compound in the series was synthesized. Briefly, tetrachloro-2-(3-hydroxyphenyl)isoindole-1,3-dione (2 μmol) was combined with

anhydrous potassium carbonate (4 μmol) in 5 mL of acetonitrile, and refluxed for 30 minutes. Pefluorohexanesulfonyl fluoride (2.4 μmol) was subsequently added, and the resulting mixture was analyzed by GC-cIMS. Technical mixtures of polyfluorochloro n-alkanes, Halocarbon oil 27 and 700, were purchased from Sigma-Aldrich and stock solutions (406.7 and 434.5 $\mu\text{g mL}^{-1}$, respectively) were prepared in 10 mL of hexane.



Scheme 5.1 Synthesis of Cl/F-1

5.2.2 Instrumental analysis

Gas chromatography-cyclic ion mobility mass spectrometry (GC-cIMS) experiments were performed using a Waters Cyclic ion mobility mass spectrometer (Wilmslow, UK) coupled to an Agilent 8890 Gas chromatograph using Atmospheric pressure chemical ionization (APCI). Analyte separation was performed with a rtx-5 column (30 m \times 0.25 mm \times 0.25 μm). The initial temperature was set to 90 $^{\circ}\text{C}$; the oven was then ramped to 325 $^{\circ}\text{C}$ at 8.4 $^{\circ}\text{C}/\text{min}$, and then held for 6 minutes. Sample extracts and standard solutions (1 μL) were injected in the splitless mode. The inlet temperature was set to 280 $^{\circ}\text{C}$ and the helium carrier gas flow was set to 1.4 mL/min. GC eluant exiting the column was swept through the ion volume using a make-up flow of nitrogen (\sim 99.99% purity) of 350 mL/min. Atmospheric pressure chemical ionization was initiated by a corona discharge (3 μA) in both positive and negative ion modes. The source conditions were as follows: source

temperature, 150 °C; sampling cone, 40V; extraction cone, 10V; cone gas, 175 L/hour; auxiliary gas, 100 L/hour. Column bleed ($C_9H_{27}O_5Si_5^+$ - m/z 355.0705) and background ions ($C_{16}H_{31}O_2^-$ - m/z 255.2324 and $C_{18}H_{35}O_2^-$ - 283.2637) were used to internally correct the measured m/z in the positive and negative ion modes respectively. Mass spectra were collected for m/z 50 – 1200. The cyclic ion mobility cell was operated in the single pass mode, with a separation time set to 2 ms and a traveling wave height of 22 V. The separation time was increased to 140 ms to subject selected Cl/F-phthalimide ions through 10 passes through the cyclic ion mobility cell. Calibration of the instrument to measure CCS was performed according to standard procedure using a mixture of 22 compounds (aka, "major mix") supplied by Waters Corp.

5.2.3 Chemical Databases and CCS Prediction

CCSs of 17,428 industrial chemicals compiled in the DSL and TSCA inventory were predicted using AllCCS. AllCCS is a machine-learning based program⁵⁷ which predicts CCS values from SMILES (simplified molecular input line entry system) structures. GC-APCI typically yields M^{++} and $[M+H]^+$ ions, but we have only computed ions of the latter form because predictive models do not yet exist for radical cations. The error introduced by this assumption is relatively small when identifying broad regions of m/z vs. CCS space that enclose PFAS. For selected chlorofluoro phthalimides tentatively identified in SRM 2585, MobCal mpi was employed to predict the CCS of the M^{++} molecular ions using trajectory method (TM). Optimized geometries of selected conformers were obtained using DFT calculations at the B3LYP/6-31++G(d,p) level of theory using Gaussian G.16²⁰¹. The python module provided by Ieritano *et al.*⁵⁸ was used to prepare input files and the CCS calculations.

5.2.4 Indoor Dust Samples

SRM 2585 was purchased from the National Institute of Standards and Technology. Indoor dust was also collected from floor sweepings and vacuum bags from 6 locations on the campus of Memorial University. These locations included Arts and Administration (A), Science (SN), Education (ED), Chemistry-Physics (C), Engineering (EN), and several different locations in the new Core Science Facility (CSF). Construction of CSF began in 2015 and is currently open for operation while still undergoing renovations. The other buildings were built in the 1960s and 1970s. To extract the samples, approximately 2g of dust sonicated for 30 minutes each in 5 mL of hexane, 5 mL of acetone, and 5mL of 1:1 methanol/acetonitrile. The extracts were concentrated to dryness and reconstituted into 100 μ L of hexane.

5.2.5 Data Processing

GC-cIMS contour plots were created in DriftScope (v. 3.0) and Progenesis QI was used to obtain experimental ^{13}C CCS_{N2} values of unknowns. The selection tool in DriftScope was used to filter GC-cIMS contour plots and reveal (unknown) PFASs. Kendrick mass defect (KMD) plots, originally conceived by Hughey *et al.*²⁷³, were constructed using the CF₂CFCI mass²¹². In brief, the accurate mass of an ion is multiplied by 116/115.9641, and the difference between its nominal and exact mass (*i.e.*, the apparent mass defect) is then plotted against the accurate, unmodified mass.

5.2.6 Quality Assurance and Quality Control.

Table S5.1 summarizes the proposed structures of PFASs detected in SRM 2585, a reference material widely available to other practitioners of NTS. The accurate mass and isotope ratios of the (quasi)molecular ions of all proposed identifications fall within 5 ppm

and +/- 10% of the theoretical values. Confidence in these assignments is characterized using the 5-level scale proposed by Schymanski *et al.*²⁸³ Briefly, level 1 indicates that the structure has been confirmed using an authentic reference standard in our laboratory. Level 2 indicates that there is evidence to support the exact structure proposed, but it has not been confirmed. Level 3 indicates that the proposed structure is not exact, and there are other possible isomers (*i.e.*, positional, stereochemical) that cannot be excluded using available information. Level 4 indicates that the molecular formula can be assigned with confidence, but there is no evidence to support specific structure proposals. All compounds reported herein are present at concentrations that exceed those in the method blanks by >10-fold.

5.3 Results and Discussion

5.3.1 Differentiating polyfluorinated and non-fluorinated compounds based on m/z and CCS

An ion's mobility and the CCS derived therefrom may be used akin to chromatographic retention time, or retention index, to confirm the identity of a chemical pollutant^{65,282}. This has led to the creation of libraries of experimental and predicted CCS⁵⁷. However, a drawback of this approach is that such libraries will always be incomplete because they neither account for (bio)transformation and degradation that may eventually occur during a chemical's lifecycle, nor that many substances are highly complex, poorly characterized mixtures²⁰⁵. A complementary approach is to use CCS as a metric to triage detected compounds for further characterization and investigation, rather than the confirmatory role it is more routinely used for. The analyst, when confronted with a large mass spectrometry data set, may wonder which of the many thousands of compounds detected are PFASs?

Figure 5.1(a) provides a hypothetical example: it displays c. 20,000 m/z and CCS values predicted from chemicals listed on the Canadian DSL and US TSCA inventories. No "real-world" sample is expected to contain all industrial chemicals, but this exercise may serve to demonstrate how PFAS and other halogenated pollutants occupy a unique region of chemical space defined by m/z and CCS. Indeed, chemicals containing >5 F, >3 Cl and >2 Br atoms respectively are characterized by relatively small CCSs compared to other compounds with a similar mass. Consequently, these polyhalogenated compounds tend to occupy the bottom edge of the data set in Figure 5.1(a).

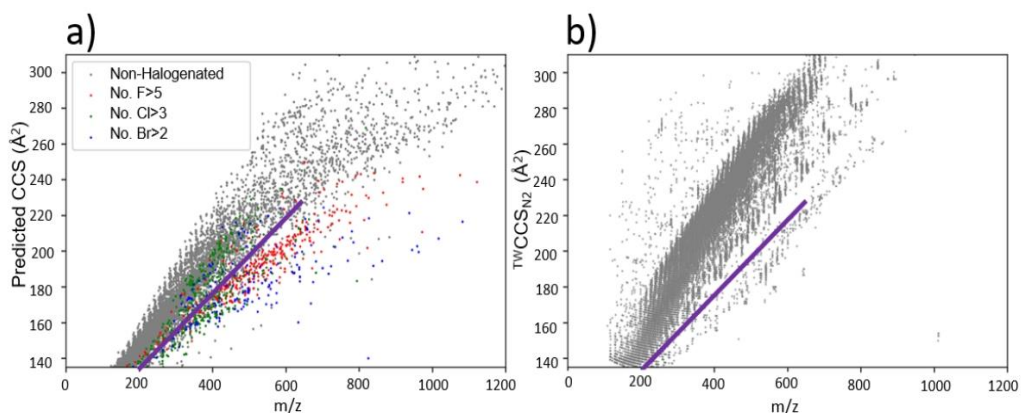


Figure 5.1 (a) Predicted CCS_{N_2} vs. m/z for c. 20,000 substances listed in the Canadian DSL and US TSCA chemical inventories; (b) Experimental $^{TW}CCS_{N_2}$ vs. m/z of ions detected in SRM 2585, a reference material of indoor dust, using GC-cIMS.

This is consistent with the experimental results reported by Mullin *et al.*³⁰, who rationalized this observation based on atom count: a polyhalogenated ion will have relatively few atoms, low molecular volume, and consequently smaller CCS compared to non-halogenated isobars. Belova *et al.*⁶⁵ have also reported this trend, remarking that the

trendline through 22 model PFASs in their study is lower than that of 126 other non-fluorinated contaminants, allowing a clear distinction between PFAS and other compound classes.

The boundary that separates PFASs from other industrial chemicals is approximated by the line drawn in Figure 5.1(a): Below this line, all compounds are characterized by a CCS that is smaller than the sum of 100 \AA^2 and one fifth of their mass. These include 65/135 (48%) compounds with >5 F atoms, 49/52 (94%) with >9 F atoms, 37/138 (27%) with >3 Cl atoms, and 26/44 (59%) with >2 Br atoms. This would suggest that a simple filter selecting compounds with $\text{CCS} < 0.2 \cdot m/z + 100 \text{ \AA}^2$ would minimize the false negative discovery of PFASs, while capturing a significant number of polychlorinated and polybrominated contaminants. However, not all of the model industrial compounds that meet the proposed criterion are halogenated. As shown in Figure 5.1(a), the false positive discovery may increase significantly above 250 \AA^2 , where non-halogenated compounds encroach on the proposed boundary line. This is because the relationship between m/z and CCS for a given compound class is nonlinear and better approximated by a power function. These potential interferences can be minimized by introducing a further constraint that PFAS and other halogenated compounds have CCS values between 150 \AA^2 and 250 \AA^2 . When these constraints are applied, approximately 20% of the compounds enclosed are halogenated, of which 44% are polyfluorinated, 33% are polychlorinated and 23% are polybrominated. A more rigorous analysis of a larger training may result in better definition of the boundaries between PFASs and other classes of chemicals, but this is beyond the scope of the present work. Nevertheless, the results suggest that the simple filter criteria proposed herein can be used to reveal PFAS and other halogenated contaminants without

prior knowledge of their structures. When applied to experimental data obtained from a reference material of indoor dust (SRM 2585), see Figure 5.1(b), it is seen that relatively few compounds are detected with CCS values greater than one fifth their mass. We hypothesize that most of these compounds are PFASs or other halogenated contaminants.

5.3.2 Evaluation of the method using a standard reference material of indoor dust

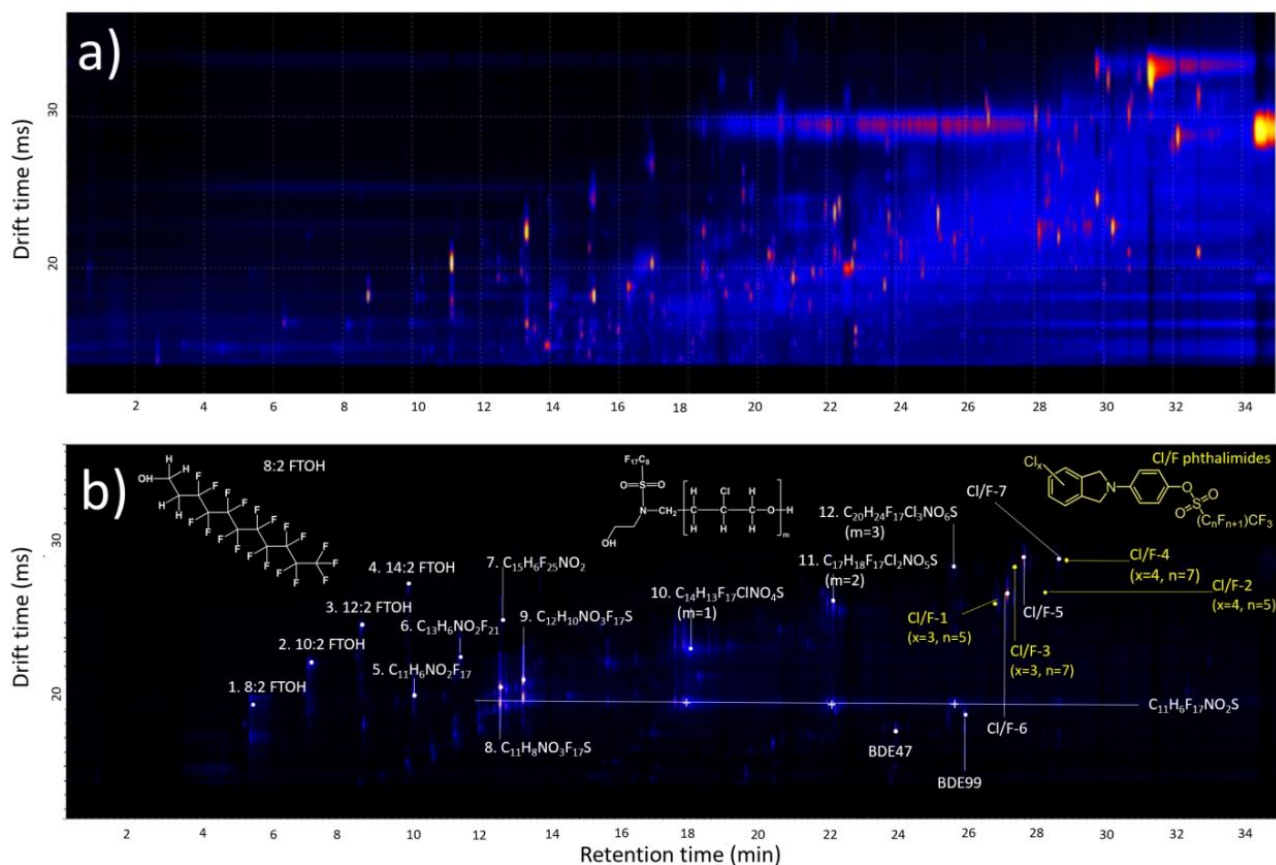


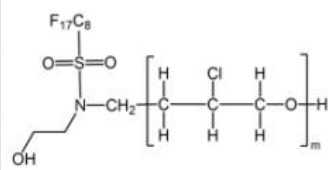
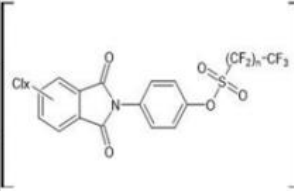
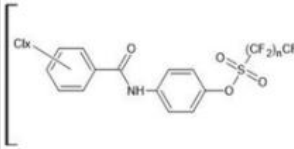
Figure 5.2 Retention time vs. drift time contour plots obtained from NIST SRM 2585 displaying (a) all ions; and (b) only ions characterized by CCS values that are less than the sum of 100 Å² and one fifth of their mass.

Figure 5.2(a) displays the contour plot of drift time vs retention time obtained from SRM 2585. It nicely illustrates the benefits of comprehensive two-dimensional dimensional separation^{284,285} as many compounds are separated by ion mobility that would otherwise co-elute from the GC. Akin to other two-dimensional separation techniques, such as GC×GC²⁶⁷ and LC×LC²⁸⁵ multiplexing GC and IMS results in separation that is "comprehensive" because it meets the following criteria^{286,287}: (i) Every part of the sample is subjected to both gas chromatography and ion mobility separations; (ii) Equal amounts of all sample components pass through both dimensions of separation and eventually reach the detector; and (iii) The separation obtained in the GC dimension is maintained.

Indeed, Figure 5.2(a) shows that a single pass through the ion mobility cell occurs on a very short time scale of <40 ms compared to the 4 - 8 second width of a GC peak. The result is dramatically improved separation of the sample SRM 2585, of which only a small fraction are fluorinated. To simplify this picture, we have filtered the detected compounds by mass and CCS, see Figure 5.2(b), such that only compounds characterized by CCS values smaller than the sum of 100 Å² and one fifth of their mass are displayed (i.e. compounds that fall below the boundary line illustrated in Figure 5.1(b)).

Elemental composition determination of each of the detected compounds in Figure 5.2(b) has led to their tentative identification, which is summarized in Table 5.1. The majority of detected peaks correspond to well-known classes of PFAS, including homologues of fluorotelomer alcohols (FTOH), and alcohol perfluoroalkyl sulfonamides (alcohol-PFSM), indicated as compounds **1-4**, and **8-9** respectively in Figure 5.2(b) and Table 5.1.

Table 5.1 Summary of tentatively identified PFASs present in NIST SRM 2585.

Compound ID	Class	Structure	Elemental Composition	I.D. Lvl	Ions	m/z	Mass error (ppm)	GC R.T.	CCS (Exp.)	CCS (Calc.)
8:2 FTOH (1)	Fluorotelomer alcohols (FTOH)	$F-(CF_2)_nCH_2CH_2OH$ $n = 8-14$	$C_{10}H_5F_{17}O$	1	$[M+H]^+$	465.0147	0.2	5.32	191.04	176.4
10:2 FTOH (2)			$C_{12}H_5F_{21}O$	2	$[M+H]^+$	565.0084	2.1	6.99	211.91	197.9
12:2 FTOH (3)			$C_{14}H_5F_{25}O$	2	$[M+H]^+$	665.002	0.6	8.50	230.83	210.8
14:2 FTOH (4)			$C_{16}H_5F_{29}O$	2	$[M+H]^+$	764.9955	1.6	9.87	-	224.1
5			$C_{11}H_6F_{17}NO_2$	4	$[M+H]^+$	508.0205	0.6	10.02	193.5	
6			$C_{13}H_6F_{21}NO_2$	4	$[M+H]^+$	608.0142	0.8	11.34	212.63	
7			$C_{15}H_6F_{25}NO_2$	4	$[M+H]^+$	708.0078	2.3	12.56	244.25	
8	Alcohol perfluoroalkyl-sulfonamides (PFSM)	$C_8F_{17}-S(=O)_2N(CH_3)CH_2CH_2OH$	$C_{11}H_8F_{17}NO_3S$	1	$[M+H]^+$	558.0032	0.9	12.51	197.62	194.1
9		$C_8F_{17}-S(=O)_2N(CH_2CH_3)CH_2CH_2OH$	$C_{12}H_{10}F_{17}NO_3S$	2	$[M+H]^+$	572.0188	1.4	13.18	200.88	198.2
10			$C_{14}H_{13}F_{17}SO_4NCl$ (m=1)	4	$[M+H]^+$	650.0060	2.6	17.8	220.74	202.4
11			$C_{17}H_{18}F_{17}SO_5NCl_2$ (m=2)	4	$[M+H]^+$	742.0090	2.4	22.21	241.15	211.5
12			$C_{20}H_{23}F_{17}SO_6NCl_3$ (m=3)	4	$[M+H]^+$	834.0149	4.2	25.6	-	
CI/F-1	Cl/F phthalimides $X = 3, 4 \quad n = 5, 7$		$C_{20}H_5NSO_5Cl_3F_{13}$ (x=3, n=5)	1	M+	724.8719	5	26.84	241.26	212.6
CI/F-2			$C_{20}H_4NSO_5Cl_4F_{13}$ (x=4, n=5)	1	M+	758.8329	4	28.16	246.8	213.5
CI/F-3			$C_{22}H_5NSO_5Cl_3F_{17}$ (x=3, n=7)	3	M+	824.8656	2.9	27.33	256.71	222
CI/F-4			$C_{22}H_4NSO_5Cl_4F_{17}$ (x=4, n=7)	3	M+	856.8328	-0.5	28.58	260.2	222.5
CI/F-5			$C_{21}H_6NSO_4Cl_4F_{17}$ (x=4, n=7)	3	M+	832.8472	5.5	27.61	263.04	220.6
CI/F-6		$C_{19}H_6NSO_4Cl_4F_{13}$ (x=4, n=5)	3	M+	732.8536	4	27.13	246	211.7	
CI/F-7		$C_{21}H_7NSO_4Cl_3F_{17}$ (x=3, n=7)	3	M+	798.8863	2.4	27.22	261.41	221.2	

Other halogenated contaminants were also identified, such as the ubiquitous polybrominated diphenyl ether congeners BDE47 and BDE99. We note that Figure 5.2(b) is structured in appearance and displays patterns that can aid the analyst in identifying compounds belonging to the same class akin to how chromatographers interpret GC×GC contour plots. All PFAS homologues fall upon a diagonal line. This is because lengthening the perfluoroalkyl chain will result in a predictable, stepwise increase in a compound's GC retention time and decrease its mobility. Homologous compounds **5-7** are also a prime example of this phenomenon as they are characterized by retention time and drift time spacing that parallel the FTOHs. Their elemental compositions were determined to be $C_{11}H_6F_{17}NO_2$, $C_{13}H_6F_{21}NO_2$ and $C_{15}H_6F_{25}NO_2$, which could potentially correspond with the $[M+H]^+$ ions of N-substituted perfluoroalkylamides. Authentic standards are not available to confirm this hypothesis and we have thus characterized these structure assignments with level 4 confidence.

In Figure 5.2(b), there is also a horizontal line connecting five peaks that share similar drift times of approximately 20 ms, yet have different GC retention times. These peaks correspond to common fragment ions $C_{11}H_6F_{17}NO_2S^{+}$ shared by six different PFASs. For example, the observed common fragment ion could result from the losses of H_2O and CH_3OH respectively from compounds **8** and **9**, which are possible isomers of the methyl and ethyl homologues of 2-(N-**alkyl**perfluoro-1-octanesulfonamido)ethanol. The presence of compound **8** was confirmed with an authentic standard. Fragment ions of the same composition are also common to compounds **10-12**, suggesting that they too are N-alkylperfluoroalkylsulfonamides (PFSM) having higher molecular weight substituents at the sulfamido nitrogen. Stepwise spacing in their retention times and drift times also

supports the proposal that compounds **10-12** belong to a homologous series. Indeed, there is a common difference of C_3H_5OCl between their elemental compositions ($C_{14}H_{13}F_{17}NSO_4Cl$, $C_{17}H_{18}F_{17}NSO_5Cl_2$ and $C_{20}H_{23}F_{17}NSO_6Cl_3$ respectively). We tentatively propose that compounds **10-12** belong to a family of PFSMs substituted with chlorinated (poly)propylene glycols, as shown in the inset of Figure 5.2(b). The presence of these compounds in a widely available reference material has not been reported previously, but without available standards these assignments remain speculative. Liu *et al.* first proposed exploiting structure-diagnostic fragment ions generated during LC-MS to help guide the discovery of unknown PFAS. It is apparent from Figure 5.2(b) that the same strategy is equally applicable to GC-MS and the inclusion of drift time and CCS data can help identify common fragments of unknown PFAS.

A series of four chloro/fluoro phthalimides (compounds **Cl/F-1 - 4** in Fig. 5.2(b)) were tentatively identified by Zhang *et al.*⁵ and Newton *et al.*²⁸⁸ The proposed structures of these suspected flame retardants are illustrated in Figure 5.2(b) and Table 5.1. Three related Cl/F compounds (**Cl/F-5 - 7** in Fig. 5.2(b)) were also tentatively identified^{5,288}. It is gratifying that these compounds have also been revealed by our GC-IMS method, but until now their identities have not been confirmed with authentic standards. Therefore, we devised a method (see Scheme 5.1) to synthesize one member of the series: **Cl/F-2**. The negative ion mode mass spectrum of **Cl/F-2** obtained from SRM 2585 is shown vis-a-vis that of the synthesized standard in Figure 5.3. The mass spectra are virtually superimposable and display structure diagnostic fragments displayed in Figure 5.3.

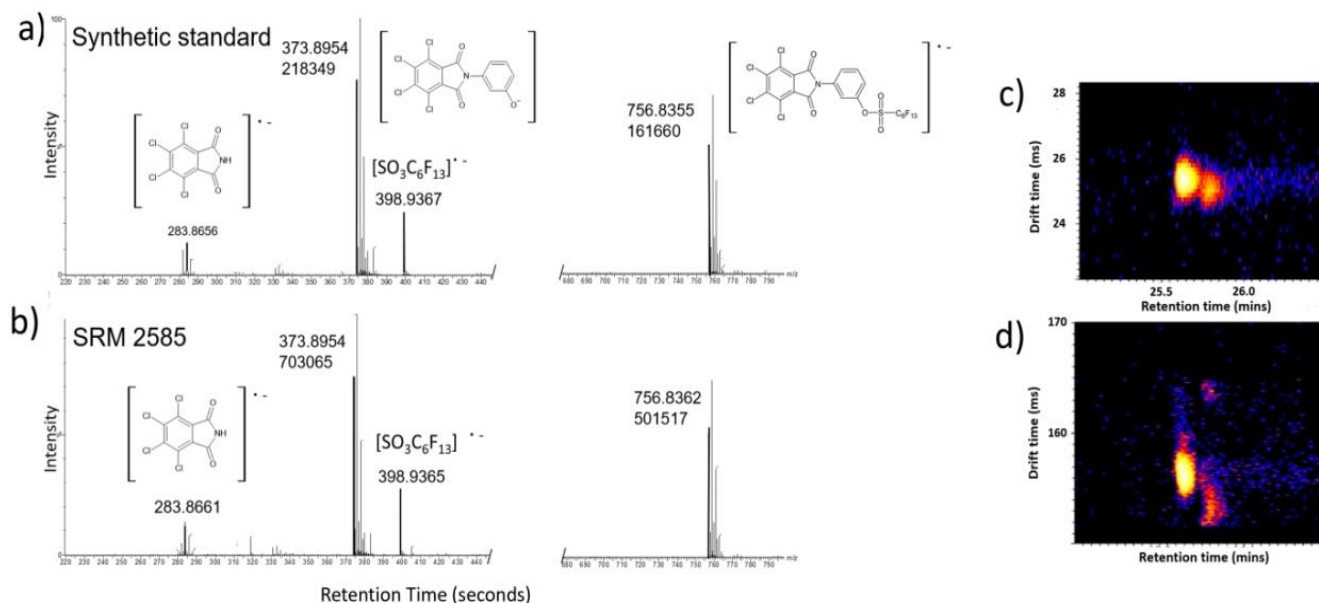


Figure 5.3 Negative ion mode mass spectra obtained from (a) the main product of the synthesis (**CI/F-1**); and (b) the same compound found in SRM 2585; Retention time vs. drift time contour plot of the molecular ions M^{+} of **CI/F-1** after (c) one pass and (d) ten passes through the cyclic ion mobility cell.

The retention time and drift time of the **CI/F-2** standard also matched with the compound in SRM 2585, see Figure 5.4, although the GC retention time was slightly longer in SRM 2585 due to the presence of matrix. We also found that **CI/F-1**, the dechlorinated analogue of **CI/F-2**, was a minor by-product of the synthesis, present at approximately 2.5% of the yield of **CI/F-2**. This is likely due to impurities in the starting material. As shown in Figure 5.4, the retention time and drift time of **CI/F-1** in SRM 2585 matched those obtained from the synthetic product.

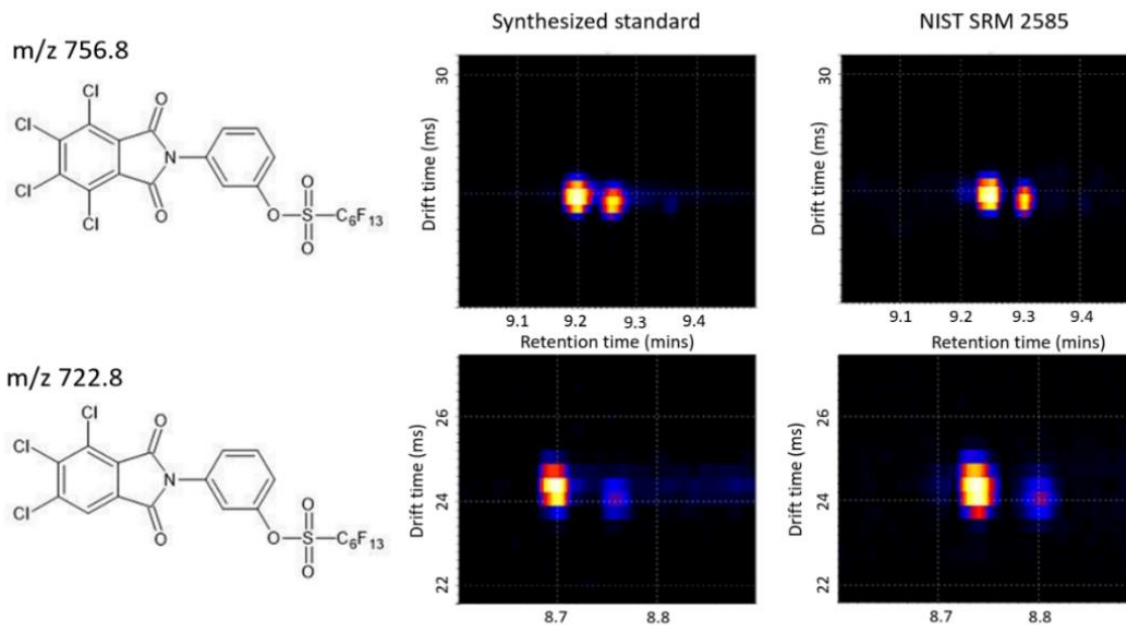


Figure 5.4 Retention times and drift times of Cl/F-1 and Cl/F-2 in SRM2585 and the synthesis product.

One unexpected observation is the fact that the GC-cIMS contour plots for compounds **Cl/F-1** and **Cl/F-2** display not one, but two different peaks, see Figures 5.3(c) and 5.4, which are characterized by closely similar mass spectra. This implies the presence of two structural isomers. In order to determine whether this is the case, a multipass experiment was performed using the cIMS. The results of this experiment are shown in Figure 5.3(d). When the number of passes around the cyclic IMS cell was increased from one to ten (Figure 5.3(d) vs. 5.3(c)), the separation in drift time increased significantly. The isomer that elutes first by GC must have a relatively large CCS because it is characterized by a longer drift time compared to the late eluting isomer.

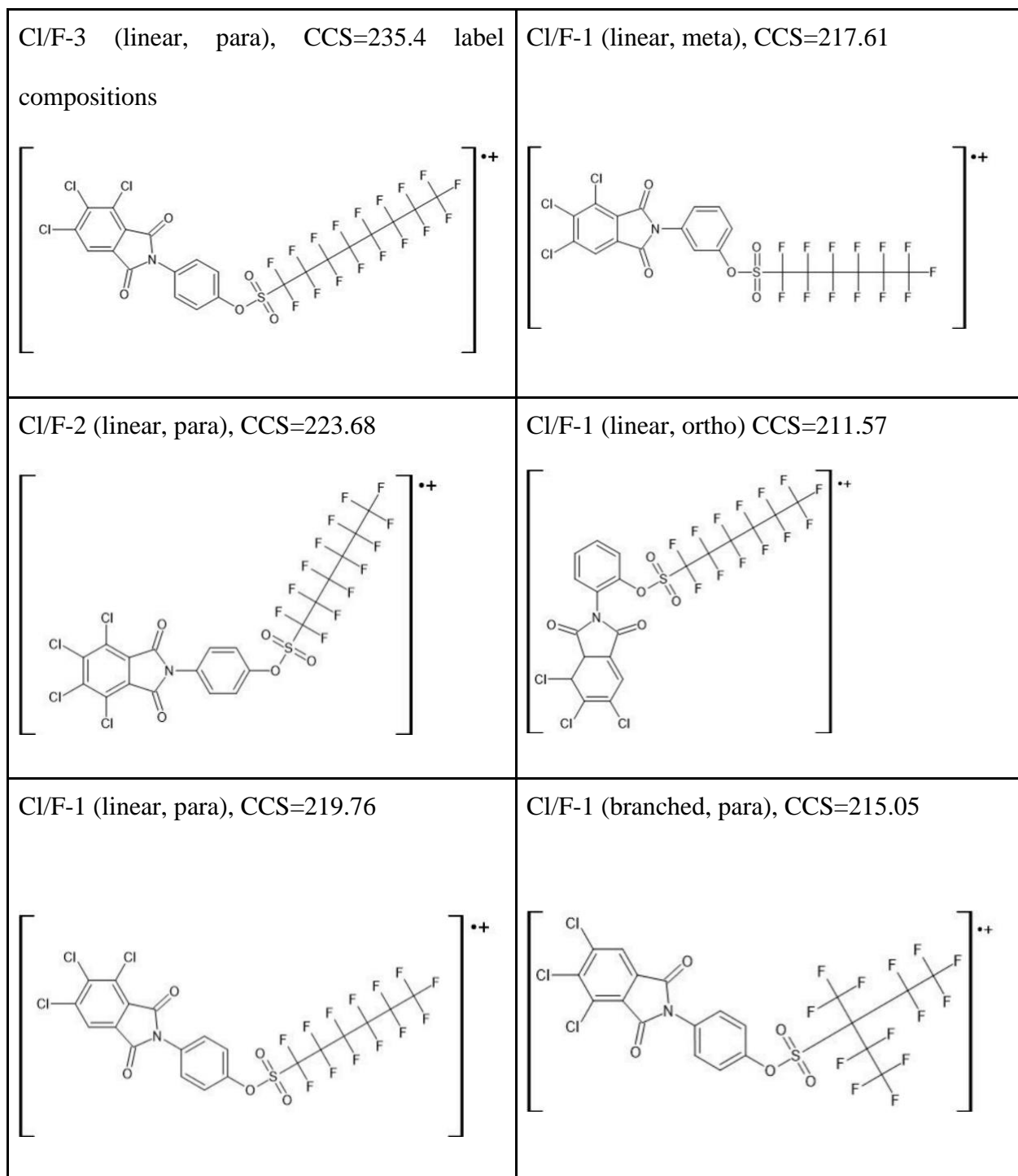


Figure 5.5 Optimized geometries of selected homologues and isomers of Cl/F-1.

The second isomer travels so quickly that it even starts to wrap-around, as witnessed by the signal forming at ~165 ms. We hypothesize that the second isomer most likely results from impurities in the perfluorohexansulfonyl fluoride starting material. Electrochemical fluorination is one process used in the production of PFAS, which can result in a mixture of linear and branched isomers in ratios³⁹ similar to that observed for the isomers of **Cl/F-1** and **Cl/F-2**. This proposal is supported by the results of theoretical calculations of the CCS of representative branched and linear isomers (see Figure 5.5), which agree that the branched isomer is more compact with a smaller CCS.

5.3.3 Identification of previously unknown chlorofluoro n-alkanes in indoor dust

Encouraged by the success of the method to characterize known and unknown PFAS in a reference material, we applied it to a set of indoor dust samples collected from six locations on the campus of Memorial University.

Figures 5.6(a) and 5.6(b) display contour plots obtained from one of these dust samples using the positive and negative ion modes respectively. Both ion modes yield highly complex contour plots, which are greatly simplified when the filter is applied, as shown in Figures 5.6(c) and 5.6(d). Both contour plots in Figures 5.6(c) and 5.6(d) display a relatively large ellipsoid shape that is consistent with the presence of a complex mixture of isomers. All mass spectra within the ellipse were co-added and transformed into a mass defect plot. Briefly, a mass defect plot is constructed from a traditional mass spectrum by graphing the m/z of each ion against its mass defect, i.e., the difference between the nominal mass and exact mass. The intensity of each ion may be conveyed by the diameter of the "bubble" marker in the plot. Often, the m/z values are scaled to assist in the search of homologues and this has been described previously. Figure 5.6(g) displays the mass defect

plot obtained in the negative ion mode. It was constructed using the CF_2CFCl mass scale after we realized that the three clusters of peaks circled in Figure 5.6(g) are spaced apart by 115.9641 Da, the exact mass of CF_2CFCl .

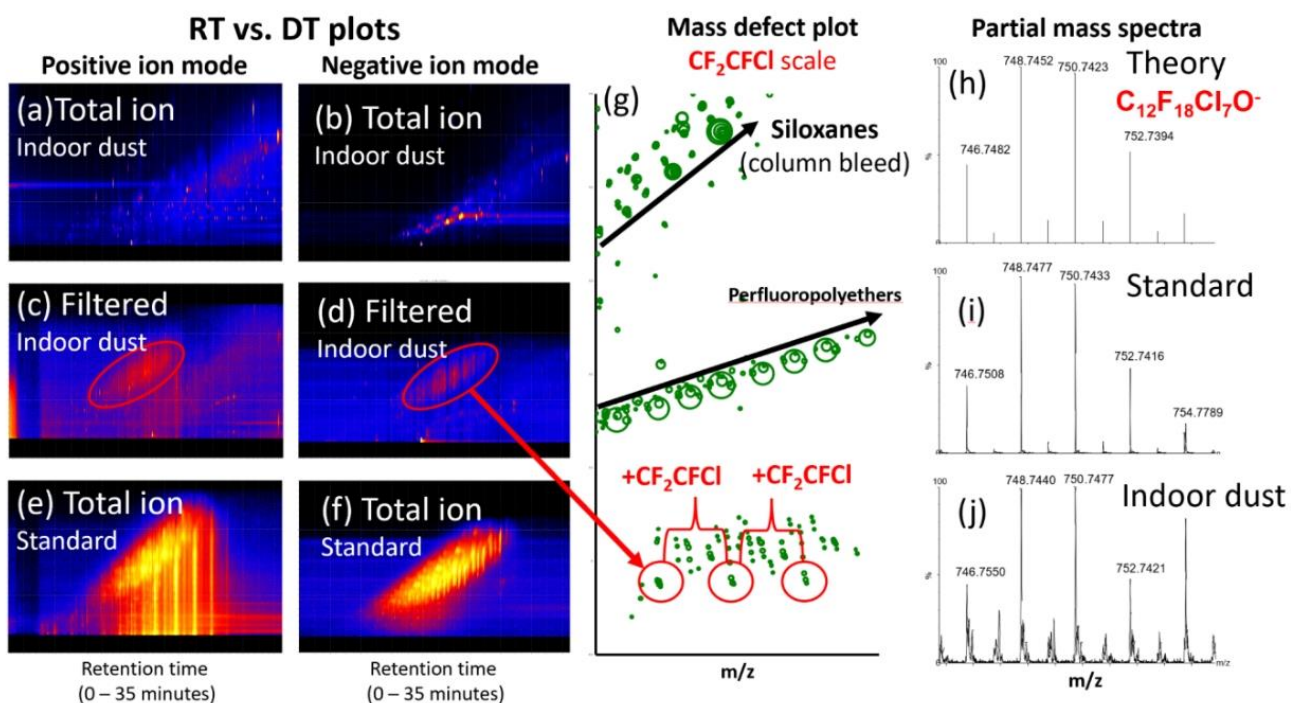


Figure 5.6 Total ion contour plots obtained from indoor dust sample CSF1 under (a) positive ion and (b) negative ion conditions; (c-d) only ions characterized by CCS values that are less than the sum of 100 \AA^2 and one fifth of their mass are displayed; (e-f) Total ion contour plots obtained from an authentic standard of Halocarbon 700; (g) Combined mass spectrum of the highlighted region in Fig. 4d depicted as a mass defect plot constructed using the CF_2CFCl scale; (h) The theoretical isotope pattern for ions $\text{C}_{12}\text{F}_{18}\text{Cl}_7\text{O}^-$ closely matches those observed in (i) an authentic standard of Halocarbon 700; and (j) the indoor dust sample collected from CSF1.

Consequently, all three ions fall upon a line parallel to the x-axis. The elemental compositions of the three peaks were determined to be $C_{12}F_{18}Cl_7O^-$, $C_{14}F_{21}Cl_8O^-$ and $C_{16}F_{24}Cl_9O^-$. Reactions with oxygen²⁸⁹ are common in APCI and the observed compositions would be consistent with the formation of the $[M-Cl+O]^-$ quasimolecular ions of the polychlorofluoro alkanes: $C_{12}F_{18}Cl_8$, $C_{14}F_{21}Cl_9$ and $C_{16}F_{24}Cl_{10}$. Silicon-containing ions and perfluoropolyethers were also observed. The former originate from the septum and GC stationary phase and the latter appeared to be background, possibly resulting from exhaust from the turbomolecular pumps, which use perfluoropolyether oils for lubrication²⁹⁰. This background can be minimized by increasing the auxiliary nitrogen flow in the ion source to prevent exhaust from entering the ion source housing²⁸⁹.

Chlorofluoroalkanes consisting of 1-2 carbon atoms are infamous for their role in ozone depletion, and have been banned for decades. However, longer chain oils, waxes and polymers have found modern use in a variety of applications from lubricants and cutting oils to non-stick coatings on smartphones¹⁸⁹. Figures 5.6(e) and 5.6(f) display contour plots obtained from Halocarbon 700, a widely available lubricant that appears to consist of a range of $\sim C_{12-20}$ chlorofluoro alkanes. The similar retention time and drift time profile of Halocarbon 700 compared to the putative Cl/F alkanes identified in indoor dust are quite similar. The theoretical and experimental isotope pattern of ions $C_{12}F_{18}Cl_7O^-$ obtained from Halocarbon 700 are also quite close to the pattern observed in the indoor dust sample. These observations strongly suggest that Cl/F alkanes are contaminants of the indoor environment. Dust was sampled from six buildings on campus, viz. The Arts and Administration (A), Science (SN), Education (ED), Chemistry-Physics (C), Engineering (EN), and several different locations in the new Core Science Facility (CSF), and halocarbon oils were

detected in three: the ED, CSF and C buildings. The detection of halocarbon oils appeared to coincide with recent renovation and construction activities as well as the presence of exposed ductwork. This is consistent with the use of halocarbons as metalworking fluids and compressor oils used in heating, cooling and ventilation¹⁸⁹. While the potential source of these contaminants is unknown, their detection is concerning because halocarbon oils are likely replacements to the short-chain chlorinated paraffins (SCCPs) that have been restricted by the Stockholm Convention. Recent environmental fate modeling²⁷ suggests that hundreds of widely used mixed halogenated n-alkanes, including the Cl/FI alkanes, are likely persistent organic pollutants. The first detection of halocarbon oils in the indoor environment underlines the need for further investigation into their environmental occurrence and risk.

5.4 Conclusions

The method reported here employs gas chromatography, hyphenated with (cyclic) ion mobility-mass spectrometry to selectively discover unknown PFAS and related halogenated contaminants without prior knowledge of their structure or occurrence. Unlike Cl- and Br-containing compounds that are easily recognized by their characteristic isotope patterns, PFASs are more difficult to recognize because ¹⁹F exists as a single stable isotope. By modeling the m/z and CCS of approximately 20,000 industrial chemicals, a simple filter was devised to select up to 94% of unknown PFAS characterized by CCS values smaller than the sum of 100 Å² and one fifth their mass. The approach was evaluated using SRM 2585, and it revealed the presence of 19 PFAS compounds, including 6 that have not been reported by other NTS methods. Four PFAS compounds detected were tentatively identified as chlorofluoro phthalimides. This proposal is confirmed in the present study by

experiments with a synthesized standard. When the method was applied to a set of indoor dust samples collected from six different buildings on the campus of Memorial University, chlorofluoro alkanes were detected in three locations. The proposed identities were confirmed by experiments with a sample of halocarbon 700 oil. Thus, GC-cIMS had enabled the first detection of this suspected class of persistent organic pollutants.

Chapter 6

Conclusion and future work

6.1 Conclusions

It is essential to evaluate the potential of a chemical to be a POP, considering its persistence, bioaccumulation, and long-range transport characteristics. Theoretical approaches, such as QSPR and DFT (discussed in Chapters 3 & 4), as well as advanced instrumental methods (described in Chapter 5), have been developed to identify previously unknown "forever" fluorinated chemicals.

Chapter 2 extensively explained the principles of atmospheric pressure ionization techniques coupled with gas chromatography and mass spectrometry, highlighting their advantages over traditional ionization approaches.

The findings presented in Chapter 3 indicate that while EPI SuiteTM offers rapid batch predictions of physical-chemical properties for halogenated chemicals, its accuracy is limited. Conversely, DFT calculations provide accurate results but are time-consuming. A linear relationship was observed between the partitioning coefficients obtained from EPI Suite and the DFT results, allowing for the correction of EPI SuiteTM predictions using this relationship. By combining these two approaches, we designed a convenient yet relatively accurate model to predict the environmental behavior of halogenated n-alkanes. The modeled results suggest that out of the 966 elemental compositions of halogenated n-alkanes analyzed, 352 (23 Br, 83 Cl/F, 119 Br/Cl, and 127 Br/F) are likely constituents of substances used as lubricants, plasticizers, and flame retardants. Complementary DFT calculations also indicate that compositions with a higher number of carbon and fluorine atoms, but fewer chlorine and bromine atoms, may pose a risk. The prioritized mixed halogenated n-alkanes in this chapter highlight the need to investigate them, particularly Cl/F n-alkanes, in real environmental samples.

In Chapter 4, the inclusion of conceptual DFT descriptors, namely global electronegativity, electrophilicity index, hardness, and polarizability, in the analysis of a chemical's potential environmental behavior revealed distinct distributions between chemicals with POPs potential and those with lower or no POPs potential. Notably, fluorinated chemicals exhibited higher hardness (>0.21) compared to other compounds. Among the chemicals with a hardness >0.20 in the POPs list, 106 out of 108 are poly or perfluorinated chemicals. Conversely, no poly or perfluorinated chemical in the POPs list has a hardness >0.20 , suggesting a similarity in hardness between poly or perfluorinated chemicals and proteins. This implies a potential for binding between poly or perfluorinated chemicals and proteins based on the HBSA theory, which could contribute to their persistence in the human body. PCA further confirmed the predictive capability of conceptual DFT properties in assessing environmental fate. This study establishes a novel link between conceptual DFT and a chemical's environmental fate, offering a new approach to environmental risk assessment. Chapter 3 supported the hypothesis that DFT descriptors can be used to prioritize pollutants with P, B, and T potential.

The outcomes presented in Chapter 3 demonstrate that high-resolution mass spectrometry is a suitable tool for the accurate identification and monitoring of suspected pollutants. The computed resolving power of approximately 60,000 (full-width half maximum) allows for distinguishing around 74% of the prioritized elemental compositions from the most likely interferences, such as chlorinated alkanes. In Chapter 5, our newly developed ion mobility spectrometer coupled with high-resolution mass spectrometry was employed to identify unknown (poly or per) fluorinated chemicals. By utilizing a computational CCS model developed with approximately 20,000 chemicals, it was

discovered that a specific filter zone, defined by CCS values less than the sum of 100 \AA^2 and one-fifth of their mass, can accommodate both PFAS and polybrominated flame retardants. This model was then applied to GC-cIMS-MS data collected from a set of 20 indoor dust samples, leading to the identification of PFAS compounds without prior knowledge of their presence. To validate this approach, a standard reference material of household dust, SRM 2585, was subjected to a validation procedure, which successfully confirmed the identification of previously (tentatively) identified PFAs using the established filter. Furthermore, the existence of a tentatively identified substance, chlorofluoro phthalimide, in SRM 2585 was confirmed through the synthesis of a corresponding standard. The method employed in this study also revealed the presence of chlorofluoro n-alkanes as an emerging class of persistent chemicals in the indoor environment, consistent with the findings of Chapter 2.

Overall, these chapters demonstrate the use of theoretical approaches and advanced instrumental methods in understanding environmental behavior and identifying unknown fluorinated chemicals in environmental samples. The research presented in the thesis contributes to the fields of environmental analytical chemistry and environmental risk assessment.

6.2 Future work

Since the models presented in Chapters 3 and 4 are based on the DSL and US TSCA, it would be advantageous to extend the application of the developed approach to include broader chemical lists. For instance, the Inventory of Existing Chemical Substances of China and the Registration, Evaluation, Authorization and Restriction of Chemicals by the European Union encompass more comprehensive chemicals and groups. This implies that

these lists may contain additional chemicals with potential risks that have yet to be investigated and identified.

In Chapter 4, only four descriptors, namely hardness, electrophilicity index, global electronegativity, and polarizability, were considered. The incorporation of other parameters could lead to a more sophisticated model. For example, molecular weight can serve as a valuable complementary factor alongside the cDFT descriptors. Additionally, the collision cross-section of a chemical provides insightful information regarding its partitioning behavior. These readily available parameters can be easily integrated into the models. Furthermore, utilizing more advanced artificial intelligence algorithms can significantly enhance the predictive capabilities of the models.

Previous studies have demonstrated that the binding energy between PFOA/PFOS and serum albumin (the primary accumulator of PFAS) can be readily measured using ESI mass spectrometry. Considering that even non-ionized PFASs tend to bind with proteins, similar experiments could be conducted to examine their binding with non-polar PFAS compounds such as perfluorooctane or, similarly, the PXAs. These experiments could provide further insights into how PFASs disrupt the normal functioning of proteins and, consequently, their potential risks to human health.

In order to enhance the non-target screening process, an extensive data analysis campaign will be carried out on the GC-cIMS-MS platform, focusing on testing a larger number of environmental samples. This approach aims to identify new contaminants that have limited prior information available. Additionally, multi-pass experiments will be conducted to maximize the resolving power provided by cIMS. These experiments will

provide a more comprehensive understanding of the samples and generate additional information regarding the detected contaminants.

References

- (1) Environment and Climate Change Canada. Canadian Domestic Substances List <https://www.canada.ca/en/environment-climate-change/services/canadian-environmental-protection-act-registry/substances-list/domestic.html> (accessed May 17, 2022).
- (2) United States Environmental Protection Agency. The Toxic Substances Control Act (TSCA) Chemical Substance Inventory <https://www.epa.gov/tsca-inventory> (accessed May 17, 2022).
- (3) Ministry of Ecology and Environment of the P.R.C. Inventory of Existing Chemical Substances of China (IECSC) https://www.mee.gov.cn/gkml/hbb/bgg/201301/t20130131_245810.htm (accessed Jun 23, 2023).
- (4) European Union. REACH Regulation https://environment.ec.europa.eu/topics/chemicals/reach-regulation_en (accessed Jun 23, 2023).
- (5) Zhang, X.; Di Lorenzo, R. A.; Helm, P. A.; Reiner, E. J.; Howard, P. H.; Muir, D. C. G.; Sled, J. G.; Jobst, K. J. Compositional Space: A Guide for Environmental Chemists on the Identification of Persistent and Bioaccumulative Organics Using Mass Spectrometry. *Environ. Int.* **2019**, *132* (December 2018), 104808. <https://doi.org/10.1016/j.envint.2019.05.002>.
- (6) Stockholm Convention; UNEP. The 16 New POPs. 25 P. **2017**, No. June, 25.
- (7) Scheringer, M.; Stempel, S.; Hukari, S.; Ng, C. A.; Blepp, M.; Hungerbuhler, K. How Many Persistent Organic Pollutants Should We Expect? *Atmos. Pollut. Res.* **2012**, *3* (4), 383–391. <https://doi.org/https://doi.org/10.5094/APR.2012.044>.
- (8) Brown, T. N.; Wania, F. Screening Chemicals for the Potential to Be Persistent Organic Pollutants: A Case Study of Arctic Contaminants. *Environ. Sci. Technol.* **2008**, *42* (14), 5202–5209. <https://doi.org/10.1021/es8004514>.
- (9) US EPA. Estimation Programs Interface Suite™ for Microsoft® Windows, v 4.11. United States Environmental Protection Agency: Washington, DC 2012.
- (10) Cramer, C. J. *Essentials Computational Chemistry*; Wiley: Hoboken, NJ, 2004.
- (11) Geerlings, P.; De Proft, F.; Langenaeker, W. Conceptual Density Functional Theory. *Chem. Rev.* **2003**, *103* (5), 1793–1874. <https://doi.org/10.1021/cr990029p>.

- (12) Koch, W.; Holthausen, M. C. Chemical Reactivity: Exploring Potential Energy Surfaces. In *A Chemist's Guide to Density Functional Theory*; 2001; pp 239–263. <https://doi.org/https://doi.org/10.1002/3527600043.ch13>.
- (13) Chermette, H. Chemical Reactivity Indexes in Density Functional Theory. *J. Comput. Chem.* **1999**, *20* (1), 129–154. [https://doi.org/https://doi.org/10.1002/\(SICI\)1096-987X\(19990115\)20:1<129::AID-JCC13>3.0.CO;2-A](https://doi.org/https://doi.org/10.1002/(SICI)1096-987X(19990115)20:1<129::AID-JCC13>3.0.CO;2-A).
- (14) Chandrakumar, K. R. S.; Pal, S. The Concept of Density Functional Theory Based Descriptors and Itsrelationwith the Reactivity of Molecular Systems: A Semi-Quantitative Study. *Int. J. Mol. Sci.* **2002**, *3* (4), 324–337. <https://doi.org/10.3390/i3040324>.
- (15) Geerlings, P. From Density Functional Theory to Conceptual Density Functional Theory and Biosystems. *Pharmaceuticals* **2022**, *15* (9). <https://doi.org/10.3390/ph15091112>.
- (16) Hati, S.; Datta, D. Hardness and Electric Dipole Polarizability. Atoms and Clusters. *J. Phys. Chem.* **1994**, *98* (41), 10451–10454. <https://doi.org/10.1021/j100092a012>.
- (17) Pearson, R. G. Recent Advances in the Concept of Hard and Soft Acids and Bases. *J. Chem. Educ.* **1987**, *64* (7), 561–567. <https://doi.org/10.1021/ed064p561>.
- (18) Parr, R. G.; Yang, W. Density Functional Approach to the Frontier-Electron Theory of Chemical Reactivity. *J. Am. Chem. Soc.* **1984**, *106* (14), 4049–4050. <https://doi.org/10.1021/ja00326a036>.
- (19) Melnikov, F.; Geohagen, B. C.; Gavin, T.; LoPachin, R. M.; Anastas, P. T.; Coish, P.; Herr, D. W. Application of the Hard and Soft, Acids and Bases (HSAB) Theory as a Method to Predict Cumulative Neurotoxicity. *Neurotoxicology* **2020**, *79* (April), 95–103. <https://doi.org/10.1016/j.neuro.2020.04.009>.
- (20) Staikova, M.; Wania, F.; Donaldson, D. J. Molecular Polarizability as a Single-Parameter Predictor of Vapour Pressures and Octanol–Air Partitioning Coefficients of Non-Polar Compounds: A Priori Approach and Results. *Atmos. Environ.* **2004**, *38* (2), 213–225. <https://doi.org/10.1016/j.atmosenv.2003.09.055>.
- (21) Staikova, M.; Messih, P.; Lei, Y. D.; Wania, F.; Donaldson, D. J. Prediction of Subcooled Vapor Pressures of Nonpolar Organic Compounds Using a One-Parameter QSPR. *J. Chem. Eng. Data* **2005**, *50* (2), 438–443. <https://doi.org/10.1021/je049732n>.

- (22) Xiaolei Li. Polarizability as a Single Parameter to Predict Octanol-Water Partitioning Coefficient and Bioconcentration Factor for Persistent Organic Pollutants. Master thesis. Memorial University **2016**, July.
- (23) Endo, S.; Hammer, J. Predicting Partition Coefficients of Short-Chain Chlorinated Paraffin Congeners by COSMO-RS-Trained Fragment Contribution Models. *Environ. Sci. Technol.* **2020**, *54* (23), 15162–15169. <https://doi.org/10.1021/acs.est.0c06506>.
- (24) Endo, S. Refinement and Extension of COSMO-RS-Trained Fragment Contribution Models for Predicting the Partition Properties of C 10-20 Chlorinated Paraffin Congeners. **2021**. <https://doi.org/10.1039/d1em00123j>.
- (25) Jobst, K. J.; Seeley, J. V; Reiner, E. J.; Mullin, L.; Ladak, A. Enhancing the Sensitivity of Atmospheric Pressure Ionization Mass Spectrometry Using Flow Modulated Gas Chromatography. *Curr. Trends Mass Spectrom.* **2018**, *16* (4), 15–19.
- (26) Organtini, K. L.; Myers, A. L.; Jobst, K. J.; Reiner, E. J.; Ross, B.; Ladak, A.; Mullin, L.; Stevens, D.; Dorman, F. L. Quantitative Analysis of Mixed Halogen Dioxins and Furans in Fire Debris Utilizing Atmospheric Pressure Ionization Gas Chromatography-Triple Quadrupole Mass Spectrometry. *Anal. Chem. (Washington, DC, United States)* **2015**, *87* (20), 10368–10377. <https://doi.org/10.1021/acs.analchem.5b02463>.
- (27) Li, X.; Chevez, T.; De Silva, A. O.; Muir, D. C. G.; Kleywegt, S.; Simpson, A.; Simpson, M. J.; Jobst, K. J. Which of the (Mixed) Halogenated n-Alkanes Are Likely To Be Persistent Organic Pollutants? *Environ. Sci. Technol.* **2021**, *55* (23), 15912–15920. <https://doi.org/10.1021/acs.est.1c05465>.
- (28) Hernández-Mesa, M.; Escourrou, A.; Monteau, F.; Le Bizec, B.; Dervilly-Pinel, G. Current Applications and Perspectives of Ion Mobility Spectrometry to Answer Chemical Food Safety Issues. *TrAC - Trends Anal. Chem.* **2017**, *94*, 39–53. <https://doi.org/10.1016/j.trac.2017.07.006>.
- (29) Stephan, S.; Hippler, J.; Köhler, T.; Deeb, A. A.; Schmidt, T. C.; Schmitz, O. J. Contaminant Screening of Wastewater with HPLC-IM-QTOF-MS and LC+LC-IM-QTOF-MS Using a CCS Database. *Anal. Bioanal. Chem.* **2016**, *408* (24), 6545–6555. <https://doi.org/10.1007/s00216-016-9820-5>.
- (30) Mullin, L.; Jobst, K.; DiLorenzo, R. A.; Plumb, R.; Reiner, E. J.; Yeung, L. W. Y. Y.; Jogsten, I. E. Liquid Chromatography-Ion Mobility-High Resolution Mass Spectrometry for Analysis of Pollutants in Indoor Dust: Identification and Predictive Capabilities. *Anal. Chim. Acta* **2020**, *1125*, 29–40. <https://doi.org/https://doi.org/10.1016/j.aca.2020.05.052>.

- (31) Menger, F.; Gago-Ferrero, P.; Wiberg, K.; Ahrens, L. Wide-Scope Screening of Polar Contaminants of Concern in Water: A Critical Review of Liquid Chromatography-High Resolution Mass Spectrometry-Based Strategies. *Trends Environ. Anal. Chem.* **2020**, *28*, e00102. <https://doi.org/10.1016/j.teac.2020.e00102>.
- (32) Fisher, C. M.; Croley, T. R.; Knolhoff, A. M. Data Processing Strategies for Non-Targeted Analysis of Foods Using Liquid Chromatography/High-Resolution Mass Spectrometry. *TrAC - Trends Anal. Chem.* **2021**, *136*, 116188. <https://doi.org/10.1016/j.trac.2021.116188>.
- (33) Hernández-Mesa, M.; Monteau, F.; Le Bizec, B.; Dervilly-Pinel, G. Potential of Ion Mobility-Mass Spectrometry for Both Targeted and Non-Targeted Analysis of Phase II Steroid Metabolites in Urine. *Anal. Chim. Acta X* **2019**, *1*. <https://doi.org/10.1016/j.acax.2019.100006>.
- (34) Hernández-Mesa, M.; Ropartz, D.; García-Campaña, A. M.; Rogniaux, H.; Dervilly-Pinel, G.; Le Bizec, B. Ion Mobility Spectrometry in Food Analysis: Principles, Current Applications and Future Trends. *Molecules* **2019**, *24* (15), 1–28. <https://doi.org/10.3390/molecules24152706>.
- (35) Dodds, J. N.; Baker, E. S. Ion Mobility Spectrometry: Fundamental Concepts, Instrumentation, Applications, and the Road Ahead. *J. Am. Soc. Mass Spectrom.* **2019**, *30* (11), 2185–2195. <https://doi.org/10.1007/s13361-019-02288-2>.
- (36) May, J. C.; McLean, J. A. Ion Mobility-Mass Spectrometry: Time-Dispersive Instrumentation. *Anal. Chem.* **2015**, *87* (3), 1422–1436. <https://doi.org/10.1021/ac504720m>.
- (37) Waters. T-WAVE DEVICES Unique Technology for Advanced MS Capabilities. **2012**, *5*.
- (38) Kurulugama, R.; Imatani, K. The Agilent Ion Mobility Q-TOF Mass Spectrometer System, Technical Overview by Agilent Technologies. **2013**.
- (39) Hogan, C. J.; Fernández De La Mora, J. Ion Mobility Measurements of Nondenatured 12-150 KDa Proteins and Protein Multimers by Tandem Differential Mobility Analysis-Mass Spectrometry (DMA-MS). *J. Am. Soc. Mass Spectrom.* **2011**, *22* (1), 158–172. <https://doi.org/10.1007/s13361-010-0014-7>.
- (40) Arnaud, C. H. Resolving power for the people: Ion mobility-mass spec expands its offerings <https://cen.acs.org/analytical-chemistry/mass-spectrometry/Resolving-power-people-Ion-mobility/98/i20>.
- (41) Deng, L.; Webb, I. K.; Garimella, S. V. B.; Hamid, A. M.; Zheng, X.; Norheim, R. V.; Prost, S. A.; Anderson, G. A.; Sandoval, J. A.; Baker, E. S.; Ibrahim, Y. M.;

- Smith, R. D. Serpentine Ultralong Path with Extended Routing (SUPER) High Resolution Traveling Wave Ion Mobility-MS Using Structures for Lossless Ion Manipulations. *Anal. Chem.* **2017**, *89* (8), 4628–4634. <https://doi.org/10.1021/acs.analchem.7b00185>.
- (42) Giles, K.; Ujma, J.; Wildgoose, J.; Pringle, S.; Richardson, K.; Langridge, D.; Green, M. A Cyclic Ion Mobility-Mass Spectrometry System. *Anal. Chem.* **2019**, *91* (13), 8564–8573. <https://doi.org/10.1021/acs.analchem.9b01838>.
- (43) Breen, J.; Hashemihedeshi, M.; Amiri, R.; Dorman, F. L.; Jobst, K. J. Unwrapping Wrap-around in Gas (or Liquid) Chromatographic Cyclic Ion Mobility-Mass Spectrometry. *Anal. Chem.* **2022**, *94* (32), 11113–11117. <https://doi.org/10.1021/acs.analchem.2c02351>.
- (44) Merenbloom, S. I.; Glaskin, R. S.; Henson, Z. B.; Clemmer, D. E. High-Resolution Ion Cyclotron Mobility Spectrometry. *Anal. Chem.* **2009**, *81* (4), 1482–1487. <https://doi.org/10.1021/ac801880a>.
- (45) Waters. Ion Mobility Mass Spectrometry https://www.waters.com/waters/en_US/Ion-Mobility-Mass-Spectrometry/nav.htm?cid=134656158&locale=en_US (accessed Mar 26, 2022).
- (46) Bruker. timsTOF <https://www.azom.com/equipment-details.aspx?EquipID=6677> (accessed Mar 26, 2022).
- (47) Ewing, M. A.; Glover, M. S.; Clemmer, D. E. Hybrid Ion Mobility and Mass Spectrometry as a Separation Tool. *J. Chromatogr. A* **2016**, *1439*, 3–25. <https://doi.org/10.1016/j.chroma.2015.10.080>.
- (48) Poltash, M. L.; McCabe, J. W.; Shirzadeh, M.; Laganowsky, A.; Clowers, B. H.; Russell, D. H. Fourier Transform-Ion Mobility-Orbitrap Mass Spectrometer: A Next-Generation Instrument for Native Mass Spectrometry. *Anal. Chem.* **2018**, *90* (17), 10472–10478. <https://doi.org/10.1021/acs.analchem.8b02463>.
- (49) Rus, J.; Moro, D.; Sillero, J. A.; Royuela, J.; Casado, A.; Estevez-Molinero, F.; Fernández de la Mora, J. IMS-MS Studies Based on Coupling a Differential Mobility Analyzer (DMA) to Commercial API-MS Systems. *Int. J. Mass Spectrom.* **2010**, *298* (1–3), 30–40. <https://doi.org/10.1016/j.ijms.2010.05.008>.
- (50) Revercomb, H. E.; Mason, E. A. Theory of Plasma Chromatography/Gaseous Electrophoresis. A Review. *Anal. Chem.* **1975**, *47* (7), 970–983. <https://doi.org/10.1021/ac60357a043>.
- (51) Smith, D. P.; Knapman, T. W.; Campuzano, L.; Malham, R. W.; Berryman, J. T.; Radford, S. E.; Ashcroft, A. E. Deciphering Drift Time Measurements from

- Travelling Wave Ion Mobility Spectrometry- Mass Spectrometry Studies. *Eur. J. Mass Spectrom.* **2009**, *15* (2), 113–130. <https://doi.org/10.1255/ejms.947>.
- (52) Marchand, A.; Livet, S.; Rosu, F.; Gabelica, V. Drift Tube Ion Mobility: How to Reconstruct Collision Cross Section Distributions from Arrival Time Distributions? *Anal. Chem.* **2017**, *89* (23), 12674–12681. <https://doi.org/10.1021/acs.analchem.7b01736>.
- (53) Ruotolo, B. T.; Benesch, J. L. P.; Sandercock, A. M.; Hyung, S. J.; Robinson, C. V. Ion Mobility-Mass Spectrometry Analysis of Large Protein Complexes. *Nat. Protoc.* **2008**, *3* (7), 1139–1152. <https://doi.org/10.1038/nprot.2008.78>.
- (54) Hinnenkamp, V.; Klein, J.; Meckelmann, S. W.; Balsaa, P.; Schmidt, T. C.; Schmitz, O. J. Comparison of CCS Values Determined by Traveling Wave Ion Mobility Mass Spectrometry and Drift Tube Ion Mobility Mass Spectrometry. *Anal. Chem.* **2018**, *90* (20), 12042–12050. <https://doi.org/10.1021/acs.analchem.8b02711>.
- (55) Stow, S. M.; Causon, T. J.; Zheng, X.; Kurulugama, R. T.; Mairinger, T.; May, J. C.; Rennie, E. E.; Baker, E. S.; Smith, R. D.; McLean, J. A.; Hann, S.; Fjeldsted, J. C. An Interlaboratory Evaluation of Drift Tube Ion Mobility-Mass Spectrometry Collision Cross Section Measurements. *Anal. Chem.* **2017**, *89* (17), 9048–9055. <https://doi.org/10.1021/acs.analchem.7b01729>.
- (56) Righetti, L.; Dreolin, N.; Celma, A.; McCullagh, M.; Barknowitz, G.; Sancho, J. V.; Dall'Asta, C. Travelling Wave Ion Mobility-Derived Collision Cross Section for Mycotoxins: Investigating Interlaboratory and Interplatform Reproducibility. *J. Agric. Food Chem.* **2020**, *68* (39), 10937–10943. <https://doi.org/10.1021/acs.jafc.0c04498>.
- (57) Zhou, Z.; Luo, M.; Chen, X.; Yin, Y.; Xiong, X.; Wang, R.; Zhu, Z. J. Ion Mobility Collision Cross-Section Atlas for Known and Unknown Metabolite Annotation in Untargeted Metabolomics. *Nat. Commun.* **2020**, *11* (1), 1–13. <https://doi.org/10.1038/s41467-020-18171-8>.
- (58) Ieritano, C.; Crouse, J.; Campbell, J. L.; Hopkins, W. S. A Parallelized Molecular Collision Cross Section Package with Optimized Accuracy and Efficiency. *Analyst* **2019**, *144* (5), 1660–1670. <https://doi.org/10.1039/C8AN02150C>.
- (59) Kim, S.; Rodgers, R. P.; Marshall, A. G. Truly "Exact" Mass: Elemental Composition Can Be Determined Uniquely from Molecular Mass Measurement at ~0.1mDa Accuracy for Molecules up to ~500Da. *Int. J. Mass Spectrom.* **2006**, *251* (2), 260–265. <https://doi.org/https://doi.org/10.1016/j.ijms.2006.02.001>.

- (60) Zhou, Z.; Tu, J.; Zhu, Z. J. Advancing the Large-Scale CCS Database for Metabolomics and Lipidomics at the Machine-Learning Era. *Curr. Opin. Chem. Biol.* **2018**, *42*, 34–41. <https://doi.org/10.1016/j.cbpa.2017.10.033>.
- (61) Hellhake, S.; Meckelmann, S. W.; Empl, M. T.; Rentmeister, K.; Wißdorf, W.; Steinberg, P.; Schmitz, O. J.; Benter, T.; Schebb, N. H. Non-Targeted and Targeted Analysis of Oxylipins in Combination with Charge-Switch Derivatization by Ion Mobility High-Resolution Mass Spectrometry. *Anal. Bioanal. Chem.* **2020**, *412* (23), 5743–5757. <https://doi.org/10.1007/s00216-020-02795-2>.
- (62) Mccullagh, M.; Goshawk, J.; Gosciny, S. [APPLICATION NOTE] Use of Ion Mobility TW CCS N 2 Values in Non-Targeted Food Additives Screening [APPLICATION NOTE]. 1–7.
- (63) Chiaia-Hernandez, A. C.; Schymanski, E. L.; Kumar, P.; Singer, H. P.; Hollender, J. Suspect and Nontarget Screening Approaches to Identify Organic Contaminant Records in Lake Sediments. *Anal. Bioanal. Chem.* **2014**, 7323–7335. <https://doi.org/10.1007/s00216-014-8166-0>.
- (64) McCabe, J. W.; Hebert, M. J.; Shirzadeh, M.; Mallis, C. S.; Denton, J. K.; Walker, T. E.; Russell, D. H. The Ims Paradox: A Perspective on Structural Ion Mobility-Mass Spectrometry. *Mass Spectrom. Rev.* **2021**, *40* (3), 280–305. <https://doi.org/10.1002/mas.21642>.
- (65) Belova, L.; Caballero-Casero, N.; van Nuijs, A. L. N.; Covaci, A. Ion Mobility-High-Resolution Mass Spectrometry (IM-HRMS) for the Analysis of Contaminants of Emerging Concern (CECs): Database Compilation and Application to Urine Samples. *Anal. Chem.* **2021**, *93* (16), 6428–6436. <https://doi.org/10.1021/acs.analchem.1c00142>.
- (66) Castellanos, A.; Benigni, P.; Hernandez, D. R.; DeBord, J. D.; Ridgeway, M. E.; Park, M. A.; Fernandez-Lima, F. Fast Screening of Polycyclic Aromatic Hydrocarbons Using Trapped Ion Mobility Spectrometry - Mass Spectrometry. *Anal. Methods* **2014**, *6* (23), 9328–9332. <https://doi.org/10.1039/C4AY01655F>.
- (67) Muir, D. C. G.; Howard, P. H. Are There Other Persistent Organic Pollutants? A Challenge for Environmental Chemists. *Environ. Sci. Technol.* **2006**, *40* (23), 7157–7166. <https://doi.org/10.1021/es061677a>.
- (68) McGuire, J. M.; Collette, T. W.; Thurston, A. D.; Richardson, S. D.; Payne, W. D. *Multispectral Identification and Confirmation of Organic Compounds in Wastewater Extracts.*; Environ. Res. Lab., 1990.
- (69) UN. UN report: Urgent action needed to tackle chemical pollution as global production is set to double by 2030 <https://www.unep.org/news-and-stories/press-release/un-report-urgent-action-needed-tackle-chemical-pollution-global>.

- (70) Stockholm Convention. What are POPs
<http://www.pops.int/TheConvention/ThePOPs/tabid/673/Default.aspx>.
- (71) Hites, R. A.; Jobst, K. J. Is Nontargeted Screening Reproducible? *Environ. Sci. Technol.* **2018**, *52* (21), 11975–11976. <https://doi.org/10.1021/acs.est.8b05671>.
- (72) Rostkowski, P.; Haglund, P.; Aalizadeh, R.; Alygizakis, N.; Thomaidis, N.; Arandes, J. B.; Nizzetto, P. B.; Booiij, P.; Budzinski, H.; Brunswick, P.; Covaci, A.; Gallampos, C.; Grosse, S.; Hindle, R.; Ipolyi, I.; Jobst, K.; Kaserzon, S. L.; Leonards, P.; Lestremau, F.; Letzel, T.; Magnér, J.; Matsukami, H.; Moschet, C.; Oswald, P.; Plassmann, M.; Slobodnik, J.; Yang, C. The Strength in Numbers: Comprehensive Characterization of House Dust Using Complementary Mass Spectrometric Techniques. *Anal. Bioanal. Chem.* **2019**, *411* (10), 1957–1977. <https://doi.org/10.1007/s00216-019-01615-6>.
- (73) Andreasen, B.; van Bavel, B.; Fischer, S.; Haglund, P.; Rostkowski, P.; Reid, M. J.; Samanipour, S.; Schlabach, M.; Veenaas, C.; Dam, M. *Maximizing Output from Non-Target Screening*; Nordisk Ministerråd: Copenhagen, 2021. <https://doi.org/10.6027/temanord2021-526>.
- (74) Hertz, H. S.; Hites, R. A.; Biemann, K. Identification of Mass Spectra by Computer-Searching a File of Known Spectra. *Anal. Chem.* **1971**, *43* (6), 681–691. <https://doi.org/10.1021/ac60301a009>.
- (75) Harrison, A. G. *Chemical Ionization Mass Spectrometry*, 2nd ed.; CRC Press, 1992.
- (76) Kauppila, T. J.; Syage, J. A.; Benter, T. Recent Developments in Atmospheric Pressure Photoionization-Mass Spectrometry. *Mass Spectrom. Rev.* **2017**, *36* (3), 423–449. <https://doi.org/10.1002/mas.21477>.
- (77) Gross, J. H. *From the Discovery of Field Ionization to Field Desorption and Liquid Injection Field Desorption/Ionization-Mass Spectrometry—A Journey from Principles and Applications to a Glimpse into the Future*; 2020; Vol. 26. <https://doi.org/10.1177/1469066720939399>.
- (78) McEwen, C. N. GC/MS on an LC/MS Instrument Using Atmospheric Pressure Photoionization. *Int. J. Mass Spectrom.* **2007**, *259* (1), 57–64. <https://doi.org/10.1016/j.ijms.2006.07.004>.
- (79) Horning, E. C., Horning, M. G., Carroll, D. I., Dzidic, I., & Stillwell, R. N. New Picogram Detection System Based on a Mass Spectrometer with an External Ionization Source at Atmospheric Pressure. *Anal. Chem.* **1973**, *45* (6), 936–943.
- (80) Revelsky, I. A.; Yashin, Y. S.; Sobolevsky, T. G.; Revelsky, A. I.; Miller, B.; Oriedo, V. Electron Ionization and Atmospheric Pressure Photochemical

Ionization in Gas Chromatography- Mass Spectrometry Analysis of Amino Acids. **2003**, *507*, 497–507. <https://doi.org/10.1255/ejms.581>.

- (81) Schiewek, R.; Schellentra, M.; Mo, R.; Lorenz, M.; Giese, R.; Brockmann, K. J.; Ga, S. Ultrasensitive Determination of Polycyclic Aromatic Compounds with Atmospheric-Pressure Laser Ionization as an Interface for GC / MS. **2007**, *79* (11), 4135–4140.
- (82) Brenner, N.; Haapala, M.; Vuorensola, K.; Kostianen, R. Simple Coupling of Gas Chromatography to Electrospray Ionization Mass Spectrometry. *Anal. Chem.* **2008**, *80* (21), 8334–8339. <https://doi.org/10.1021/ac801406t>.
- (83) Niu, Y.; Liu, J.; Yang, R.; Zhang, J.; Shao, B. Atmospheric Pressure Chemical Ionization Source as an Advantageous Technique for Gas Chromatography-Tandem Mass Spectrometry. *TrAC - Trends Anal. Chem.* **2020**, *132*, 116053. <https://doi.org/10.1016/j.trac.2020.116053>.
- (84) Fang, J.; Zhao, H.; Zhang, Y.; Lu, M.; Cai, Z. Atmospheric Pressure Chemical Ionization in Gas Chromatography-Mass Spectrometry for the Analysis of Persistent Organic Pollutants. *Trends Environ. Anal. Chem.* **2020**, *25*, e00076. <https://doi.org/10.1016/j.teac.2019.e00076>.
- (85) Schreckenbach, S. A.; Simmons, D.; Ladak, A.; Mullin, L.; Muir, D. C. G.; Simpson, M. J.; Jobst, K. J. Data-Independent Identification of Suspected Organic Pollutants Using Gas Chromatography-Atmospheric Pressure Chemical Ionization-Mass Spectrometry. *Anal. Chem.* **2021**, *93* (3), 1498–1506. <https://doi.org/10.1021/acs.analchem.0c03733>.
- (86) Lipok, C.; Hippler, J.; Schmitz, O. J. A Four Dimensional Separation Method Based on Continuous Heart-Cutting Gas Chromatography with Ion Mobility and High Resolution Mass Spectrometry. *J. Chromatogr. A* **2018**, *1536*, 50–57. <https://doi.org/10.1016/j.chroma.2017.07.013>.
- (87) García-Villalba, R.; Pacchiarotta, T.; Carrasco-Pancorbo, A.; Segura-Carretero, A.; Fernández-Gutiérrez, A.; Deelder, A. M.; Mayboroda, O. A. Gas Chromatography-Atmospheric Pressure Chemical Ionization-Time of Flight Mass Spectrometry for Profiling of Phenolic Compounds in Extra Virgin Olive Oil. *J. Chromatogr. A* **2011**, *1218* (7), 959–971. <https://doi.org/10.1016/j.chroma.2010.12.014>.
- (88) Hurtado-Fernández, E.; Pacchiarotta, T.; Mayboroda, O. A.; Fernández-Gutiérrez, A.; Carrasco-Pancorbo, A. Metabolomic Analysis of Avocado Fruits by GC-APCI-TOF MS: Effects of Ripening Degrees and Fruit Varieties. *Anal. Bioanal. Chem.* **2015**, *407* (2), 547–555. <https://doi.org/10.1007/s00216-014-8283-9>.
- (89) Garlito, B.; Portolés, T.; Niessen, W. M. A.; Navarro, J. C.; Hontoria, F.; Monroig; Varó, I.; Serrano, R. Identification of Very Long-Chain (>C 24) Fatty Acid

Methyl Esters Using Gas Chromatography Coupled to Quadrupole/Time-of-Flight Mass Spectrometry with Atmospheric Pressure Chemical Ionization Source. *Anal. Chim. Acta* **2019**, *1051*, 103–109. <https://doi.org/10.1016/j.aca.2018.11.001>.

- (90) Allers, M.; Langejuergen, J.; Gaida, A.; Holz, O.; Schuchardt, S.; Hohlfeld, J. M.; Zimmermann, S. Measurement of Exhaled Volatile Organic Compounds from Patients with Chronic Obstructive Pulmonary Disease (COPD) Using Closed Gas Loop GC-IMS and GC-APCI-MS. *J. Breath Res.* **2016**, *10* (2), 026004/1-026004/10. <https://doi.org/10.1088/1752-7155/10/2/026004>.
- (91) Hennig, K.; Antignac, J. P.; Bichon, E.; Morvan, M.-L.; Miran, I.; Delalogue, S.; Feunteun, J.; Le Bizec, B. Steroid Hormone Profiling in Human Breast Adipose Tissue Using Semi-Automated Purification and Highly Sensitive Determination of Estrogens by GC-APCI-MS/MS. *Anal. Bioanal. Chem.* **2018**, *410* (1), 259–275. <https://doi.org/10.1007/s00216-017-0717-8>.
- (92) Li, D. X.; Gan, L.; Bronja, A.; Schmitz, O. J. Gas Chromatography Coupled to Atmospheric Pressure Ionization Mass Spectrometry (GC-API-MS): Review. *Anal. Chim. Acta* **2015**, *891*, 43–61. <https://doi.org/10.1016/j.aca.2015.08.002>.
- (93) Canellas, E.; Vera, P.; Domeño, C.; Alfaro, P.; Nerín, C. Atmospheric Pressure Gas Chromatography Coupled to Quadrupole-Time of Flight Mass Spectrometry as a Powerful Tool for Identification of Non Intentionally Added Substances in Acrylic Adhesives Used in Food Packaging Materials. *J. Chromatogr. A* **2012**, *1235*, 141–148. <https://doi.org/10.1016/j.chroma.2012.02.039>.
- (94) Sales, C.; Portolés, T.; Sancho, J. V.; Abad, E.; Ábalos, M.; Sauló, J.; Fiedler, H.; Gómara, B.; Beltrán, J. Potential of Gas Chromatography-Atmospheric Pressure Chemical Ionization-Tandem Mass Spectrometry for Screening and Quantification of Hexabromocyclododecane. *Anal. Bioanal. Chem.* **2016**, *408* (2), 449–459. <https://doi.org/10.1007/s00216-015-9146-8>.
- (95) Hernández, F.; Ibáñez, M.; Portolés, T.; Cervera, M. I.; Sancho, J. V.; López, F. J. Advancing towards Universal Screening for Organic Pollutants in Waters. *J. Hazard. Mater.* **2015**, *282*, 86–95. <https://doi.org/10.1016/j.jhazmat.2014.08.006>.
- (96) Sheu, R.; Marcotte, A.; Khare, P.; Charan, S.; Ditto, J. C.; Gentner, D. R. Advances in Offline Approaches for Chemically Speciated Measurements of Trace Gas-Phase Organic Compounds via Adsorbent Tubes in an Integrated Sampling-to-Analysis System. *J. Chromatogr. A* **2018**, *1575*, 80–90. <https://doi.org/10.1016/j.chroma.2018.09.014>.
- (97) Li, X.; Zhen, Y.; Wang, R.; Li, T.; Dong, S.; Zhang, W.; Cheng, J.; Wang, P.; Su, X. Application of Gas Chromatography Coupled to Triple Quadrupole Mass Spectrometry (GC-(APCI)MS/MS) in Determination of PCBs (Mono-to Deca-)

and PCDD/Fs in Chinese Mitten Crab Food Webs. *Chemosphere* **2021**, 265, 129055. <https://doi.org/10.1016/j.chemosphere.2020.129055>.

- (98) Larson, E. A.; Hutchinson, C. P.; Lee, Y. J. Gas Chromatography-Tandem Mass Spectrometry of Lignin Pyrolyzates with Dopant-Assisted Atmospheric Pressure Chemical Ionization and Molecular Structure Search with CSI:FingerID. *J. Am. Soc. Mass Spectrom.* **2018**, 29 (9), 1908–1918. <https://doi.org/10.1007/s13361-018-2001-3>.
- (99) Ojanperä, I.; Mesihää, S.; Rasanen, I.; Pelander, A.; Ketola, R. A. Simultaneous Identification and Quantification of New Psychoactive Substances in Blood by GC-APCI-QTOFMS Coupled to Nitrogen Chemiluminescence Detection without Authentic Reference Standards. *Anal. Bioanal. Chem.* **2016**, 408 (13), 3395–3400. <https://doi.org/10.1007/s00216-016-9461-8>.
- (100) Mesihää, S.; Ketola, R. A.; Pelander, A.; Rasanen, I.; Ojanperä, I. Development of a GC-APCI-QTOFMS Library for New Psychoactive Substances and Comparison to a Commercial ESI Library. *Anal. Bioanal. Chem.* **2017**, 409 (8), 2007–2013. <https://doi.org/10.1007/s00216-016-0148-y>.
- (101) Ma, S.; Ma, C.; Qian, K.; Zhou, Y.; Shi, Q. Characterization of Phenolic Compounds in Coal Tar by Gas Chromatography/Negative-Ion Atmospheric Pressure Chemical Ionization Mass Spectrometry. *Rapid Commun. Mass Spectrom.* **2016**, No. March, 1806–1810. <https://doi.org/10.1002/rcm.7608>.
- (102) Geng, D.; Jogsten, I. E.; Dunstan, J.; Hagberg, J.; Wang, T.; Ruzzin, J.; Rabasa-Lhoret, R.; van Bavel, B. Gas Chromatography/Atmospheric Pressure Chemical Ionization/Mass Spectrometry for the Analysis of Organochlorine Pesticides and Polychlorinated Biphenyls in Human Serum. *J. Chromatogr. A* **2016**, 1453, 88–98. <https://doi.org/10.1016/j.chroma.2016.05.030>.
- (103) Mesihää, S.; Rasanen, I.; Ojanpera, I. Quantitative Estimation of α -PVP Metabolites in Urine by GC-APCI-QTOFMS with Nitrogen Chemiluminescence Detection Based on Parent Drug Calibration. *Forensic Sci. Int.* **2018**, 286, 12–17. <https://doi.org/10.1016/j.forsciint.2018.02.017>.
- (104) Zacs, D.; Perkons, I.; Bartkevics, V. Evaluation of Analytical Performance of Gas Chromatography Coupled with Atmospheric Pressure Chemical Ionization Fourier Transform Ion Cyclotron Resonance Mass Spectrometry (GC-APCI-FT-ICR-MS) in the Target and Non-Targeted Analysis of Brominated and Chlo. *Chemosphere* **2019**, 225, 368–377. <https://doi.org/10.1016/j.chemosphere.2019.03.047>.
- (105) Raro, M.; Portolés, T.; Pitarch, E.; Sancho, J. V.; Hernández, F.; Garrosta, L.; Marcos, J.; Ventura, R.; Segura, J.; Pozo, O. J. Potential of Atmospheric Pressure Chemical Ionization Source in Gas Chromatography Tandem Mass Spectrometry

for the Screening of Urinary Exogenous Androgenic Anabolic Steroids. *Anal. Chim. Acta* **2016**, *906*, 128–138. <https://doi.org/10.1016/j.aca.2015.11.041>.

- (106) Geng, D.; Kukucka, P.; Jogsten, I. E. Analysis of Brominated Flame Retardants and Their Derivatives by Atmospheric Pressure Chemical Ionization Using Gas Chromatography Coupled to Tandem Quadrupole Mass Spectrometry. *Talanta* **2017**, *162*, 618–624. <https://doi.org/10.1016/j.talanta.2016.10.060>.
- (107) Zhang, Y.; Chen, Y.; Li, R.; Chen, W.; Song, Y.; Hu, D.; Cai, Z. Determination of PM_{2.5}-Bound Polyaromatic Hydrocarbons and Their Hydroxylated Derivatives by Atmospheric Pressure Gas Chromatography-Tandem Mass Spectrometry. *Talanta* **2019**, *195*, 757–763. <https://doi.org/10.1016/j.talanta.2018.12.006>.
- (108) Gill, B.; Mell, A.; Shanmuganathan, M.; Jobst, K.; Zhang, X.; Kinniburgh, D.; Cherry, N.; Britz-McKibbin, P. Urinary Hydroxypyrene Determination for Biomonitoring of Firefighters Deployed at the Fort McMurray Wildfire: An Inter-Laboratory Method Comparison. *Anal. Bioanal. Chem.* **2019**, *411* (7), 1397–1407. <https://doi.org/10.1007/s00216-018-01569-1>.
- (109) Organtini, K. L.; Myers, A. L.; Jobst, K. J.; Reiner, E. J.; Ross, B.; Ladak, A.; Mullin, L.; Stevens, D.; Dorman, F. L. Quantitative Analysis of Mixed Halogen Dioxins and Furans in Fire Debris Utilizing Atmospheric Pressure Ionization Gas Chromatography-Triple Quadrupole Mass Spectrometry. *Anal. Chem.* **2015**, *87* (20), 10368–10377. <https://doi.org/10.1021/acs.analchem.5b02463>.
- (110) Organtini, K. L.; Haimovici, L.; Jobst, K. J.; Reiner, E. J.; Ladak, A.; Stevens, D.; Cochran, J. W.; Dorman, F. L. Comparison of Atmospheric Pressure Ionization Gas Chromatography-Triple Quadrupole Mass Spectrometry to Traditional High-Resolution Mass Spectrometry for the Identification and Quantification of Halogenated Dioxins and Furans. *Anal. Chem.* **2015**, *87* (15), 7902–7908. <https://doi.org/10.1021/acs.analchem.5b01705>.
- (111) Portoles, T.; Sales, C.; Abalos, M.; Saulo, J.; Abad, E. Evaluation of the Capabilities of Atmospheric Pressure Chemical Ionization Source Coupled to Tandem Mass Spectrometry for the Determination of Dioxin-like Polychlorobiphenyls in Complex-Matrix Food Samples. *Anal. Chim. Acta* **2016**, *937*, 96–105. <https://doi.org/10.1016/j.aca.2016.06.038>.
- (112) Megson, D.; Robson, M.; Jobst, K. J.; Helm, P. A.; Reiner, E. J. Determination of Halogenated Flame Retardants Using Gas Chromatography with Atmospheric Pressure Chemical Ionization (APCI) and a High-Resolution Quadrupole Time-of-Flight Mass Spectrometer (HRqTOFMS). *Anal. Chem.* **2016**, *88* (23), 11406–11411. <https://doi.org/10.1021/acs.analchem.6b01550>.
- (113) Mirabelli, M. F.; Zenobi, R. Solid-Phase Microextraction Coupled to Capillary Atmospheric Pressure Photoionization-Mass Spectrometry for Direct Analysis of

Polar and Nonpolar Compounds. *Anal. Chem.* **2018**, *90* (8), 5015–5022.
<https://doi.org/10.1021/acs.analchem.7b04514>.

- (114) Deibel, E.; Klink, D.; Schmitz, O. J. New Derivatization Strategies for the Ultrasensitive Analysis of Non-Aromatic Analytes with APLI-TOF-MS. *Anal. Bioanal. Chem.* **2015**, *407* (24), 7425–7434. <https://doi.org/10.1007/s00216-015-8908-7>.
- (115) Ayala-Cabrera, J. F.; Contreras-Llin, A.; Moyano, E.; Santos, F. J. A Novel Methodology for the Determination of Neutral Perfluoroalkyl and Polyfluoroalkyl Substances in Water by Gas Chromatography-Atmospheric Pressure Photoionization-High Resolution Mass Spectrometry. *Anal. Chim. Acta* **2020**, *1100*, 97–106. <https://doi.org/10.1016/j.aca.2019.12.004>.
- (116) Cervera, M. I.; Portolés, T.; López, F. J.; Beltrán, J.; Hernández, F. Screening and Quantification of Pesticide Residues in Fruits and Vegetables Making Use of Gas Chromatography-Quadrupole Time-of-Flight Mass Spectrometry with Atmospheric Pressure Chemical Ionization. *Anal. Bioanal. Chem.* **2014**, *406* (27), 6843–6855. <https://doi.org/10.1007/s00216-014-7853-1>.
- (117) Richter-Brockmann, S.; Dettbarn, G.; Jessel, S.; John, A.; Seidel, A.; Achten, C. GC-APLI-MS as a Powerful Tool for the Analysis of BaP-Tetraol in Human Urine. *J. Chromatogr. B Anal. Technol. Biomed. Life Sci.* **2018**, *1100–1101*, 1–5. <https://doi.org/10.1016/j.jchromb.2018.08.006>.
- (118) Leider, A.; Richter-Brockmann, S.; Nettersheim, B. J.; Achten, C.; Hallmann, C. Low-Femtogram Sensitivity Analysis of Polyaromatic Hydrocarbons Using GC-APLI-TOF Mass Spectrometry: Extending the Target Window for Aromatic Steroids in Early Proterozoic Rocks. *Org. Geochem.* **2019**, *129*, 77–87. <https://doi.org/10.1016/j.orggeochem.2019.01.015>.
- (119) Dohmann, J. F.; Thiäner, J. B.; Achten, C. Ultrasensitive Detection of Polycyclic Aromatic Hydrocarbons in Coastal and Harbor Water Using GC-APLI-MS. *Mar. Pollut. Bull.* **2019**, *149* (August), 110547. <https://doi.org/10.1016/j.marpolbul.2019.110547>.
- (120) Große Brinkhaus, S.; Thiäner, J. B.; Achten, C.; Grosse Brinkhaus, S.; Thiaener, J. B.; Achten, C. Ultra-High Sensitive PAH Analysis of Certified Reference Materials and Environmental Samples by GC-APLI-MS. *Anal. Bioanal. Chem.* **2017**, *409* (11), 2801–2812. <https://doi.org/10.1007/s00216-017-0224-y>.
- (121) Cha, E.; Sook, E.; Cha, S.; Lee, J. Analytica Chimica Acta Coupling of Gas Chromatography and Electrospray Ionization High Resolution Mass Spectrometry for the Analysis of Anabolic Steroids as Trimethylsilyl Derivatives in Human Urine. *Anal. Chim. Acta* **2017**, *964*, 123–133. <https://doi.org/10.1016/j.aca.2017.01.058>.

- (122) Cha, E.; Jeong, E. S.; Han, S. B.; Cha, S.; Son, J.; Kim, S.; Oh, H. Bin; Lee, J. Ionization of Gas-Phase Polycyclic Aromatic Hydrocarbons in Electrospray Ionization Coupled with Gas Chromatography. **2018**. <https://doi.org/10.1021/acs.analchem.8b00401>.
- (123) Mcewen, C. N.; Mckay, R. G. A Combination Atmospheric Pressure LC/MS:GC/MS Ion Source: Advantages of Dual AP-LC/MS:GC/MS Instrumentation. **2005**. <https://doi.org/10.1016/j.jasms.2005.07.005>.
- (124) Schiewek, R.; Lorenz, M.; Giese, R.; Brockmann, K.; Benter, T.; Gäb, S.; Schmitz, O. J. Development of a Multipurpose Ion Source for LC-MS and GC-API MS. *Anal. Bioanal. Chem.* **2008**, *392* (1–2), 87–96. <https://doi.org/10.1007/s00216-008-2255-x>.
- (125) Robb, D. B.; Covey, T. R.; Bruins, A. P. Atmospheric Pressure Photoionization: An Ionization Method for Liquid Chromatography-Mass Spectrometry. **2000**. <https://doi.org/10.1021/ac0001636>.
- (126) Syage, Jack A., Matthew D. Evans, and K. A. H. Photoionization Mass Spectrometry. *Am. Lab.* **2000**, *32* (24), 24–29.
- (127) Cody, R. B.; Laramée, J. A.; Durst, H. D. Versatile New Ion Source for the Analysis of Materials in Open Air under Ambient Conditions. *Anal. Chem.* **2005**, *77* (8), 2297–2302. <https://doi.org/10.1021/ac050162j>.
- (128) Cody, R. B. GC/MS with a DART™ Ion Source. *LC GC North Am.* **2008**, *FEV*, 59–59.
- (129) Faubert, D.; Paul, G. J. C.; Giroux, J.; Bertrand, M. J. Selective Fragmentation and Ionization of Organic Compounds Using an Energy-Tunable Rare-Gas Metastable Beam Source. *Int. J. Mass Spectrom. Ion Process.* **1993**, *124* (1), 69–77. [https://doi.org/10.1016/0168-1176\(93\)85021-5](https://doi.org/10.1016/0168-1176(93)85021-5).
- (130) Nudnova, M. M.; Zhu, L.; Zenobi, R. Active Capillary Plasma Source for Ambient Mass Spectrometry. *Rapid Commun. Mass Spectrom.* **2012**, *26* (12), 1447–1452. <https://doi.org/https://doi.org/10.1002/rcm.6242>.
- (131) Niu, Y.; Liu, J.; Yang, R.; Zhang, J.; Shao, B. Atmospheric Pressure Chemical Ionization Source as an Advantageous Technique for Gas Chromatography-Tandem Mass Spectrometry. *TrAC, Trends Anal. Chem.* **2020**, *132*, 116053. <https://doi.org/10.1016/j.trac.2020.116053>.
- (132) Ayala-Cabrera, J. F.; Galceran, M. T.; Moyano, E.; Santos, F. J. Chloride-Attachment Atmospheric Pressure Photoionisation for the Determination of Short-Chain Chlorinated Paraffins by Gas Chromatography-High-Resolution Mass

Spectrometry. *Anal. Chim. Acta* **2021**, *1172*, 338673.
<https://doi.org/10.1016/j.aca.2021.338673>.

- (133) Di Lorenzo, R. A.; Lobodin, V. V.; Cochran, J.; Kolic, T.; Besevic, S.; Sled, J. G.; Reiner, E. J.; Jobst, K. J. Fast Gas Chromatography-Atmospheric Pressure (Photo)Ionization Mass Spectrometry of Polybrominated Diphenylether Flame Retardants. *Anal. Chim. Acta* **2019**, *1056*, 70–78.
<https://doi.org/10.1016/j.aca.2019.01.007>.
- (134) Kauppila, T. J.; Kersten, H.; Benter, T. Ionization of EPA Contaminants in Direct and Dopant- and Atmospheric Pressure Laser Ionization. **2015**, 1036–1045.
<https://doi.org/10.1007/s13361-015-1092-3>.
- (135) Stader, C.; Beer, F. T.; Achten, C. Environmental PAH Analysis by Gas Chromatography-Atmospheric Pressure Laser Ionization-Time-of-Flight-Mass Spectrometry (GC-APLI-MS). *Anal. Bioanal. Chem.* **2013**, *405* (22), 7041–7052.
<https://doi.org/10.1007/s00216-013-7183-8>.
- (136) Mollah, S.; Pris, A. D.; Johnson, S. K.; Gwizdala III, A. B.; Houk, R. S. Identification of Metal Cations, Metal Complexes, and Anions by Electrospray Mass Spectrometry in the Negative Ion Mode. *Anal. Chem.* **2000**, *72*, 985–991.
<https://doi.org/10.1021/ac9908647>.
- (137) Cody, R. B. Observation of Molecular Ions and Analysis of Nonpolar Compounds with the Direct Analysis in Real Time Ion Source. *Anal. Chem.* **2009**, *81* (3), 1101–1107. <https://doi.org/10.1021/ac8022108>.
- (138) Moore, S. Use of the Metastable Atom Bombardment (MAB) Ion Source for the Elimination of PCDE Interference in PCDD/PCDF Analysis. *Chemosph.* **2002**, *49* (2), 121–125. [https://doi.org/10.1016/S0045-6535\(02\)00329-6](https://doi.org/10.1016/S0045-6535(02)00329-6).
- (139) Nørgaard, A. W.; Kofoed-Sørensen, V.; Svensmark, B.; Wolkoff, P.; Clausen, P. A. Gas Chromatography Interfaced with Atmospheric Pressure Ionization-Quadrupole Time-of-Flight-Mass Spectrometry by Low-Temperature Plasma Ionization. *Anal. Chem.* **2013**, *85* (1), 28–32. <https://doi.org/10.1021/ac301859r>.
- (140) Mirabelli, M. F.; Wolf, J. C.; Zenobi, R. Atmospheric Pressure Soft Ionization for Gas Chromatography with Dielectric Barrier Discharge Ionization-Mass Spectrometry (GC-DBDI-MS). *Analyst* **2017**, *142* (11), 1909–1915.
<https://doi.org/10.1039/c7an00245a>.
- (141) Hagenhoff, S.; Korf, A.; Markgraf, U.; Brandt, S.; Schütz, A.; Franzke, J.; Hayen, H. Screening of Semifluorinated N-Alkanes by Gas Chromatography Coupled to Dielectric Barrier Discharge Ionization Mass Spectrometry. *Rapid Commun. Mass Spectrom.* **2018**, *32* (13), 1092–1098. <https://doi.org/10.1002/rcm.8139>.

- (142) Schymanski, E. L.; Singer, H. P.; Slobodnik, J.; Ipolyi, I. M.; Oswald, P.; Krauss, M.; Schulze, T.; Haglund, P.; Letzel, T.; Grosse, S.; Thomaidis, N. S.; Bletsou, A.; Zwiener, C.; Ibáñez, M.; Portolés, T.; De Boer, R.; Reid, M. J.; Onghena, M.; Kunkel, U.; Schulz, W.; Guillon, A.; Noyon, N.; Leroy, G.; Bados, P.; Bogialli, S.; Stipaničev, D.; Rostkowski, P.; Hollender, J. Non-Target Screening with High-Resolution Mass Spectrometry: Critical Review Using a Collaborative Trial on Water Analysis. *Anal. Bioanal. Chem.* **2015**, *407* (21), 6237–6255. <https://doi.org/10.1007/s00216-015-8681-7>.
- (143) Pitarch, E.; Cervera, M. I.; Portolés, T.; Ibáñez, M.; Barreda, M.; Renau-Pruñonosa, A.; Morell, I.; López, F.; Albarrán, F.; Hernández, F. Comprehensive Monitoring of Organic Micro-Pollutants in Surface and Groundwater in the Surrounding of a Solid-Waste Treatment Plant of Castellón, Spain. *Sci. Total Environ.* **2016**, *548–549*, 211–220. <https://doi.org/10.1016/j.scitotenv.2015.12.166>.
- (144) Ballesteros-Gómez, A.; de Boer, J.; Leonards, P. E. G. Novel Analytical Methods for Flame Retardants and Plasticizers Based on Gas Chromatography, Comprehensive Two-Dimensional Gas Chromatography, and Direct Probe Coupled to Atmospheric Pressure Chemical Ionization-High Resolution Time-of-Flight-Mass Spectrom. *Anal. Chem.* **2013**, *85* (20), 9572–9580. <https://doi.org/10.1021/ac4017314>.
- (145) Jobst, K. J.; Arora, A.; Pollitt, K. G.; Sled, J. G. Dried Blood Spots for the Identification of Bioaccumulating Organic Compounds: Current Challenges and Future Perspectives. *Curr. Opin. Environ. Sci. Heal.* **2020**, *15*, 66–73. <https://doi.org/10.1016/j.coesh.2020.07.001>.
- (146) Patterson, D. G.; Welch, S. M.; Turner, W. E.; Sjödin, A.; Focant, J.-F. Cryogenic Zone Compression for the Measurement of Dioxins in Human Serum by Isotope Dilution at the Attogram Level Using Modulated Gas Chromatography Coupled to High Resolution Magnetic Sector Mass Spectrometry. *J. Chromatogr. A* **2011**, *1218* (21), 3274–3281. <https://doi.org/10.1016/j.chroma.2010.10.084>.
- (147) Seeley, J. V.; Schimmel, N. E.; Seeley, S. K. The Multi-Mode Modulator: A Versatile Fluidic Device for Two-Dimensional Gas Chromatography. *J. Chromatogr. A* **2018**, *1536*, 6–15. <https://doi.org/10.1016/j.chroma.2017.06.030>.
- (148) Bowman, D. T.; Jobst, K. J.; Helm, P. A.; Kleywegt, S.; Diamond, M. L. Characterization of Polycyclic Aromatic Compounds in Commercial Pavement Sealcoat Products for Enhanced Source Apportionment. *Environ. Sci. Technol.* **2019**, *53* (6), 3157–3165. <https://doi.org/10.1021/acs.est.8b06779>.
- (149) Venable, J. D.; Dong, M.; Wohlschlegel, J.; Dillin, A.; Iii, J. R. Y. Automated Approach for Quantitative Analysis of Complex Peptide Mixtures from Tandem Mass Spectra. **2004**, *1* (1), 1–8. <https://doi.org/10.1038/NMETH705>.

- (150) Gillet, L. C.; Navarro, P.; Tate, S.; Ro, H.; Selevsek, N.; Reiter, L.; Bonner, R.; Aebersold, R. Targeted Data Extraction of the MS / MS Spectra Generated by Data-Independent Acquisition : A New Concept for Consistent and Accurate Proteome Analysis. **2012**, 1–17. <https://doi.org/10.1074/mcp.O111.016717>.
- (151) Moseley, M. A.; Hughes, C. J.; Juvvadi, P. R.; Soderblom, E. J.; Lennon, S.; Perkins, S. R.; Thompson, J. W.; Steinbach, W. J.; Geromanos, S. J.; Wildgoose, J.; Langridge, J. I.; Richardson, K.; Vissers, J. P. C. Scanning Quadrupole Data-Independent Acquisition, Part A: Qualitative and Quantitative Characterization. **2018**. <https://doi.org/10.1021/acs.jproteome.7b00464>.
- (152) Waters. MassFragment for Structural Elucidation in Metabolite ID using Exact Mass MS
https://www.waters.com/waters/library.htm?locale=en_US&lid=10064396.
- (153) Waters. UNIFI Scientific Information System
https://www.waters.com/waters/en_US/UNIFI-Scientific-Information-System/nav.htm?cid=134801359&locale=en_US.
- (154) Wolf, S.; Schmidt, S.; Müller-Hannemann, M.; Neumann, S. In Silico Fragmentation for Computer Assisted Identification of Metabolite Mass Spectra. *BMC Bioinformatics* **2010**, *11* (1), 148. <https://doi.org/10.1186/1471-2105-11-148>.
- (155) Dührkop, K.; Shen, H.; Meusel, M.; Rousu, J.; Böcker, S.; Dührkop, K.; Shen, H.; Meusel, M.; Rousu, J.; Böcker, S. Searching Molecular Structure Databases with Tandem Mass Spectra Using CSI : FingerID. **2015**, *112* (41), 12580–12585. <https://doi.org/10.1073/pnas.1509788112/-/DCSupplemental>. www.pnas.org/cgi/doi/10.1073/pnas.1509788112.
- (156) Allen, F.; Pon, A.; Wilson, M.; Greiner, R.; Wishart, D. CFM-ID: A Web Server for Annotation, Spectrum Prediction and Metabolite Identification from Tandem Mass Spectra. *Nucleic Acids Res.* **2014**, *42*. <https://doi.org/10.1093/nar/gku436>.
- (157) Grimme, S. Towards First Principles Calculation of Electron Impact Mass Spectra of Molecules. *Angewandte Chemie*. Verlag Chemie: Weinheim/Bergstr. : New York : 2013, pp 6306–6312. <https://doi.org/10.1002/anie.201300158>.
- (158) Kanu, A. B.; Dwivedi, P.; Tam, M.; Matz, L.; Hill, H. H. Ion Mobility-Mass Spectrometry. *Journal of mass spectrometry*. John Wiley & Sons: Chichester ; New York, NY : 2008, pp 1–22. <https://doi.org/10.1002/jms.1383>.
- (159) Olanrewaju, C. A.; Ramirez, C. E.; Fernandez-Lima, F. Comprehensive Screening of Polycyclic Aromatic Hydrocarbons and Similar Compounds Using GC-APLI-TIMS-TOFMS/GC-EI-MS. *Anal. Chem. (Washington, DC, United States)* **2021**, *93* (15), 6080–6087. <https://doi.org/10.1021/acs.analchem.0c04525>.

- (160) Scheubert, K.; Hufsky, F.; Böcker, S. Computational Mass Spectrometry for Small Molecules. *J. Cheminform.* **2013**, *5* (3), 12. <https://doi.org/10.1186/1758-2946-5-12>.
- (161) Su, Q. Z.; Vera, P.; Van de Wiele, C.; Nerín, C.; Lin, Q. B.; Zhong, H. N. Non-Target Screening of (Semi-)Volatiles in Food-Grade Polymers by Comparison of Atmospheric Pressure Gas Chromatography Quadrupole Time-of-Flight and Electron Ionization Mass Spectrometry. *Talanta* **2019**, *202* (April), 285–296. <https://doi.org/10.1016/j.talanta.2019.05.029>.
- (162) Cherta, L.; Portolés, T.; Pitarch, E.; Beltran, J.; López, F. J.; Calatayud, C.; Company, B.; Hernández, F. Analytical Strategy Based on the Combination of Gas Chromatography Coupled to Time-of-Flight and Hybrid Quadrupole Time-of-Flight Mass Analyzers for Non-Target Analysis in Food Packaging. *Food Chem.* **2015**, *188*, 301–308. <https://doi.org/10.1016/j.foodchem.2015.04.141>.
- (163) Mitchum, R. K.; Korfmacher, W. A.; Molar, G. F.; Stalling, D. L. Capillary Gas Chromatography/Atmospheric Pressure Negative Chemical Ionization Mass Spectrometry of the 22 Isomeric Tetrachlorodibenzo-p-Dioxins. *Anal. Chem.* **1982**, *54* (4), 719–722. <https://doi.org/10.1021/ac00241a028>.
- (164) Korfmacher, W. A.; Rowland, K. R.; Mitchum, R. K.; Daly, J. J.; McDaniel, R. C.; Plummer, M. V. Analysis of Snake Tissue and Snake Eggs for 2,3,7,8-Tetrachlorodibenzo-p-Dioxin via Fused Silica GC Combined with Atmospheric Pressure Ionization MS. *Chemosphere* **1984**, *13* (11), 1229–1233. [https://doi.org/10.1016/0045-6535\(84\)90123-1](https://doi.org/10.1016/0045-6535(84)90123-1).
- (165) Korfmacher, W. A.; Hansen, E. B.; Rowland, K. L. Tissue Distribution of 2,3,7,8-TCDD in Bullfrogs Obtained from a 2,3,7,8-TCDD-Contaminated Area. *Chemosphere* **1986**, *15* (2), 121–126. [https://doi.org/10.1016/0045-6535\(86\)90563-1](https://doi.org/10.1016/0045-6535(86)90563-1).
- (166) Ishaq, R.; Näf, C.; Zebühr, Y.; Broman, D.; Järnberg, U. PCBs, PCNs, PCDD/Fs, PAHs and Cl-PAHs in Air and Water Particulate Samples—Patterns and Variations. *Chemosphere* **2003**, *50* (9), 1131–1150. [https://doi.org/10.1016/S0045-6535\(02\)00701-4](https://doi.org/10.1016/S0045-6535(02)00701-4).
- (167) Fernando, S.; Green, M. K.; Organtini, K.; Dorman, F.; Jones, R.; Reiner, E. J.; Jobst, K. J. Differentiation of (Mixed) Halogenated Dibenzo-p-Dioxins by Negative Ion Atmospheric Pressure Chemical Ionization. *Anal. Chem.* **2016**, *88* (10), 5205–5211. <https://doi.org/10.1021/acs.analchem.6b00255>.
- (168) Ayerton, S. T.; Jones, R.; Douce, D. S.; Morris, M. R.; Cooks, R. G. Uncatalyzed, Regioselective Oxidation of Saturated Hydrocarbons in an Ambient Corona Discharge. *Angewandte Chemie*. Verlag Chemie: Weinheim ; [New York] : 2018, pp 777–781. <https://doi.org/10.1002/ange.201711190>.

- (169) Megson, D.; Hajimirzaee, S.; Doyle, A.; Cannon, F.; Balouet, J.-C. Investigating the Potential for Transisomerisation of Trycresyl Phosphate with a Palladium Catalyst and Its Implications for Aircraft Cabin Air Quality. *Chemosph.* **2019**, *215*, 532–534. <https://doi.org/10.1016/j.chemosphere.2018.10.082>.
- (170) Lai, A.; Singh, R. R.; Kovalova, L.; Jaeggi, O.; Kondić, T.; Schymanski, E. L. Retrospective Non-Target Analysis to Support Regulatory Water Monitoring: From Masses of Interest to Recommendations via in Silico Workflows. *Env. Sci Eur* **2021**, *33*, 43. <https://doi.org/10.1186/s12302-021-00475-1>.
- (171) Waters. MassFragment https://www.waters.com/waters/en_US/MassFragment/nav.htm?cid=1000943&locale=en_US.
- (172) Thermo Fisher. Mass Frontier Spectral Interpretation Software <https://www.thermofisher.com/ca/en/home/industrial/mass-spectrometry/liquid-chromatography-mass-spectrometry-lc-ms/lc-ms-software/multi-omics-data-analysis/mass-frontier-spectral-interpretation-software.html>.
- (173) Schreckenbach, S. A.; Anderson, J. S. M.; Koopman, J.; Grimme, S.; Simpson, M. J.; Jobst, K. J. Predicting the Mass Spectra of Environmental Pollutants Using Computational Chemistry: A Case Study and Critical Evaluation. *J. Am. Soc. Mass Spectrom.* **2021**, *32* (6), 1508–1518. <https://doi.org/10.1021/jasms.1c00078>.
- (174) Koopman, J.; Grimme, S. From QCEIMS to QCxMS : A Tool to Routinely Calculate CID Mass Spectra Using Molecular Dynamics. **2021**. <https://doi.org/10.1021/jasms.1c00098>.
- (175) EC. *Risk Profile and Summary Report for Short-Chained Chlorinated Paraffins (SCCPs). Dossier Prepared for the UNECE Convention on Long-Range Transboundary Air Pollution, Protocol on Persistent Organic Pollutants*; 2005.
- (176) Zeng, L.; Li, H.; Wang, T.; Gao, Y.; Xiao, K.; Du, Y.; Wang, Y.; Jiang, G. Behavior, Fate, and Mass Loading of Short Chain Chlorinated Paraffins in an Advanced Municipal Sewage Treatment Plant. *Environ. Sci. Technol.* **2013**, *47* (2), 732–740. <https://doi.org/10.1021/es304237m>.
- (177) Wu, Y.; Gao, S.; Ji, B.; Liu, Z.; Zeng, X.; Yu, Z. Occurrence of Short- and Medium-Chain Chlorinated Paraffins in Soils and Sediments from Dongguan City, South China. *Environ. Pollut.* **2020**, *265*, 114181. <https://doi.org/10.1016/j.envpol.2020.114181>.
- (178) Brandsma, S. H.; Brits, M.; Groenewoud, Q. R.; van Velzen, M. J. M.; Leonards, P. E. G.; de Boer, J. Chlorinated Paraffins in Car Tires Recycled to Rubber Granulates and Playground Tiles. *Environ. Sci. Technol.* **2019**, *53* (13), 7595–7603. <https://doi.org/10.1021/acs.est.9b01835>.

- (179) Gallistl, C.; Sprengel, J.; Vetter, W. High Levels of Medium-Chain Chlorinated Paraffins and Polybrominated Diphenyl Ethers on the inside of Several Household Baking Oven Doors. **2017**. <https://doi.org/10.1016/j.scitotenv.2017.09.112>.
- (180) United Nations Environment Programme. *Draft Technical Guidelines on the Environmentally Sound Management of Wastes Consisting of, Containing or Contaminated with Short-Chain Chlorinated Paraffins*; Geneva, Switzerland, 2018.
- (181) Wong, F.; Suzuki, G.; Michinaka, C.; Yuan, B.; Takigami, H.; de Wit, C. A. Dioxin-like Activities, Halogenated Flame Retardants, Organophosphate Esters and Chlorinated Paraffins in Dust from Australia, the United Kingdom, Canada, Sweden and China. *Chemosphere* **2017**, *168*, 1248–1256. <https://doi.org/10.1016/j.chemosphere.2016.10.074>.
- (182) Li, T.; Wan, Y.; Gao, S.; Wang, B.; Hu, J. High-Throughput Determination and Characterization of Short-, Medium-, and Long-Chain Chlorinated Paraffins in Human Blood. *Environ. Sci. Technol.* **2017**, *51* (6), 3346–3354. <https://doi.org/10.1021/acs.est.6b05149>.
- (183) Xia, D.; Gao, L.-R.; Zheng, M.-H.; Li, J.-G.; Zhang, L.; Wu, Y.-N.; Qiao, L.; Tian, Q.-C.; Huang, H.-T.; Liu, W.-B.; Su, G.-J.; Liu, G.-R. Health Risks Posed to Infants in Rural China by Exposure to Short-and Medium-Chain Chlorinated Paraffins in Breast Milk. **2017**. <https://doi.org/10.1016/j.envint.2017.03.013>.
- (184) Tomy, G. T.; Stern, G. A.; Lockhart, W. L.; Muir, D. C. G. Occurrence of C10–C13 Polychlorinated N-Alkanes in Canadian Midlatitude and Arctic Lake Sediments. *Environ. Sci. Technol.* **1999**, *33* (17), 2858–2863. <https://doi.org/10.1021/es990107q>.
- (185) United Nations. *Reference: C.N.766.2017.TREATIES-XXVII.15 (Depositary Notification)*; 2017.
- (186) Van Mourik, L. M.; Gaus, C.; Leonards, E. G.; De Boer, J. Chlorinated Paraffins in the Environment: A Review on Their Production, Fate, Levels and Trends between 2010 and 2015. **2016**. <https://doi.org/10.1016/j.chemosphere.2016.04.037>.
- (187) Ren, X.; Geng, N.; Zhang, H.; Wang, F.; Gong, Y.; Song, X.; Luo, Y.; Zhang, B.; Chen, J. Comparing the Disrupting Effects of Short-, Medium-and Long-Chain Chlorinated Paraffins on Cell Viability and Metabolism. *Sci. Total Environ.* **2019**, *685*, 297–307. <https://doi.org/10.1016/j.scitotenv.2019.05.388>.
- (188) Chibwe, L.; Myers, A. L.; De Silva, A. O.; Reiner, E. J.; Jobst, K.; Muir, D.; Yuan, B. C12–30 α -Bromo-Chloro "Alkenes": Characterization of a Poorly Identified Flame Retardant and Potential Environmental Implications. *Environ. Sci. Technol.* **2019**, *53* (18), 10835–10844. <https://doi.org/10.1021/acs.est.9b03760>.

- (189) Halocarbon company. Engineered Fluids <https://halocarbon.com/engineered-fluids/> (accessed May 18, 2021).
- (190) Company, D. Daikin Fluoropolymer Films <https://www.daikinchemicals.com/solutions/products/neoflon-fluoropolymers-films.html> (accessed May 18, 2021).
- (191) Company, D. Daikin fluoropolymers flame retardant <https://www.daikinchemicals.com/solutions/technical-challenges/flame-retardant.html> (accessed May 17, 2021).
- (192) Ferstandig, L. L., Astrologes, G. Polybromotrifluoroethylene. In *Fluorine Compounds, Organic*; ECT; pp 833–835.
- (193) Rtp company. polyvinylidene difluoride (PVDF) <https://www.rtpcompany.com/products/product-guide/polyvinylidene-fluoride-pvdf/> (accessed May 17, 2021).
- (194) Howard, P. H.; Muir, D. C. G. Identifying New Persistent and Bioaccumulative Organics Among Chemicals in Commerce. *Environ. Sci. Technol.* **2010**, *44* (7), 2277–2285. <https://doi.org/10.1021/es903383a>.
- (195) Rorije, E.; Emj, V.; Hollander, A.; Tp, T.; Mpm, J.; Ler. Identifying Potential POP and PBT Substances : Development of a New Persistence/Bioaccumulation-Score; 2011.
- (196) Gugisch, R.; Kerber, A.; Kohnert, A.; Laue, R.; Meringer, M.; Rücker, C.; Wassermann, A. MOLGEN 5.0, A Molecular Structure Generator; 2014.
- (197) Yuan, B.; Lysak, D. H.; Soong, R.; Haddad, A.; Hisatsune, A.; Moser, A.; Golotvin, S.; Argyropoulos, D.; Simpson, A. J.; Muir, D. C. G. Chlorines Are Not Evenly Substituted in Chlorinated Paraffins: A Predicted NMR Pattern Matching Framework for Isomeric Discrimination in Complex Contaminant Mixtures. *Environ. Sci. Technol. Lett.* **2020**, *7* (7), 496–503. <https://doi.org/10.1021/acs.estlett.0c00244>.
- (198) Gawor, A.; Wania, F. Using Quantitative Structural Property Relationships, Chemical Fate Models, and the Chemical Partitioning Space to Investigate the Potential for Long Range Transport and Bioaccumulation of Complex Halogenated Chemical Mixtures. *Environ. Sci. Process. & impacts* **2013**, *15* 9, 1671–1684.
- (199) Nedyalkova, M. A.; Madurga, S.; Tobiszewski, M.; Simeonov, V. Calculating the Partition Coefficients of Organic Solvents in Octanol/Water and Octanol/Air. *J. Chem. Inf. Model.* **2019**, *59* (5), 2257–2263. <https://doi.org/10.1021/acs.jcim.9b00212>.

- (200) O'Boyle, N. M.; Banck, M.; James, C. A.; Morley, C.; Vandermeersch, T.; Hutchison, G. R. Open Babel: An Open Chemical Toolbox. *J. Cheminform.* **2011**, *3* (1), 33. <https://doi.org/10.1186/1758-2946-3-33>.
- (201) Frisch, M. J., Trucks, G. W., Schlegel, H. B., Scuseria, G. E., Robb, M. A., Cheeseman, J. R., Scalmani, G., Barone, V., Petersson, G. A., Nakatsuji, H., Li, X., Caricato, M., Marenich, A. V., Bloino, J., Janesko, B. G., Gomperts, R., Mennucci, B., Hratch, D. J. Gaussian 16. Gaussian, Inc.: Wallingford CT 2016.
- (202) Czub, G.; Wania, F.; McLachlan, M. S. Combining Long-Range Transport and Bioaccumulation Considerations to Identify Potential Arctic Contaminants. *Environ. Sci. Technol.* **2008**, *42* (10), 3704–3709. <https://doi.org/10.1021/es7028679>.
- (203) Yuan, B.; Benskin, J. P.; Chen, C.-E. L.; Bergman, Å. Determination of Chlorinated Paraffins by Bromide-Anion Attachment Atmospheric-Pressure Chemical Ionization Mass Spectrometry. *Environ. Sci. Technol. Lett.* **2018**, *5* (6), 348–353. <https://doi.org/10.1021/acs.estlett.8b00216>.
- (204) Loos, M.; Gerber, C.; Corona, F.; Hollender, J.; Singer, H. Accelerated Isotope Fine Structure Calculation Using Pruned Transition Trees. *Anal. Chem.* **2015**, *87* (11), 5738–5744. <https://doi.org/10.1021/acs.analchem.5b00941>.
- (205) Howard, P. H.; Muir, D. C. G. Identifying New Persistent and Bioaccumulative Organics Among Chemicals in Commerce. III: Byproducts, Impurities, and Transformation Products. *Environ. Sci. Technol.* **2013**, *47* (10), 5259–5266. <https://doi.org/10.1021/es4004075>.
- (206) Henschler, D. Metabolism of Chlorinated Alkenes and Alkanes as Related to Toxicity. *J. Environ. Pathol. Toxicol.* **1977**, *1* (2), 125–133.
- (207) Glüge, J.; Bogdal, C.; Scheringer, M.; Buser, A. M.; Hungerbühler, K. Calculation of Physicochemical Properties for Short- and Medium-Chain Chlorinated Paraffins. *J. Phys. Chem. Ref. Data* **2013**, *42* (2), 23103. <https://doi.org/10.1063/1.4802693>.
- (208) Mackay, D. *Handbook of Physical-Chemical Properties and Environmental Fate for Organic Chemicals*, 2nd ed.; CRC/Taylor & Francis: Boca Raton, FL, 2006.
- (209) Bettina, H.; Hermann, F.; Wolfgang, V.; Mehmet, C. Effects of Chain Length, Chlorination Degree, and Structure on the Octanol–Water Partition Coefficients of Polychlorinated n-Alkanes. *Environ. Sci. Technol.* **2011**, *45* (7), 2842–2849. <https://doi.org/10.1021/es103098b>.
- (210) Fisk, A. T.; Wiens, S. C.; Webster, G. R. B.; Bergman, Å.; Muir, D. C. G. Accumulation and Depuration of Sediment-Sorbed C12- and C16-Polychlorinated

- Alkanes by Oligochaetes (*Lumbriculus Variegatus*). *Environ. Toxicol. Chem.* **1998**, *17* (10), 2019–2026. <https://doi.org/https://doi.org/10.1002/etc.5620171018>.
- (211) Renberg, L.; Sundström, G.; Sundh-Nygård, K. Partition Coefficients of Organic Chemicals Derived from Reversed Phase Thin Layer Chromatography: Evaluation of Methods and Application on Phosphate Esters, Polychlorinated Paraffins and Some PCB-Substitutes. *Chemosphere* **1980**, *9* (11), 683–691. [https://doi.org/https://doi.org/10.1016/0045-6535\(80\)90120-4](https://doi.org/https://doi.org/10.1016/0045-6535(80)90120-4).
- (212) Myers, A. L.; Jobst, K. J.; Mabury, S. A.; Reiner, E. J. Using Mass Defect Plots as a Discovery Tool to Identify Novel Fluoropolymer Thermal Decomposition Products. *J. Mass Spectrom.* **2014**, *49* (4), 291–296. <https://doi.org/https://doi.org/10.1002/jms.3340>.
- (213) Nakajima, Y.; Arinami, Y.; Yamamoto, K. Selective Separation of Fluorinated Compounds from Complex Organic Mixtures by Pyrolysis-Comprehensive Two-Dimensional Gas Chromatography Coupled to High-Resolution Time-of-Flight Mass Spectrometry. *J. Chromatogr. A* **2014**, *1374*, 231–237. <https://doi.org/10.1016/j.chroma.2014.11.062>.
- (214) Bergmann, M.; Wirzberger, V.; Krumpfen, T.; Lorenz, C.; Primpke, S.; Tekman, M. B.; Gerdts, G. High Quantities of Microplastic in Arctic Deep-Sea Sediments from the HAUSGARTEN Observatory. *Environ. Sci. Technol.* **2017**, *51* (19), 11000–11010. <https://doi.org/10.1021/acs.est.7b03331>.
- (215) Plassmann, M. M.; Berger, U. Trace Analytical Methods for Semifluorinated N-Alkanes in Snow, Soil, and Air. *Anal. Chem.* **2010**, *82* (11), 4551–4557. <https://doi.org/10.1021/ac1005519>.
- (216) Beyer, A.; Wania, F.; Gouin, T.; Mackay, D.; Matthies, M. Selecting Internally Consistent Physicochemical Properties of Organic Compounds. *Environ. Toxicol. Chem.* **2002**, *21* (5), 941–953. <https://doi.org/https://doi.org/10.1002/etc.5620210508>.
- (217) Zhou, Y.; de Wit, C. A.; Yin, G.; Du, X.; Yuan, B. Shorter than Short-Chain: Very Short-Chain Chlorinated Paraffins (VSCCPs) Found in Wildlife from the Yangtze River Delta. *Environ. Int.* **2019**, *130*, 104955. <https://doi.org/10.1016/j.envint.2019.104955>.
- (218) Yuan, B.; Muir, D.; MacLeod, M. Methods for Trace Analysis of Short-, Medium-, and Long-Chain Chlorinated Paraffins: Critical Review and Recommendations. *Anal. Chim. Acta* **2019**, *1074*, 16–32. <https://doi.org/https://doi.org/10.1016/j.aca.2019.02.051>.
- (219) Yeung, L. W. Y.; Miyake, Y.; Taniyasu, S.; Wang, Y.; Yu, H.; So, M. K.; Jiang, G.; Wu, Y.; Li, J.; Giesy, J. P.; Yamashita, N.; Lam, P. K. S. Perfluorinated

- Compounds and Total and Extractable Organic Fluorine in Human Blood Samples from China. *Environ. Sci. Technol.* **2008**, *42* (21), 8140–8145.
<https://doi.org/10.1021/es800631n>.
- (220) United Nations Environment Programme. *United Nations Global Chemicals Outlook*; 2019.
- (221) European Union. Green Deal: Commission adopts new Chemicals Strategy towards a toxic-free environment
https://ec.europa.eu/commission/presscorner/detail/en/ip_20_1839.
- (222) Hollender, J.; Schymanski, E. L.; Singer, H. P.; Ferguson, P. L. Nontarget Screening with High Resolution Mass Spectrometry in the Environment: Ready to Go? *Environ. Sci. Technol.* **2017**, *51* (20), 11505–11512.
<https://doi.org/10.1021/acs.est.7b02184>.
- (223) Covention, S. All POPs listed in the Stockholm Convention
<http://chm.pops.int/TheConvention/ThePOPs/ListingofPOPs/tabid/2509/Default.aspx>.
- (224) Wania, F. Assessing the Potential of Persistent Organic Chemicals for Long-Range Transport and Accumulation in Polar Regions. *Environ. Sci. Technol.* **2003**, *37* (7), 1344–1351. <https://doi.org/10.1021/es026019e>.
- (225) Muir, D.; Zhang, X.; de Wit, C. A.; Vorkamp, K.; Wilson, S. Identifying Further Chemicals of Emerging Arctic Concern Based on ‘in Silico’ Screening of Chemical Inventories. *Emerg. Contam.* **2019**, *5*, 201–210.
<https://doi.org/10.1016/j.emcon.2019.05.005>.
- (226) Megson, D.; Robson, M.; Jobst, K. J.; Helm, P. A.; Reiner, E. J. Determination of Halogenated Flame Retardants Using Gas Chromatography with Atmospheric Pressure Chemical Ionization (APCI) and a High-Resolution Quadrupole Time-of-Flight Mass Spectrometer (HRqTOFMS). *Anal. Chem. (Washington, DC, United States)* **2016**, *88* (23), 11406–11411.
<https://doi.org/10.1021/acs.analchem.6b01550>.
- (227) PFAS Master List of PFAS Substance
<https://comptox.epa.gov/dashboard/chemical-lists/pfasmaster>.
- (228) Beyer, A.; Mackay, D.; Matthies, M.; Wania, F.; Webster, E. Assessing Long-Range Transport Potential of Persistent Organic Pollutants. *Environ. Sci. Technol.* **2000**, *34* (4), 699–703. <https://doi.org/10.1021/es990207w>.
- (229) Hohenberg, P.; Kohn, W. Inhomogeneous Electron Gas. *Phys. Rev.* **1964**, *136* (3B), B864–B871. <https://doi.org/10.1103/PhysRev.136.B864>.

- (230) Kohn, W.; Sham, L. J. Self-Consistent Equations Including Exchange and Correlation Effects. *Phys. Rev.* **1965**, *140* (4A), A1133–A1138. <https://doi.org/10.1103/PhysRev.140.A1133>.
- (231) Levy, M. Universal Variational Functionals of Electron Densities, First-Order Density Matrices, and Natural Spin-Orbitals and Solution of the v -Representability Problem. *Proc. Natl. Acad. Sci.* **1979**, *76* (12), 6062–6065. <https://doi.org/10.1073/pnas.76.12.6062>.
- (232) Parr, R. G.; Pearson, R. G. Absolute Hardness: Companion Parameter to Absolute Electronegativity. *J. Am. Chem. Soc.* **1983**, *105* (26), 7512–7516. <https://doi.org/10.1021/ja00364a005>.
- (233) Geerlings, P.; Chamorro, E.; Chattaraj, P. K.; De Proft, F.; Gázquez, J. L.; Liu, S.; Morell, C.; Toro-Labbé, A.; Vela, A.; Ayers, P. Conceptual Density Functional Theory: Status, Prospects, Issues. *Theor. Chem. Acc.* **2020**, *139* (2), 36. <https://doi.org/10.1007/s00214-020-2546-7>.
- (234) Johnson, P. A.; Bartolotti, L. J.; Ayers, P. W.; Fievez, T.; Geerlings, P. Charge Density and Chemical Reactions: A Unified View from Conceptual DFT BT - Modern Charge-Density Analysis; Gatti, C., Macchi, P., Eds.; Springer Netherlands: Dordrecht, 2012; pp 715–764. https://doi.org/10.1007/978-90-481-3836-4_21.
- (235) Liu, S. B. *Conceptual Density Functional Theory: Towards a New Chemistry Reactivity Theory*; Wiley-VCH: Weinheim: German, 2022.
- (236) Parr, R. G.; Szentpály, L. v.; Liu, S. Electrophilicity Index. *J. Am. Chem. Soc.* **1999**, *121* (9), 1922–1924. <https://doi.org/10.1021/ja983494x>.
- (237) Ghanty, T. K.; Ghosh, S. K. Correlation between Hardness, Polarizability, and Size of Atoms, Molecules, and Clusters. *J. Phys. Chem.* **1993**, *97* (19), 4951–4953. <https://doi.org/10.1021/j100121a015>.
- (238) Vela, A.; Gázquez, J. L. A Relationship between the Static Dipole Polarizability, the Global Softness, and the Fukui Function. *J. Am. Chem. Soc.* **1990**, *112* (4), 1490–1492. <https://doi.org/10.1021/ja00160a029>.
- (239) Stott, M. J.; Zaremba, E. Erratum: Linear-Response Theory within the Density-Functional Formalism: Application to Atomic Polarizabilities. *Phys. Rev. A* **1980**, *22* (5), 2293. <https://doi.org/10.1103/PhysRevA.22.2293.2>.
- (240) Yang, W.; Parr, R. G.; Pucci, R. Electron Density, Kohn–Sham Frontier Orbitals, and Fukui Functions. *J. Chem. Phys.* **1984**, *81* (6), 2862–2863. <https://doi.org/10.1063/1.447964>.

- (241) Ayers, P. W.; Levy, M. Perspective on "Density Functional Approach to the Frontier-Electron Theory of Chemical Reactivity." *Theor. Chem. Acc.* **2000**, *103* (3), 353–360. <https://doi.org/10.1007/s002149900093>.
- (242) Anderson, J. S. M.; Melin, J.; Ayers, P. W. Conceptual Density-Functional Theory for General Chemical Reactions, Including Those That Are Neither Charge- nor Frontier-Orbital-Controlled. 1. Theory and Derivation of a General-Purpose Reactivity Indicator. *J. Chem. Theory Comput.* **2007**, *3* (2), 358–374. <https://doi.org/10.1021/ct600164j>.
- (243) The Open Babel Package <http://openbabel.org>.
- (244) Lee, C.; Yang, W.; Parr, R. G. Development of the Colle-Salvetti Correlation-Energy Formula into a Functional of the Electron Density. *Phys. Rev. B* **1988**, *37* (2), 785–789. <https://doi.org/10.1103/PhysRevB.37.785>.
- (245) Becke, A. D. Density-Functional Exchange-Energy Approximation with Correct Asymptotic Behavior. *Phys. Rev. A* **1988**, *38* (6), 3098–3100. <https://doi.org/10.1103/PhysRevA.38.3098>.
- (246) Becke, A. D. Density-functional Thermochemistry. III. The Role of Exact Exchange. *J. Chem. Phys.* **1993**, *98* (7), 5648–5652. <https://doi.org/10.1063/1.464913>.
- (247) Stephens, P. J.; Devlin, F. J.; Chabalowski, C. F.; Frisch, M. J. Ab Initio Calculation of Vibrational Absorption and Circular Dichroism Spectra Using Density Functional Force Fields. *J. Phys. Chem.* **1994**, *98* (45), 11623–11627. <https://doi.org/10.1021/j100096a001>.
- (248) Clark, T.; Chandrasekhar, J.; Spitznagel, G. W.; Schleyer, P. V. R. Efficient Diffuse Function-Augmented Basis Sets for Anion Calculations. III. The 3-21+G Basis Set for First-Row Elements, Li–F. *J. Comput. Chem.* **1983**, *4* (3), 294–301. <https://doi.org/https://doi.org/10.1002/jcc.540040303>.
- (249) Curtiss, L. A.; McGrath, M. P.; Blaudeau, J.; Davis, N. E.; Binning Jr., R. C.; Radom, L. Extension of Gaussian-2 Theory to Molecules Containing Third-row Atoms Ga–Kr. *J. Chem. Phys.* **1995**, *103* (14), 6104–6113. <https://doi.org/10.1063/1.470438>.
- (250) Francl, M. M.; Pietro, W. J.; Hehre, W. J.; Binkley, J. S.; Gordon, M. S.; DeFrees, D. J.; Pople, J. A. Self-consistent Molecular Orbital Methods. XXIII. A Polarization-type Basis Set for Second-row Elements. *J. Chem. Phys.* **1982**, *77* (7), 3654–3665. <https://doi.org/10.1063/1.444267>.

- (251) Krishnan, R.; Binkley, J. S.; Seeger, R.; Pople, J. A. Self-consistent Molecular Orbital Methods. XX. A Basis Set for Correlated Wave Functions. *J. Chem. Phys.* **2008**, *72* (1), 650–654. <https://doi.org/10.1063/1.438955>.
- (252) Koopmans, T. Über Die Zuordnung von Wellenfunktionen Und Eigenwerten Zu Den Einzelnen Elektronen Eines Atoms. *Physica* **1934**, *1* (1), 104–113. [https://doi.org/https://doi.org/10.1016/S0031-8914\(34\)90011-2](https://doi.org/https://doi.org/10.1016/S0031-8914(34)90011-2).
- (253) Bartolotti, L. J.; Ayers, P. W. An Example Where Orbital Relaxation Is an Important Contribution to the Fukui Function. *J. Phys. Chem. A* **2005**, *109* (6), 1146–1151. <https://doi.org/10.1021/jp0462207>.
- (254) Arulmozhiraja, S.; Fujii, T. Torsional Barrier, Ionization Potential, and Electron Affinity of Biphenyl—A Theoretical Study. *J. Chem. Phys.* **2001**, *115* (23), 10589–10594. <https://doi.org/10.1063/1.1418438>.
- (255) De Proft, F.; Geerlings, P. Relative Hardness as a Measure of Aromaticity. *Phys. Chem. Chem. Phys.* **2004**, *6* (2), 242–248. <https://doi.org/10.1039/B312566C>.
- (256) Zhan, C.-G. G.; Nichols, J. A.; Dixon, D. A. Ionization Potential, Electron Affinity, Electronegativity, Hardness, and Electron Excitation Energy: Molecular Properties from Density Functional Theory Orbital Energies. *J. Phys. Chem. A* **2003**, *107* (20), 4184–4195. <https://doi.org/10.1021/jp0225774>.
- (257) Damoun, S.; Langenaeker, W.; Van de Woude, G.; Geerlings, P. Acidity of Halogenated Alcohols and Silanols: Competition of Electronegativity and Softness in Second and Higher Row Atoms. *J. Phys. Chem.* **1995**, *99* (32), 12151–12157. <https://doi.org/10.1021/j100032a016>.
- (258) Nian, M.; Luo, K.; Luo, F.; Aimuzi, R.; Huo, X.; Chen, Q.; Tian, Y.; Zhang, J. Association between Prenatal Exposure to PFAS and Fetal Sex Hormones: Are the Short-Chain PFAS Safer? *Environ. Sci. Technol.* **2020**, *54* (13), 8291–8299. <https://doi.org/10.1021/acs.est.0c02444>.
- (259) Pétré, M.-A.; Genereux, D. P.; Koropecykj-Cox, L.; Knappe, D. R. U.; Duboscq, S.; Gilmore, T. E.; Hopkins, Z. R. Per- and Polyfluoroalkyl Substance (PFAS) Transport from Groundwater to Streams near a PFAS Manufacturing Facility in North Carolina, USA. *Environ. Sci. Technol.* **2021**, *55* (9), 5848–5856. <https://doi.org/10.1021/acs.est.0c07978>.
- (260) Forsthuber, M.; Kaiser, A. M.; Granitzer, S.; Hassl, I.; Hengstschläger, M.; Stangl, H.; Gundacker, C. Albumin Is the Major Carrier Protein for PFOS, PFOA, PFHxS, PFNA and PFDA in Human Plasma. *Environ. Int.* **2020**, *137* (February), 105324. <https://doi.org/10.1016/j.envint.2019.105324>.

- (261) Raevskii, O. A.; Grigor'ev, V. Y. Lipophilicity of Organic Compounds: A Quantitative Description Based on the Concepts of Polarizability and Acceptor Ability to Hydrogen Bond Formation. *Pharm. Chem. J.* **1999**, *33* (5), 274–277. <https://doi.org/10.1007/BF02510052>.
- (262) Zhang, L.; Ren, X.-M.; Guo, L.-H. Structure-Based Investigation on the Interaction of Perfluorinated Compounds with Human Liver Fatty Acid Binding Protein. *Environ. Sci. Technol.* **2013**, *47* (19), 11293–11301. <https://doi.org/10.1021/es4026722>.
- (263) Beesoon, S.; Martin, J. W. Isomer-Specific Binding Affinity of Perfluorooctanesulfonate (PFOS) and Perfluorooctanoate (PFOA) to Serum Proteins. *Environ. Sci. Technol.* **2015**, *49* (9), 5722–5731. <https://doi.org/10.1021/es505399w>.
- (264) Mishra, V.; Heath, R. J. Structural and Biochemical Features of Human Serum Albumin Essential for Eukaryotic Cell Culture. *Int. J. Mol. Sci.* **2021**, *22* (16), 8411. <https://doi.org/10.3390/ijms22168411>.
- (265) Zhou, P.; Zou, J.; Tian, F.; Shang, Z. Fluorine Bonding — How Does It Work In Protein–Ligand Interactions? *J. Chem. Inf. Model.* **2009**, *49* (10), 2344–2355. <https://doi.org/10.1021/ci9002393>.
- (266) Han, X.; Hinderliter, P. M.; Snow, T. A.; Jepson, G. W. Binding of Perfluorooctanoic Acid to Rat Liver-form and Kidney-form A2u-Globulins. *Drug Chem. Toxicol.* **2004**, *27* (4), 341–360. <https://doi.org/10.1081/DCT-200039725>.
- (267) Hites, R. A. Mass Spectrometric Identification of Pollutants in the Environment: A Personal and Bibliometric Perspective. *J. Am. Soc. Mass Spectrom.* **2022**, *33* (4), 620–626. <https://doi.org/10.1021/jasms.1c00374>.
- (268) GUY, W. S.; TAVES, D. R.; BREY, W. S. J. R. Organic Fluorocompounds in Human Plasma: Prevalence and Characterization. In *Biochemistry Involving Carbon-Fluorine Bonds*; ACS Symposium Series; AMERICAN CHEMICAL SOCIETY, 1976; Vol. 28, pp 117-134 SE – 7. <https://doi.org/doi:10.1021/bk-1976-0028.ch007>.
- (269) Hansen, K. J.; Clemen, L. A.; Ellefson, M. E.; Johnson, H. O. Compound-Specific, Quantitative Characterization of Organic Fluorochemicals in Biological Matrices. *Environ. Sci. Technol.* **2001**, *35* (4), 766–770. <https://doi.org/10.1021/es001489z>.
- (270) Land, M.; de Wit, C. A.; Cousins, I. T.; Herzke, D.; Johansson, J.; Martin, J. W. What Is the Effect of Phasing out Long-Chain per- and Polyfluoroalkyl Substances on the Concentrations of Perfluoroalkyl Acids and Their Precursors in the Environment? A Systematic Review Protocol. *Environ. Evid.* **2015**, *4* (1), 3. <https://doi.org/10.1186/2047-2382-4-3>.

- (271) Liu, Y.; D'Agostino, L. A.; Qu, G.; Jiang, G.; Martin, J. W. High-Resolution Mass Spectrometry (HRMS) Methods for Nontarget Discovery and Characterization of Poly- and per-Fluoroalkyl Substances (PFASs) in Environmental and Human Samples. *TrAC Trends Anal. Chem.* **2019**, *121*, 115420. <https://doi.org/https://doi.org/10.1016/j.trac.2019.02.021>.
- (272) Jobst, K.; Shen, L.; Reiner, E.; Taguchi, V.; Helm, P.; Mccrindle, R.; Backus, S. The Use of Mass Defect Plots for the Identification of (Novel) Halogenated Contaminants in the Environment. *Anal. Bioanal. Chem.* **2013**, *405*. <https://doi.org/10.1007/s00216-013-6735-2>.
- (273) Hughey, C. A.; Hendrickson, C. L.; Rodgers, R. P.; Marshall, A. G.; Qian, K. Kendrick Mass Defect Spectrum: A Compact Visual Analysis for Ultrahigh-Resolution Broadband Mass Spectra. *Anal. Chem.* **2001**, *73* (19), 4676–4681. <https://doi.org/10.1021/ac010560w>.
- (274) Taguchi, V. Y.; Nieckarz, R. J.; Clement, R. E.; Krolik, S.; Williams, R. Dioxin Analysis by Gas Chromatography-Fourier Transform Ion Cyclotron Resonance Mass Spectrometry (GC-FTICRMS). *J. Am. Soc. Mass Spectrom.* **2010**, *21* (11), 1918–1921. <https://doi.org/10.1016/j.jasms.2010.07.010>.
- (275) Ballesteros-Gómez, A.; Ballesteros, J.; Ortiz, X.; Jonker, W.; Helmus, R.; Jobst, K. J.; Parsons, J. R.; Reiner, E. J. Identification of Novel Brominated Compounds in Flame Retarded Plastics Containing TBBPA by Combining Isotope Pattern and Mass Defect Cluster Analysis. *Environ. Sci. Technol.* **2017**, *51* (3), 1518–1526. <https://doi.org/10.1021/acs.est.6b03294>.
- (276) Shen, L.; Jobst, K. J.; Reiner, E. J.; Helm, P. A.; McCrindle, R.; Taguchi, V. Y.; Marvin, C. H.; Backus, S.; MacPherson, K. A.; Brindle, I. D. Identification and Occurrence of Analogues of Dechlorane 604 in Lake Ontario Sediment and Their Accumulation in Fish. *Environ. Sci. Technol.* **2014**, *48* (19), 11170–11177. <https://doi.org/10.1021/es503089c>.
- (277) Sührling, R.; Ortiz, X.; Pena-Abaurrea, M.; Jobst, K. J.; Freese, M.; Pohlmann, J.-D.; Marohn, L.; Ebinghaus, R.; Backus, S.; Hanel, R.; Reiner, E. J. Evidence for High Concentrations and Maternal Transfer of Substituted Diphenylamines in European Eels Analyzed by Two-Dimensional Gas Chromatography–Time-of-Flight Mass Spectrometry and Gas Chromatography–Fourier Transform Ion Cyclotron Resonance Mass Spe. *Environ. Sci. Technol.* **2016**, *50* (23), 12678–12685. <https://doi.org/10.1021/acs.est.6b04382>.
- (278) Aznar-Alemany, Ò.; Sala, B.; Jobst, K. J.; Reiner, E. J.; Borrell, A.; Aguilar, À.; Eljarrat, E. Temporal Trends of Halogenated and Organophosphate Contaminants in Striped Dolphins from the Mediterranean Sea. *Sci. Total Environ.* **2021**, *753*, 142205. <https://doi.org/https://doi.org/10.1016/j.scitotenv.2020.142205>.

- (279) Fernando, S.; Jobst, K. J.; Taguchi, V. Y.; Helm, P. A.; Reiner, E. J.; McCarry, B. E. Identification of the Halogenated Compounds Resulting from the 1997 Plastimet Inc. Fire in Hamilton, Ontario, Using Comprehensive Two-Dimensional Gas Chromatography and (Ultra)High Resolution Mass Spectrometry. *Environ. Sci. Technol.* **2014**, *48* (18), 10656–10663. <https://doi.org/10.1021/es503428j>.
- (280) Ubukata, M.; Jobst, K. J.; Reiner, E. J.; Reichenbach, S. E.; Tao, Q.; Hang, J.; Wu, Z.; Dane, A. J.; Cody, R. B. Non-Targeted Analysis of Electronics Waste by Comprehensive Two-Dimensional Gas Chromatography Combined with High-Resolution Mass Spectrometry: Using Accurate Mass Information and Mass Defect Analysis to Explore the Data. *J. Chromatogr. A* **2015**, *1395*, 152–159. <https://doi.org/10.1016/j.chroma.2015.03.050>.
- (281) Dodds, J. N.; Hopkins, Z. R.; Knappe, D. R. U. U.; Baker, E. S. Rapid Characterization of Per- and Polyfluoroalkyl Substances (PFAS) by Ion Mobility Spectrometry–Mass Spectrometry (IMS-MS). *Anal. Chem.* **2020**, *92* (6), 4427–4435. <https://doi.org/10.1021/acs.analchem.9b05364>.
- (282) Gabelica, V.; Shvartsburg, A. A.; Afonso, C.; Barran, P.; Benesch, J. L. P.; Bleiholder, C.; Bowers, M. T.; Bilbao, A.; Bush, M. F.; Campbell, J. L.; Campuzano, I. D. G.; Causon, T.; Clowers, B. H.; Creaser, C. S.; De Pauw, E.; Far, J.; Fernandez-Lima, F.; Fjeldsted, J. C.; Giles, K.; Groessl, M.; Hogan Jr, C. J.; Hann, S.; Kim, H. I.; Kurulugama, R. T.; May, J. C.; McLean, J. A.; Pagel, K.; Richardson, K.; Ridgeway, M. E.; Rosu, F.; Sobott, F.; Thalassinou, K.; Valentine, S. J.; Wyttenbach, T. Recommendations for Reporting Ion Mobility Mass Spectrometry Measurements. *Mass Spectrom. Rev.* **2019**, *38* (3), 291–320. <https://doi.org/10.1002/mas.21585>.
- (283) Schymanski, E. L.; Jeon, J.; Gulde, R.; Fenner, K.; Ruff, M.; Singer, H. P.; Hollender, J. Identifying Small Molecules via High Resolution Mass Spectrometry: Communicating Confidence. *Environ. Sci. Technol.* **2014**, *48* (4), 2097–2098. <https://doi.org/10.1021/es5002105>.
- (284) Muscalu, A. M.; Górecki, T. Comprehensive Two-Dimensional Gas Chromatography in Environmental Analysis. *TrAC Trends Anal. Chem.* **2018**, *106*, 225–245. <https://doi.org/10.1016/j.trac.2018.07.001>.
- (285) Pirok, B. W. J.; Stoll, D. R.; Schoenmakers, P. J. Recent Developments in Two-Dimensional Liquid Chromatography: Fundamental Improvements for Practical Applications. *Anal. Chem.* **2019**, *91* (1), 240–263. <https://doi.org/10.1021/acs.analchem.8b04841>.
- (286) Wu, Z.; Schoenmakers, P.; Marriott, P. J. Nomenclature and Conventions in Comprehensive Multidimensional Chromatography – An Update

<https://www.chromatographyonline.com/view/nomenclature-and-conventions-comprehensive-multidimensional-chromatography-update> (accessed May 5, 2022).

- (287) Giddings, J. C. Concepts and Comparisons in Multidimensional Separation. *J. High Resolut. Chromatogr.* **1987**, *10* (5), 319–323.
<https://doi.org/https://doi.org/10.1002/jhrc.1240100517>.
- (288) Newton, S. R.; McMahan, R. L.; Sobus, J. R.; Mansouri, K.; Williams, A. J.; McEachran, A. D.; Strynar, M. J. Suspect Screening and Non-Targeted Analysis of Drinking Water Using Point-of-Use Filters. *Environ. Pollut.* **2018**, *234*, 297–306.
<https://doi.org/10.1016/j.envpol.2017.11.033>.
- (289) Fernando, S.; Green, M. K.; Organtini, K.; Dorman, F.; Jones, R.; Reiner, E. J.; Jobst, K. J. Differentiation of (Mixed) Halogenated Dibenzo-p-Dioxins by Negative Ion Atmospheric Pressure Chemical Ionization. *Anal. Chem.* **2016**, *88* (10), 5205–5211. <https://doi.org/10.1021/acs.analchem.6b00255>.
- (290) Gross, J. H. *Mass Spectrometry*, 3rd ed.; Springer: Heidelberg, Germany, 2017.